UNIVERSITY OF TRENTO - Italy

International PhD Program in Biomolecular Sciences
Department of Cellular, Computational and Integrative Biology – CIBIO 32st Cycle

Identification and validation of small molecules targeting the YTH domain

Tutor: Prof. ALESSANDRO PROVENZANI

Department of Cellular, Computational and Integrative Biology – CIBIO Laboratory of Genomic Screening

Ph.D. Thesis of

MARIACHIARA MICAELLI

Department of Cellular, Computational and Integrative Biology – CIBIO
Laboratory of Genomic Screening

Academic Year 2018-2019

Original authorship

Declaration:

I, Mariachiara Micaelli, confirm that this is my own work and the use of all material from other sources has been properly and fully acknowledged.

Trento, 05/09/20

ABSTRACT

N6-methyladenosine (m6A) is one of the most common reversible RNA modifications, conserved in all eukaryotes from yeast to humans. It is mainly observed in the 3'UTR, the 5'UTR and near the Transcription Start Sites (TSS), inside a consensus sequence identified as [G/A/U][A/G][m6A-C][U/A/C. The m6A modification is involved in the regulation of many different biological phenomena, starting from development, stemness, adipogenesis, spermatogenesis and many others. Its misregulation has been found to be the driving force of different pathologies, most importantly has been widely described as having a major role in carcinogenesis. The methylation machinery is composed of methyltransferases, erasers and readers, the latter recognizing the modification upon target RNAs and guiding them to different fates. The proteins that act as readers of the methylation belong to the YTH-domain family, with four cytoplasmic isoforms (YTHDF1-3;YTHDC2), involved in the regulation of translation and decay of m6A-containing mRNAs, and one nuclear isoform (YTHDC1), involved in alternative splicing. The YTH domain proteins have been identified to have major roles in cancer development, mainly causing misregulation of cancer-related RNA targets. However, its role in the development of the pediatric tumor Neuroblastoma was still largely unknown.

In my PhD project I focused on characterizing the role of the YTHDF1 protein in Neuroblastoma development, reporting that YTHDF1 supports Neuroblastoma aggressiveness by enhancing its proliferation, tumour-sphere forming ability and its invasiveness. To address whether modulating the YTHDF1-mediated regulation of m6A transcripts signaling through YTHDF1 could represent a new pharmacological strategy target in NB, I performed for the first time an High Throughput Screening aiming to interfere with the RNA binding ability of the YTH domain, testing a 2000 compound library of small molecules. Among others, only one molecule was identified for as a strong binder, and consequently demonstrated its direct interaction with the binding pocket of the YTHD by different biochemical approaches. For the first time has been proposed an encouraging proof-of-concept of m6A readers as potential pharmacological targets for the treatment of NB, that led to the repurposing of an already FDA approved drug as an inhibitor for this novel target.

Table of Contents

ABBREVIATIONS AND ACRONYMS

m6A	N6-methyladenosine
RBP	RNA Binding Protein
mRNA	Messenger Ribonucleic Acid
RIP	RNA Immunoprecipitation
RRM	RNA Recognition Motif
UTR	Untranslated Region
YTHDF1-3	YTH N6-methyladenosine RNA binding protein 1-3
YTHDC1-2	YTH Domain Containing 1-2
METTL3/14	Methyltransferase like 3/14
FTO	Fat mass and obesity-associated protein
ALKBH5	AlkB Homolog 5, RNA Demethylase
VIRMA	Vir Like M6A Methyltransferase Associated
WTAP	WT1 Associated Protein
RBM15/15B	RNA binding motifs protein 15/15B
SAM	S-Adenosyl-Methionine
ZC3H13	Zinc Finger CCCH-Type Containing 13
MAT2A	methionine adenosyltransferase 2A
Mmi1	meiotic mRNA interception
XIST	X Inactive Specific Transcript

HNRNPA2B1	Heterogeneous Nuclear Ribonucleoprotein A2/B1
EIF3	Eukaryotic Translation Initiation Factor 3
IGF2BP1–3	insulin growth factor 2 mRNA binding proteins 1, 2 and 3
HUR	Human Antigen R protein
AML	Acute Myeloid Leukemia
PCa	Prostate Cancer
CRC	Colorectal Cancer
LUSC	Lung Squamous Cell Carcinoma
HCC	Hepatocellular Carcinoma
GBM	Glioblastoma
NB	Neuroblastoma
PAR-CLIP	Photoactivatable Ribonucleoside-enhanced Crosslinking and Immunoprecipitation
i-CLIP	Individual-nucleotide Resolution Cross-Linking and Immunoprecipitation
NMR	Nuclear Magnetic Resonance Spectroscopy
DMR	Dynamic Mass Redistribution
REMSA	RNA Electrophoretic Mobility Shift Assay
qRT-PCR	Quantitative Real Time PCR
siRNA	Silencing RNA
Act-D	Actinomycin D

DMSO	Dimethyl Sulfoxide
HRTR-FRET	High Resolution Time-Resolved Forster Resonance Transfer
HTS	High Throughput Screening
IC50	Half Maximal Inhibitory Concentration
PAINS	Pan-Assay Interference Compounds

1.Introduction

1.1 The epitranscriptome and RNA modifications: a brief introduction

DNA, and the study of DNA modifications, has always had a privileged eye in biological research. The discovery that also RNA bears modifications happened a while ago, around the 70' (Iwanami & Brown, 1968), but, at that time, there were no techniques to measure and localize the modifications. Therefore, this observation was forgotten for decades.

Since DNA modifications undergo the term "epigenetics", meaning all the modifications happening among the genome that are not conserved and do not cause changes in the nucleotide sequence, and that cause permanent or transient modification in gene expression, also all RNA modifications that cause changes in the transcriptome but not in the ribonucleotide sequence were classified as "epitranscriptome". RNA modifications are more than 100, and are all classified on databases that are continuously updated, such as https://mods.rna.albany.edu/ , but still, the enzymes that catalyze the covalent modification reaction are unknown for many of them, and also are their main regulatory roles. Since all kind of RNAs, from ribosomal RNAs (rRNAs), to transfer RNAs (tRNAs), messenger RNAs (mRNAs), small nuclear RNAs (snRNAs) and others, have been discovered to be modified at different sites, studying the matter is not easy at it could be. RNA modifications can be divided in reversible and non-reversible, the first being the ones that does not cause any changes in the information content of RNA, while the other are the ones responsible for the direct and permanent change of information, as for example the editing of Adenosine to Inosine catalyzed by the enzyme ADAR. Many are the known reversible RNA modifications, but less are the ones that have been completely characterized and of which is also known the biological function. Methylation, hydroxymethylation, deamination, reduction, and oxidation are some examples of modifications that can occur on RNA, and also base ribose methylation and pseudourydilation, which are considered the most common (S. Li & Mason, 2014).Starting from the 5', the most common includes 2′-Omethylated ribonucleotides, such as N6,2′-O-dimethyladenosine (m6Am), N6 (m6A), N6,2′O-trimethyladenosine (m62Am), and 3,2′-O-dimethyluridine (m3Um), and of course also the 7-methylguanosine (m7G) cap that is set during normal RNA processing, that is fundamental for the stability of mRNAs, avoiding them to be degraded prior to be translated. Anyway, modifications occur in all the regions of the transcripts, and on all the four RNA bases of coding and non-coding RNA. Adenosine modifications include mostly

methylation, occurring in different positions of the nucleoside. They include N6-methyladenosine (m6A), on which this thesis will focus exclusively and will be discussed later, N1-methyladenosine (m1a) and N6,2'-O-dimethyladenosine (m6Am), that are the most common ones (Jia et al., 2013). m1a blocks the Watson-Crick base pairing causing the formation of a positive charge, altering dramatically protein-RNA interaction and the formation of RNA secondary structures. It is mainly located near translation start sites, in fact it is correlated to translational upregulation (Dominissini et al., 2016)). N6,2'-Odimethyladenosine (m6Am) decorates the 5' cap of mRNAs in higher eukaryotes, and it was found to share one demethylase with the m6A modification (Mauer et al., 2017). Methylation can also occur on Cytosine, as in the most common 5-methylcytosine (m5C), which was firstly discovered in 1974(Desrosiers et al., 1974a). NSUN2, a tRNA methyltransferase, catalyzes the methylation reaction (Hussain et al., 2013), but the reaction can also be catalyzed by the DNA methyltransferase DNMT2. m5C occurs in different kind of RNAs, but it is mostly been studied in tRNAs, in rRNAs and of course in mRNAs.

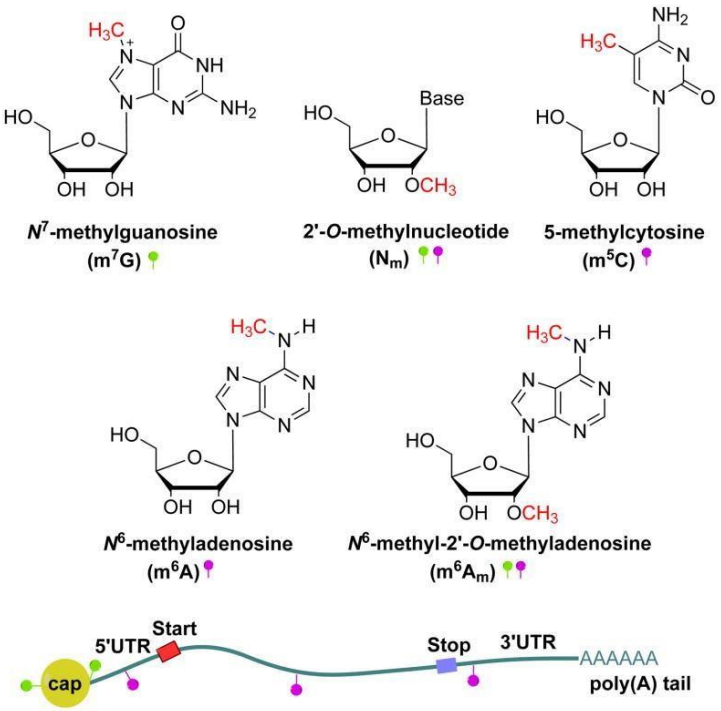

Fig.1. Chemical structure of some of the most common methylation occurring on RNA bases. In red is highlighted the methyl group, and on the bottom are indicated the positions in which each modification mainly occurs on mRNAs. (Jia et. al, 2013).

1.2 N6-methyladenosine (m6A)

N6-methyladenosine (m6A) is one of the most abundant post transcriptional RNA modifications, well conserved from yeasts to humans. It is firstly been discovered in the 1970s (Desrosiers et al., 1974b; Perry & Kelley, 1974), but only in the past decades it is been started to look at its biological relevance in more detail, also thanks to the discovery of the methyltransferase-like protein 3, METTL3 (Bokar et al., 1997) which is responsible for the synthesis of nearly all the m6A modifications present on RNA, and more recently of the demethylase fat mass and obesity-associated protein (FTO) (Jia et al., 2011a), and ALKBH5 (leading to the understanding that this RNA modification is reversible.

The growing interest in the biological role of this modification led to the development of new transcriptome-wide isolating and sequencing techniques, that were able to discriminate the pool of methylated RNAs between the total mRNAs, and also where the modification was precisely located along the transcripts. The first technique to be published, MeRIP-seq, combined an RNA-immunoprecipitation approach carried out with a specific m6A-antibody towards randomly fragmented transcripts, with next-generation sequencing (Dominissini et al., 2012).

This led also to the identification of the consensus sequence in which the modification is set, PuPuACX (Pu = purine; X = A, C, or U) after following clustering of all enriched motifs, and mostly importantly to the identification of all the transcriptome-wide m6A enriched locations on mRNAs, which are mostly near stop codons or in 3'UTRs (Meyer et al., 2012). Due to technical limitations with MeRIP-seq it is not possible to detect m6A residues at a single nucleotide resolution, so to overcome this it was developed another sequencing method called miCLIP, capable of recognising single m6A residues, thanks to crosslinking with m6A antibodies that create a specific mutation signature after crosslinking (Linder et al., 2015). Using an RNA affinity chromatography approach that used methylated and control versions of an RNA bait followed by mass spectrometry, it has been possible to find three proteins associated with m6A, two YTH (YT521-B homology) domain-containing proteins,YTHDF2 and YTHDF3, that were acting as "readers" of the modification.

Also two additional proteins, WTAP and METTL14, were identified as required for methylation (Jianzhao Liu et al., 2014a; Schwartz et al., 2014) and this raised the question

whether methylation is a regulated and selective process, in which different mRNAs could be differentially methylated, meaning that there must be a fining tuning to it. Proteomic analysis helped discover that these three proteins, METTL3, METTL14 and WTAP coevolved together and form a multi-complex that is required for the methylation of target RNAs. It was also possible to understand that some mRNAs were methylated in a WTAP dependent way, while others were methylated even after the complete silencing of the protein, leading the RNAs to different fates.

Other than the “writers” proteins, also protein acting as “erasers” were discovered. The first to be discovered was FTO (fat mass and obesity-associated protein) a protein belonging to the AlkB family of non-heme FeII/ α-ketoglutarate (α-KG)-dependent dioxygenase, already knew as being associated to obesity in GWAS studies (Jia et al., 2011a). FTO has single stranded RNAs as a substrate, and m6A-containing RNAs in particular. Its demethylation process has been found to be dependent on its oxidative activity. Not many years after, also another demethylase was discovered, ALKBH5, who belong to the same family of proteins as FTO, and was found to co-localize with nuclear speckles and to be involved in the regulation of mRNAs export from nucleus (Zheng et al., 2013). As I already mentioned, also another class of proteins was found to interact with m6A-modified RNAs, the YTH domain family of proteins, that comprehend four cytoplasmic proteins (YTHDF1-3; YTHDC2) and a nuclear one (YTHDC1).

1.3 m6A writers, erasers and readers

1.3.1 Methyltransferases

As already discussed in the beginning, m6A methyltransferases are a special class of enzymes that uses SAM (S-Adenosyl-Methionine) as a catalytic substrate for the methylation of target RNAs. Methyltransferases like 3/14 (METTL3/14), Wilm’s Tumor1 Associating Protein (WTAP), KIAA1429 and RNA binding motifs protein 15/15B (RBM15/15B) are all m6A methyltransferases that associate together and work as a complex. METTL3 was first identified in 1997 (Bokar et al., 1997) as the catalytic subunit of a bigger methyltransferase complex, and later was observed that its knockdown caused

apoptosis in HeLa cells (69). METTL14 was discovered years after, firstly recognized as a homolog of METTL3, with which shares the 43% of homology (Bujnicki et al., 2002). METTL14 does not transfer the methyl group on RNA on its own, because it lacks a functional SAM binding pocket, while METTL3 has its own catalytic ability, and can function independently from METTL14, even if it's been demonstrated that the two protein associate within each other in 1:1 ratio, forming a complex that is more efficient than METTL3 alone ((Jianzhao Liu et al., 2014b);(Xiang Wang et al., 2017). This means that METTL14 has a role in guiding the complex to the substrate RNAs. WTAP, on the other hand, does not have a catalytic activity but binds to the complex formed by METTL3 and METTL14 guiding it to nuclear speckles enriched with pre-mRNA to process and decorate with the methylation, and it's been observed that upon its knockdown the activity of the methylation complex is seriously impaired (Ping et al., 2014). METTL3 and WTAP are also involved in alternative splicing of target mRNAs involved in transcription and RNA processing. Vir-like m6A methyltransferase associated (VIRMA), KIAA1429, is a large protein, with nearly 200kDa of molecular weight, homologous protein of the Virilizer protein in Drosophila, that is been found to catalyze the recruitment of the METTL3/METTL14/WTAP preferentially to 3'UTR and near the stop codon (Yue et al., 2018), acting as a scaffold of the complex itself.

The proteins RBM15 and its paralog RBM15B have been recently discovered to be also part of the methylation complex, interacting with METTL3 in a WTAP dependent manner (Patil et al., 2016). Upon their knockdown it was observed a reduction of the m6A level, meaning that these proteins are necessary for the methylation machinery. iCLIP also showed that RBM15 and RBM15B bind to Uridine reach regions that are close to the m6A consensus sequence, probably recruiting the rest of the methylation complex from that binding site. For sure, an important role played by RBM15 and RBM15B has been observed in the methylation of XIST, the long non-coding RNA responsible for the chromosome X silencing during development (Patil et al., 2016).

Another auxiliary protein of the methyltransferase complex in Drosophila and mice is Zc3h13/FLACC (Knuckles et al., 2018). Lack of their expression cause in both organisms a dramatic reduction of the m6A levels, while in Drosophila loss of FLACC causes an aberrant splicing of the Sex Lethal (Sxl) gene. FLACC has been observed to act as an adaptor between the Drosophila WTAP homolog Fl(2)d and the RBM15 homolog

Nito, with the aim of stabilizing the complex and help the deposition of the m6A modification.

Also, the methyltransferase METTL16 has been lately added at the methylation machinery as a m6A forming enzyme, at least on one gene (Pendleton et al. 2017), MAT2A (methionine adenosyltransferase 2A), the principal SAM forming enzyme present in cells. This gene undergoes a splicing event thanks to the presence of a methylated hairpin loop that resembles the one present on the U6 RNA. The methylation upon the hairpin is fundamental for the splicing to occur, and since METTL3 failed to methylate this region alone, METTL16 was investigated and found to be responsible for this methylation, since its homolog in yeast methylates the structurally similar U6 RNA. For the moment, MAT2A is the only known gene to be methylated by METTL16, so further investigations are needed to better understand the role of this methyltransferase, focusing mostly on SAM metabolism where it could be more needed.

1.3.2 Demethylases

FTO is the first demethylase to be discovered (Jia et al., 2011b). It belongs to the ALK family of demethylases, a subfamily of Fe^{II}/α-ketoglutarate-dependent dioxygenases, that is composed of eight other members (ALKBH1-8) that oxidate different substrates. FTO reversely oxidates m6A in adenosine and is mainly set in the nucleus and partly in nuclear speckles, suggesting that the demethylation happens in concert with the deposition of the methylation upon target mRNAs. As its name suggests, FTO (Fat mass and obesity associated protein) is involved in adipogenesis, and in particular, it has been observed that the level of methylation and FTO expression are inversely correlated during that process (Zhao et al., 2014). FTO regulates the level of m6A methylation near splice sites, that in the absence of FTO enhance the RNA-binding capacity of SRSF2 protein, thus increasing the inclusion of exonic regions that are normally spliced. In this way FTO regulates the splicing of the adipogenic factor RUNX1T1, inducing the differentiation of preadipocytes. Levels of expression of FTO change during the different stages of adipogenesis, decreasing almost totally after the differentiation is complete in mature adipocytes (Zhao et al., 2014).

Recently the specificity of FTO towards m6A has been put in discussion after the MeRIPseq analysis on a mice FTO knockout model, which highlighted that the general level of m6A was not increased apart in a small subset of peaks located mostly at the 5'UTR of mRNAs (Mauer et al., 2017). Since the 5'UTR is the location at which is commonly located the m6Am modification too, has been suggested that FTO could be m6Am demethylase.

In the same work, it was also observed that FTO, when located near the m7G cap at the 5'UTR, has a catalytic activity towards m6Am that is one hundred-fold higher with respect to m6A. Since there are not so many evidences that FTO is exclusively a m6Am eraser, at least not from other working groups, FTO still is generally and wide accepted as a m6A eraser that possibly has also a good catalytic activity towards m6Am.

With totally different biological functions, ALKBH5 was discovered a while after FTO as a m6A demethylase (Zheng et al., 2013), with a catalytic activity comparable to the one described for FTO, and found also to be localized in nuclear speckles. It was found to be involved in mRNA metabolism and export since it colocalizes with SFRSF2, a splicing factor but also an adaptor for mRNAs export when hyperphosphorylated, and after its depletion also the phosphorylation level of SFRSF2 decreased. its knockout in mice affects male fertility, as ALKBH5 has high levels of expression in testis. This was also confirmed by another study (Iwanami & Brown, 1968), in which the molecular action of ALKBH5 depletion in mice testis was further analyzed. ALKBH5 expression during late meiosis and the haploid phase in spermatocytes is fundamental to abrogate m6A methylation around splice sites, and so to permit the genesis of longer transcripts, that will not be randomly spliced and fast degraded. So ALKBH5 is fundamental for the early stages of spermatogenesis, to fine tune the metabolism of target transcripts that are involved in that process. It has no demethylase activity towards m6Am.

1.3.3 Readers of m6A

The YTH domain family of proteins

The YTH domain was first identified in 2002 (Stoilov et al., 2002) inside the already known human splicing factor YT521-B, that was discovered in 1998 in a two-hybrid screening for

proteins interacting with the RNA binding protein RA301 (Imai et al., 1998). The domain turned out to be the only conserved region in a series of proteins homologous to YT521-B, and alignments of this region alone lead to the discovery of a series of uncharacterized proteins belonging exclusively to eukaryotic genomes, and most abundantly to plants. This portion of around 100-150 amino acids, with 14 invariants and 19 highly conserved residues, was so termed YT homology domain (YTH), and was the only sequence to be shared between all this unknown proteins, apart from the ones closely related to YT521-B. Analysis of the predicted structure lead to the identification of conserved aromatic residues inside the β-sheet, a characteristic typical of RNA Recognition Motifs (RRM), suggesting that the role of this domain was to bind RNA. Until 2010, no attention was put on investigating more on the members of the YTH domain family of proteins, apart for some works on the nuclear yeast RNA binding protein Mmi1 (meiotic mRNA interception) that was found to be a part of a yeast mRNA-destruction system that eliminates meiotic specific mRNAs; in fact, in that year a paper was published (Z. Zhang et al., 2010) that finally recognized the YTH domain as RNA-binding domain, also identifying a highly degenerate recognized sequence, GCAUAC, and generating a NMR structure of the domain that revealed an high presence of positively charged amino acid residues. There were also identified three residues that resulted to be fundamental for the RNA binding ability of the domain and modulating selection of the splice site, Trp-380, Phe-412, and Gly-414, all belonging to the hydrophobic core.

Two eukaryotic YTH-containing proteins were then associated to methylated RNAs in a RNA affinity chromatography experiment (Dominissini et al., 2012), so these findings revealed that the function of these proteins was to bind the modification inside the consensus sequence G(m6A)C and to guide directly or indirectly the fate of their target RNAs. In the vertebrates, the YTH domain carrying proteins were also divided on the basis of their subcellular distribution in YTHDF (YTH Domain Family) and YTHDC (YTH Domain Containing), with three proteins belonging to the first group (YTHDF1-3) located in the cytoplasm, and two proteins of the second group located one in the nucleus (YTHDC1) and the other in the cytoplasm as the YTHDFs (YTHDC2).

The way the YTH domain interacts with the m6A modification was then deeply studied. The first crystal structure of the domain was obtained from the yeast YTH domain

containing protein MRB1 (Luo & Tong, 2014), that was also found to be able to recognize the m6A modification (Schwartz et al., 2013). MRB1, also known as Phob2(Kang et al., 2014), bounds the m6A modification through a hydrophobic pocket that forms an aromatic cage in which the methylation is sandwiched between two Trp residues, and perpendicular to a third one, and has a hydrogen bond with a Tyr residue. Other studies reported the structural basis of interaction between the YTH domain of the DF and the DC types from yeast and animal proteins and the m6A modification; showing that the methylation is lying inside a hydrophobic pocket (Theler et al., 2014; Xu et al., 2014, 2015). It was also reported that the YTH domain is also able to bind GA-containing RNA, with a 50 fold difference in binding affinity with respect to m6A-containing ones ((Theler et al., 2014), even if another work stated that the YTHDC1 YTH domain has a preferential recognition for the GG-m6A sequence, and that is the only domain to show a selective binding modality to the nucleotide proceeding the m6A (Xu et al., 2015). Crystal structures of YTHDF1 (aa residues 365-554, PDB entry 4RCJ) were obtained both as a complex with a 5-mer RNA, GG(m6A)CU, and as an apo structure (aa residues 361-559, PDB entry 4RCI) (Xu et al., 2015), and these structures were superimposed to the crystal structure of the YTH domain of YTHDC1 to understand the different sequence selectivity of the two toward the nucleotide proceeding the modification. It turned out that the two proteins use different binding pockets to bind the modification, and that other residues outside of the tryptophan cage in the YTHDC1 YTH domain are involved and conserved, for example a Met and a Leu residue that does not have any role in binding nucleotides of the sequence in the YTHDF1 protein. This differential ways of recognizing the consensus sequence could be the only explanation for the different roles of the members of this family of proteins, which is still not fully understood. YTHDF1 and YTHDF2 share the 87% of similarity, they bound the consensus sequence with no nucleotide selectivity at the -1, but they have opposite roles in regulating the fate of the target mRNAs they bind.

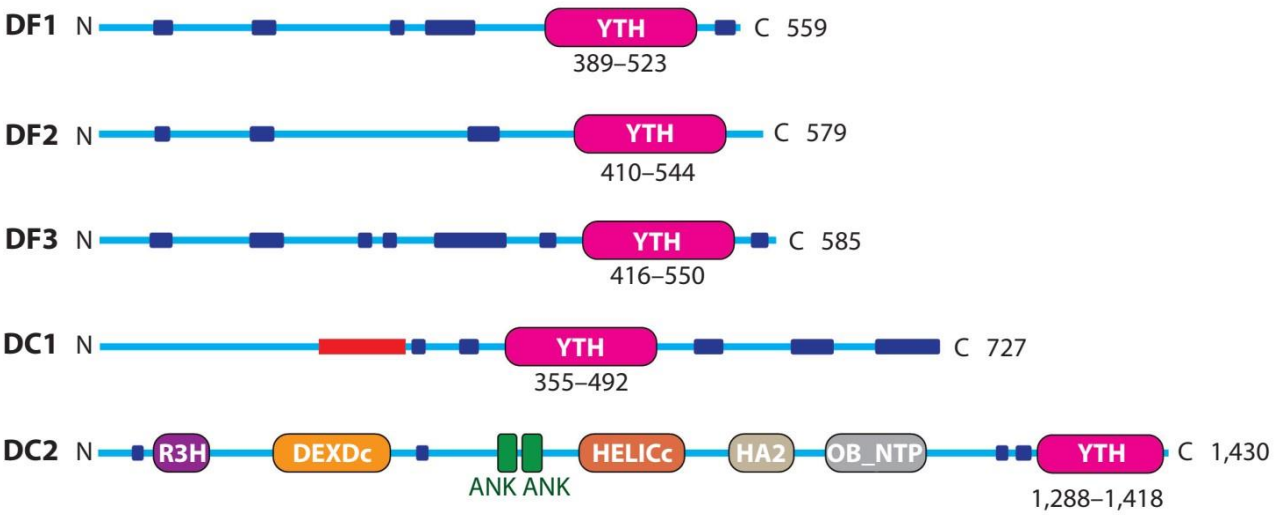

Fig.2. Schematic representation of the five human YTH proteins. The YTH domain in magenta is located at the C-terminal of the protein, apart from YTHDC1 in which the structure is organized in a different way and the domain is in the center of the protein, not far from the Glu-rich region in red. YTHDC2 is the biggest and most complex protein of the family, with a R3H domain, a DEAD-BOX domain flanked by two Ankirin repeats from the Helicase domain, an HA2 domain and a oligonucleotide binding domain (OB). In blue are the low complexity regions. Adapted from Jaffrey and Meyer, 2017

YTHDF2 has been characterized as deputed to the degradation of mRNAs in a methylation-dependent manner (Xiao Wang et al., 2014). More than 3000 targets were identified in HeLa cells through RIP-seq experiments, while with photoactivatable ribonucleoside crosslinking and immunoprecipitation (PAR-CLIP), were identified the locations of the binding sites on the mRNAs, confirming that are mostly located on 3'UTR, inside stop codons or CDS, though suggesting a role in translational regulation of the YTHDF2 protein. With ribosome profiling and RNA lifetime profiling with Actinomycin D it was possible to observe that the increased binding of YTHDF2 on its target transcripts correlates with reduced mRNA lifetime and that there is an increase of input mRNA and an increase of mRNA lifetime in the YTHDF2 KO samples. This is because YTHDF2 increases the number of mRNAs in the non-ribosome mRNPs from the translatable pool (Fig.3). YTHDF2 was also found to localize with three markers of the processing bodies, DCP1a, GW182 and DDX6, that are located in the cytoplasm, and responsible for this localization is N-terminal part of the protein, containing a P/Q/N rich region, while the C-terminal part containing the YTH domain is responsible for RNA binding. Later it was also demonstrated that the degradation process of m6A containing mRNAs is guided by a

YTHDF2-dependent recruitment of the CCR4-NOT deadenylation complex, through the interaction of the N-terminal of the protein with the SH domain of CNOT1 (Du et al., 2016). Has also been observed that, upon heat shock, YTHDF2 localize in the nucleus, with a consequent increase of m6A decoration upon the 5' UTR of stress inducible mRNAs, and an increase in their ribosomal occupancy (J. Zhou et al., 2015). This could be due to the direct recruitment of the translation initiation factor complex 3, eIF3, upon m6A sites on the 5'UTR (Meyer et al., 2015).

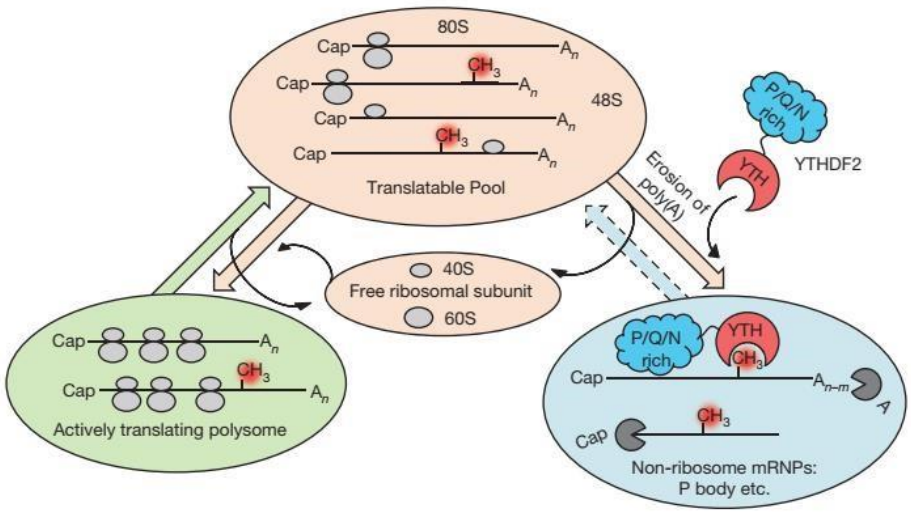

Fig.3. Degradation of target mRNA by YTHDF2. In the cytoplasm, mRNA is divided in three different pool depending on its translational state. It could derive from the translatable pool, in which are present all the mRNA ready for translation, it could be associated with polysome and actively translated, or associated to non-ribosome mRNP and send to degradation in P-bodies. YTHDF2 enhances the number of mRNA send to decay deriving from the translatable pool. From Wang et al, 2014.

On the other hand, YTHDF1 has been observed to enhance the translation of its target mRNAs (Xiao Wang et al., 2015) in a way that is different from the one described for the stress induced mRNAs, with the direct recruitment of eIF3 independently from YTHDF1. Similarly to YTHDF2, the binding sites of the protein on methylated RNAs were identified with PAR-CLIP experiments, and target transcripts with RIP-seq, leading to the discovery of more than 1000 high-confident targets of YTHDF1 deriving from the shared mRNAs between CLIP and IP. With ribosome profiling it was then observed that YTHDF1 increases the occupancy on ribosomes of its mRNA targets, regulating their subcellular localization from the non-translatable fractions to the translatable ones. The role of

YTHDF1 in regulating the translation of modified mRNAs was also confirmed by the characterization of its interactome, mostly composed of translation initiation factors, such as eIF3, ribosomal subunits but also markers of stress granuli. The translation of m6Acontaining mRNAs regulated by YTHDF1 happens on a small number of transcripts, depending on the cellular context and the physiological conditions.YTHDF3, the third YTH domain-containing mammal protein located in the cytoplasm, has also been observed to be involved in the translational regulation of m6A containing mRNAs (H. Shi et al., 2018). As for the other two cytoplasmic proteins, the localization of the binding sites and the mRNA targets were identified in HeLa cells and was found that 58% of YTHDF3 targets are also recognized by YTHDF1, and 60% by YTHDF2. YTHDF3 was found to enhance translation as YTHDF1, probably working in tandem with it on their shared targets. Differently from YTHDF1, YTHDF3 does not recruit translation initiator factors, but its depletion has been observed to cause a decrease in the number of target transcripts bound by both YTHDF1 and YTHDF2, and an increase in binding of the non-targets. This could mean that the functions of the three proteins are interconnected in the cytoplasm, and that the RNA exported from the nucleus is distributed between the different proteins and ends bound by YTHDF2 to be degraded. Differently from the other two cytoplasmic proteins, YTHDF3 can be relocated in stress granuli upon oxidative stress, were it recognizes stress-induced mRNAs helping relocated them in the stress granuli from the translatable pool (Anders et al., 2018).

The cytoplasmic YTHDF proteins do also recognize m6A marks upon viral RNA, and some works focused their attention on the mechanisms of infection of different virus related to m6A modification and YTHDFs regulation (Gokhale et al., 2016; Kennedy et al., 2016; Krug et al., 1976). For example, has been demonstrated that the recognition of YTHDF1 of the viral genome of the Zika virus blocks its reverse transcription (Lichinchi et al., 2016). Some papers have also focus on the role of YTHDF1-3 in HIV-1 infection, with different results (Kennedy et al., 2016; Tirumuru et al., 2016). In (Tirumuru et al., 2016), it was shown that YTHDF1-3 binding to HIV-1 RNA inhibit HIV-1 infection in cell lines and primary CD4+ T-cells, mostly by decreasing its reverse transcription, and decreasing the levels of the GAG protein. In (Kennedy et al., 2016) instead, found that the increased m6A decoration on 3’UTR of HIV-1 mRNAs enhances the recruitment of YTHDF1 and consequently their translation, while the knockdown of YTHDF1 blocks the reverse

transcription of the mRNA of the virus. In conclusion, for what concerns the role of the YTH domain cytoplasmic readers in the regulation of viral infection, and in HIV-1 infection in particular, there are still many questions to answer.

A recently published review (Zaccara et al.,2020) proposes for the first time a different model explaining the function of the YTHDFs, suggesting that they function redundantly in promoting mRNA degradation, while according to them there is no strong evidence of a role in translational regulation of gene expression. The YTHDFs also shares the same RNA binding properties, with no significant difference in the amino acids involved in RNA binding inside the hydrophobic pocket; other than this, also a more accurate transcriptome wide analysis of the i-CLIP data published by the same group (Patil et al.,2016) lead to the conclusion that all the paralogs recognize with the same frequency the same m6a containing sequence, without showing a preference to a certain submotif. They also concluded that there are no m6A sites uniquely bound by a certain paralog, analyzing again i-CLIP data performed on HEK 293T (Patil et al.,2016) and PAR-CLIP data performed on HeLa cells (Wang et al.,2015). These discoveries have put in discussion the differential roles predicted for the different paralog in regulating translation and degradation of mRNAs, since there is no unique paralog recognition of m6A containing sites on the transcriptome. They hypothesize that their differential roles could be driven by the differential protein network established by their effector domains, that resulted to share 70% sequence similarity and the same distribution of the disordered regions. A more accurate analysis of a Bio-ID proteomic analysis showed that the three paralogs share almost the same protein networks and that eIF3A and eIF3B are weak binders of YTHDF1, suggesting that there is no strong evidence of a regulation of translational initiation role, while all the three paralogs appeared to share strong interaction with the RNA degradation CCR4-NOT complex. They also knocked down all the three paralogs simultaneously, obtaining that there is a substantially higher increase of m6A-containing mRNAs expression, that was also visible knocking down any combination of two paralogs compared to the effect observed upon YTHDF2 knockdown alone. In contrast with previous findings (Wang et al.,2015), they concluded that the fact that none of the three paralog is found in the highly translatable mRNA pool, and all of them is excluded from the polysome fraction, while enriched in the cytoplasmic mRNPs, meaning that there is no consistency in associating the DFs with translational regulation and stable 3’UTR binding.

In conclusion, this new study rediscusses again all that has been said about the biological role of the YTHDFs, proposing that they do not bind unique m6A sites, that there are no paralog uniquely bound sets of mRNAs, that they act redundantly in mRNAs degradation, with no consistent involvement in the translational regulation.

The YTHDC proteins do not share similarities with the YTHDF proteins apart from the YTH domain and have a completely different role in the nucleus. The YTH domain of YTHDC1 is the only predicted folded portion of the protein which is surrounded by charged residues, such as Glu-rich, Arg-rich and Arg-Asp-Glu-rich, P-rich and RED segments. YTHDC1 has been reported to bind to modified pre-mRNA regulating their splicing and their affinity to splicing factors (Xiao et al., 2016). It has been observed with PAR-CLIP analysis coupled with RNA-seq that YTHDC1 recruits on mRNA the splicing factor SRSF3, enhancing exon inclusion, while antagonizes the SRSF10 splicing factor that instead is involved in exon skipping. YTHDC1 also mediates the nuclear export of target m6A-containing RNAs by interacting with SRSF3 (Roundtree et al., 2017) and collaborating with NXF1, in fact upon its depletion the m6A/A ratio in the nucleus increases and there is a consequent depletion of transcripts in the cytoplasm. Together with SRSF3, YTHDC1 is responsible of the alternative polyadenylation of modified pre-mRNAs during murine oocyte development guiding them to the pre-mRNA 3' processing factors CPSF6, but is indispensable for their growth, as its depletion caused embryonic lethality (Kasowitz et al., 2018). In *Drosophila Melanogaster* the ortholog of YTHDC1, YT521-B, is involved in the alternative splicing of the Sex Lethal (Sxl) gene, which is fundamental in sex determination and compensation during fruit fly development (Lence et al., 2016). The gene is present in both males and females, but in males it has an additional exon that cause the formation of a premature stop codon and consequently the production of a truncated and nonfunctional protein. YT521-B binds to intronic m6A-containing sites and represses the inclusion of the male specific exon. Its ablation phenocopies flies lacking Ime4, which is the Drosophila ortholog of METTL3, that are completely missing m6A modification upon their mRNAs. These flies are anyway viable, but unable to fly and with a sex bias toward maleness for the impossibility to cause the m6A-regulated alternative splicing of Sxl. (Haussmann et al., 2016).

YTHDC1 is also required for the regulation of the long non-coding RNA XIST, found to be highly methylated with at least 78 m6A sites (Patil et al., 2016), that is involved in X-linked gene silencing during development of female mammalians. Silencing of METTL3 alters the methylation pattern of XIST and consequently its regulation, but this can be restored by tethering YTHDC1 to the methylation depleted cells.

YTHDC2 has been reported to be located mostly in the cytoplasm (Hsu et al., 2017) and to be the most different and largest protein of the family, with 160kDA of molecular weight. It is also characterized by the presence of different domains that are separated by Ankyrin repeats, respectively a N-terminal arginine-histidine-rich domain (R3H), a helicase associated 2 domain (HA2), an OB-fold (oligonucleotide / oligosaccharide-binding fold) and a DEAH-box helicase domain. This peculiar structure suggest that this protein could interact with a wide range of proteins, like the cytoplasmic 5′–3′ exoribonuclease XRN1 through the ankyrin repeats (Kretschmer et al., 2018; Wojtas et al., 2017), suggesting a putative role in the regulation of mRNAs turnover, and that the presence of the helicase domains could be involved in the regulation of the RNA secondary structure and in its binding. This hypothesis has been indeed validated by the observation that YTHDC2 is involved in the regulation of translation efficiency and stability of targets involved in mouse spermatogenesis, as upon its knockout male and female mice developed reduced testes and ovaries, resulting infertile, and that it has an RNA-induced ATPase activity, translocating on RNAs in a 3'-5' direction (Wojtas et al., 2017). Another work (Mao et al., 2019) pointed out the importance of YTHDC2 in enhancing translation efficiency of m6Acontaining mRNAs, through the interaction with the head of the 40S ribosomal subunit, in particular at the level of mRNA entry and exit sites, maybe explaining the double and opposite role that the protein plays in the regulation of mRNAs fate. As observed after its knockdown, the level of protein synthesis decreased of nearly the 40%, more than what was obtained upon silencing of the three cytoplasmic proteins. Its role in enhancing translation was previously observed in colon cancer cells, in which YTHDC2 enhances transcription of metastasis related gene HIFa (Tanabe et al., 2016) by unwinding the 5' UTR untranslated region.

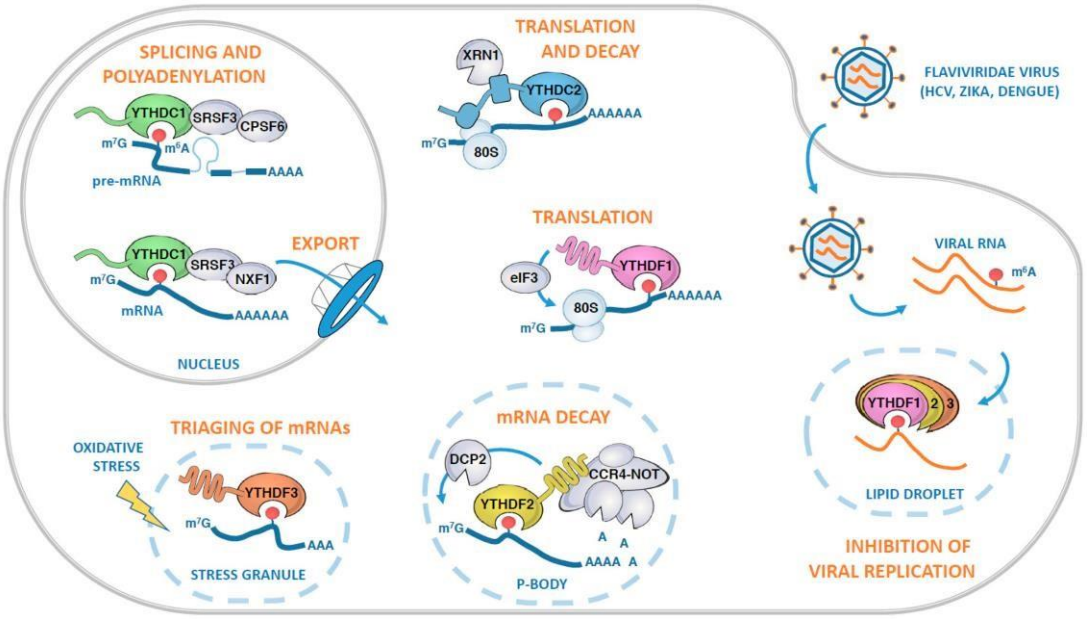

Fig.4. Main model of the different roles of YTH domain family of proteins. In nucleus, YTHDC1 regulates mRNA splicing, polyadenylation and nuclear export, while the others in the cytoplasm have different roles regarding mRNA translation and decay, and last but not least regarding viral infection. Adapted from Hazra et al, 2019.

Other readers

As previously reported, also eIF3 can be considered a sort of m6A reader, for its direct binding to the m6A modification on target mRNAs in response to stress condition. mRNA bearing the m6A modification are capable of directly recruiting eIF3 for translation initiation without needing the initiation translation complex formed by eIF4 proteins, and in particular eiF4E, which is often impaired in stress or in disease state conditions (Meyer et al., 2015; J. Zhou et al., 2015).To be more precise, eIF3 is linked to two different ways of translating m6A containing mRNAs. In the first, it is directly recruited on the 5'UTR of stress associated methylated RNAs (J. Zhou et al., 2015), while in the second this recruitment happens indirectly through the interaction with YTHDF1 (Meyer et al., 2015).

A protein belonging to the family of heterogeneous ribonucleoproteins (hnRNPs), HNRNPA2B1, was proposed and further identified as binding to m6A-bearing RNAs (Alarcón et al., 2015), both *in vitro* and *in vivo,* even without a YTH domain. It was found to bind a subset of transcripts in the nucleus and to regulate their alternative splicing, with a particular focus on pri-miRNA processing, interacting with the pri-miRNA microprocessor

complex protein DGCR8. The binding mode of HNRNPA2B1 is still not clear, but it was reported that the specificity was probably mediated by one of the RRM domains, in particular the RRM1. Another study (K. I. Zhou & Pan, 2018) pointed out that HNRNPA2B1 is not a specific m6A reader, but it could be that it binds to sequences that are close to m6A containing sites, for it was found to recognize UAG and UUAGGG motifs, so it could be easily mistaken as one. Still, this does not mean that is to exclude some sort of indirect interaction that control the regulation of m6A-containing RNAs, so this still needs further investigation.

Lately, other proteins have been reported to be m6A readers: the insulin growth factor 2 mRNA binding proteins 1, 2 and 3 (IGF2BP1–3) (K. I. Zhou & Pan, 2018). These group of proteins was isolate after a pull-down experiment using an RNA methylated probe as bait and were found to play a role in the stabilization of their target transcripts. To further understand the mechanism by which IGF2BP1-3 stabilize their targets, the proteins interacting with them were characterized after co-immunoprecipitation. Between these was found the Human Antigen R protein (HuR), also co-localizing with them in P-bodies, suggesting that there could be a sharing of targets between HuR and the IGF2BPs. IGF2BPs were also found enriched in polysome fractions, with IGF2BP1 recruiting its mRNA target C-MYC to active translation.

After the identification of other proteins acting as m6A readers, it was felt the need to divide them in two class based on RNA-binding modes. The first class is composed of all the proteins that contain a YTH domain, and in which the recognition of the consensus sequence happens through an aromatic cage. The second class is composed of the proteins that does not contain a YTH domain, some of which belong to the family of heterogeneous nuclear proteins. In the case of the IGF2BPs, the mechanism of binding differs from the other two, because they do not bear a YTH domain but they have two RNA recognition motifs (RRMs) and four KH domains, which are commonly present in other RBPs. It was reported that the KH domains mediated the specific recognition of the m6A modification in this family of proteins, in particular through the third and the fourth KH domains, with the regions flanking the domains probably playing an additional role in the binding specificity, even if this still lack a complete explanation.

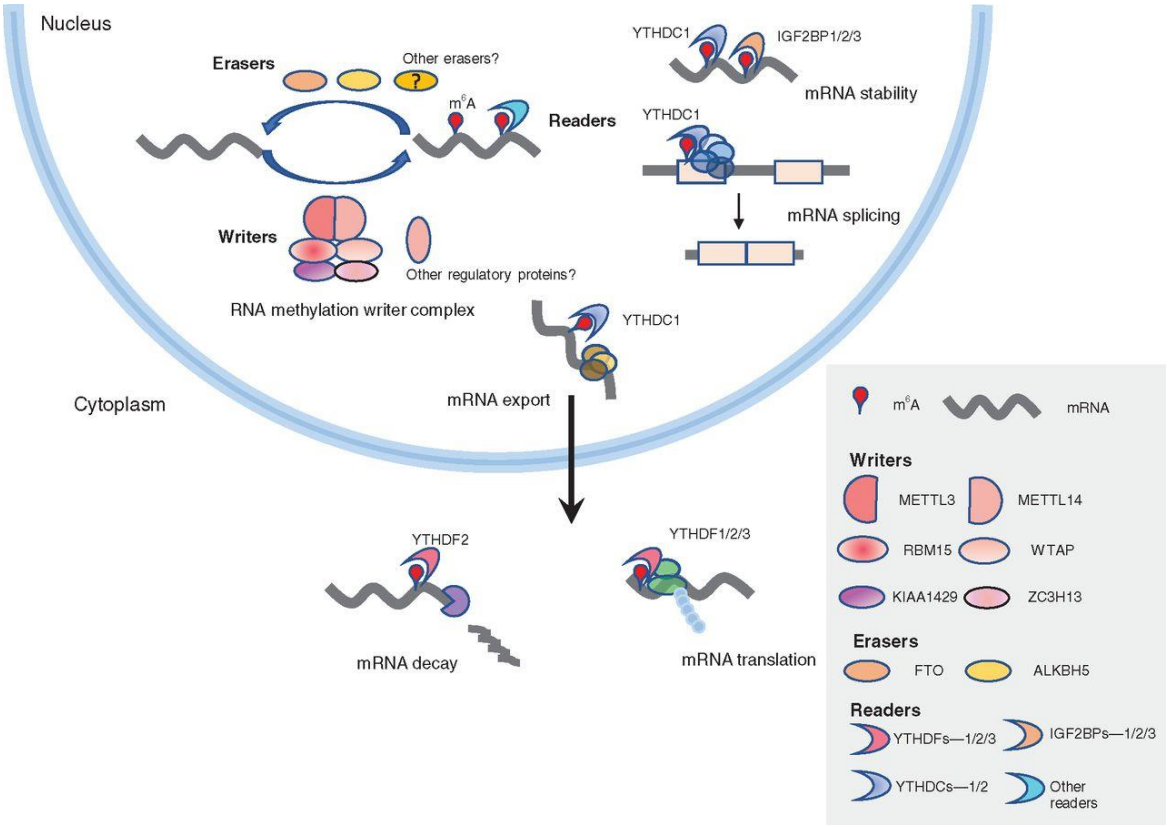

Fig.5. The methylation machinery. METTL3, METTL14 and WTAP form a complex that serves as a "writer" of the m6A methylation upon target sites, with the help of also VIRMA, RBM15, KIAA1429 and the Zinc Finger protein ZC3H13. FTO and ALKBH5 works as "erasers" of the methylation mark, while the YTH domain family of proteins, the newly discovered IGF2BP1-3 and in the same cases also METTL3 and the elongation factor eiF3, act as "readers" and guide the RNAs to different fates inside the cells. From (Vu et al., 2019)

1.4 Role of m6A in development and disease

As we already stated, the biological roles of m6A in the regulation of RNA metabolism are multiples, starting from mRNA processing, export, translation and biogenesis of miRNA and lncRNA. These multiple facets influence consequently other biological processes such as stem cell renewal, adipogenesis, spermatogenesis, development and carcinogenesis (Yamei Niu et al., 2013). For our purposes we will mostly focus on the role of m6A in the latest. Depending on the type of cancer, the effect of the m6A modification could be different, so for this reason we will report a series of examples to elucidate the mechanisms that are affected in different tumors.

1.4.1 Cancer

Acute Myeloid Leukemia

In AML (Acute Myeloid Leukemia) patient cells have been observed that the methyltransferase METTL3 is overexpressed (Vu et al., 2017) and plays an oncogenic role by increasing the translation of c-MYC, BCL2 and PTEN, thus enhancing cell proliferation and inhibiting apoptosis. Independently of METTL14, METTL3 bounds to the promoter of active genes through the interaction with the CAAT-box binding protein CEBPZ, inducing the establishment of the m6A modification on the associated mRNA transcripts and enhancing their translation (Barbieri et al., 2017).METTL14 is also involved in leukemia development by stabilizing the MYB and MYC RNA, while negatively regulated by the SP1I protein (Weng et al., 2018). YTHDF2 has been also observed as playing an important role in the pathogenesis of AML (Paris J et al, 2019).

High levels of YTHDF2 were found in patient samples, and in the samples with Leukemic Stem Cells (LSCs) activity in particular. YTHDF2 depletion in hematopoietic and progenitors stem cells (HSPCs) resulted in altered LSC activity and propagation, with inability to propagate AML after transplantation in mice. On the contrary, YTHDF2 conditional ablation in adult mice failed to generate aggressive tumors and increased the animals overall survival rate, and also did not derail normal hematopoiesis, indeed it cause an increase in the number of progenitors enhancing also their differentiation rate, and at the same time increasing the numbers of LSCs. Analysis of the transcriptome of the YTHDF2 KO lines revealed that the ablation of the protein cause the downregulation and the upregulation of a certain number of target genes, and in particular the upregulated ones resulted also to be more m6A-decorated and with increased half-lives compared to the control sample, while there was no difference in Translational Efficiency (TE) between the two genotypes. A further analysis of the upregulated genes led to the discovery that they were mostly negatively correlated with YTHDF2 expression and related to loss of leukemogenic potential.

YTHDF2 when normally expressed, caused the degradation of mRNAs encoding for genes that limit LSCs activity, such as TNFRSF2, a necrosis factor that showed to have increased half-life upon YTHDF2 KO and caused the increased sensitivity of LSCs to TNF induced apoptosis. To conclude, although YTHDF2 ablation in adult mice is permissive, targeting YTHDF2 in AML would cause a decrease of LSCs activity but at the same time

the expansion of the HSPCs, that normally are difficult to isolate for transplantation means. This makes YTHDF2 an interesting target for AML therapy.

Glioblastoma

In glioblastoma, the knockdown of METTL3 and METTL14 cause an upregulation of oncogenes such as ADAM19, EPHA3, and KLF4 (Cui et al., 2017), and this is also supported by the observation that ALKBH5 expression correlates with poor prognosis in glioblastoma patients, and that it has an high level of expression mainly in GSC (Glioblastoma Stem Cells), suggesting a role in the maintenance of their self-renewal capability (S. Zhang et al., 2017). In particular, it was found that ALKBH5 regulates the expression of FOXM1, which is a transcription factor involved in cell cycle regulation and in the regulation of stem cell renewal and tumorigenesis in GSC. On the contrary, in a latter study it was observed that the overexpression of METTL3 is a marker of poor patient survival, and that its silencing can cause the depletion of SOX2 mRNA and consequently the inhibition of tumor growth and loss of resistance to γ-irradiation *in vitro* (Visvanathan et al., 2018).

Hepatocellular Carcinoma

In Hepatocellular carcinoma (HCC), which is the main type of liver cancer, the knockdown of METTL3 cause a drastic reduction in tumorigenicity of HCC cells and lung metastasis (M. Chen et al., 2018). METTL3 was found to bind the mRNA of SOCS2 (suppressor of cytokine signaling 2) and upon its knockdown the methylation of SOCS2 was reduced and its expression increased, because YTHDF2 was found to be responsible of its degradation. At the same time, also METTL14 has a role in the development of HCC, as observed in (Ma et al., 2017), but in contrast with METTL3, its downregulation cause the enhancement of the metastatic potential of HCC cells, because normally it would regulate the maturation of the tumor suppressor miRNA-126 in a m6A-dependent manner, so blocking tumor metastasis. YTHDF2 is also negatively regulated by a miRNA in HCC, miRNA-145, that binds to its 3'UTR blocking its translation. In HCC patient tissues was observed that the level of expression of miRNA-145 were reduced, causing the overexpression of YTHDF2(Yang et al., 2017) and a decrease in the methylation levels. On the contrary, in a more recent article, YTHDF2 was reported to be downregulated by hypoxia in HCC, while

its overexpression cause a decrease in cell proliferation(Zhong et al., 2019) and of MEK and ERK activation by direct binding to the 3'UTR of EGFR mRNA, a gene upstream of the ERK/MAPK signaling, destabilizing it. Silencing of YTHDF2 in HCC cells was also reported to promote tumor growth, vascular remodeling and metastasis under hypoxic conditions (Hou et al., 2019). RNA-seq lead to the discovery of a series of upregulated transcripts related to cancer inflammation, and the consequent selection of targets increased both upon YTHDF2 knockdown and hypermethylated upon hypoxic conditions to the cancer-promoting inflammation related targets IL11 and SERPINE2. YTHDF2 process their mRNAs to decay in normal conditions, in fact both genes were overexpressed in YTHDF2-deficient cells.

Breast Cancer

Hypoxia plays a pivotal role also in the development of breast cancer, another very common solid tumor. For what concerns the epitranscriptome factors, hypoxia increase the levels of ALKBH5 in breast cancer cells, decreasing the methylation levels and increasing the stabilization of NANOG mRNA, thus inducing a stem cell phenotype (C. Zhang, Samanta, et al., 2016). The same outcome was observed in another paper (C. Zhang, Zhi, et al., 2016), in which HIF-induced protein ZNF217 decreased the m6A decoration on NANOG and KLF4 mRNA, sequestering METTL3 and promoting tumorigenesis and a BCSC phenotype.

More recently METTL3 (H. Wang et al., 2020) was found to be upregulated in breast cancer and to correlate with poor prognosis and outcome. Silencing of METTL3 induces apoptosis in breast cancer cells and the decrease of BCL2 expression which, like in acute myelocytic leukemia, was found to be its target.

FTO was found to be upregulated in breast cancer and increasing the demethylation of the pro-apoptotic gene BNIP3 (Yi Niu et al., 2019). FTO negatively regulates its expression in a YTHDF2-independent manner, as the overexpression of YTHDF2 does not affect the level of expression of BNIP3 in FTO deficient cells, suggesting another mechanism for the increased stability of BNIP3 mRNA that the paper does not investigate further.

Prostate Cancer

YTHDF2 was found to be upregulated in prostate cancer (PCa) tissue, and in particular its expression is negatively correlated with the tumor suppressor miR-493-3p (J. Li et al., 2018). Silencing of YTHDF2 cause an increase of the global m6A levels and inhibition of cells proliferation, colony formation ability and migration, while the overexpression of miR493-3p cause the decrease of YTHDF2 expression levels causing the same phenotype, as the tumor suppressor was found to directly target the 3'UTR of YTHDF2.

METTL3 was also found to be overexpressed in PCa (Cai et al., 2019) enhancing tumor progression, colony formation, proliferation, by interacting with the Sonic Hedgehog pathway (SHH), that is known to play an important role in the development of this kind of cancer. It was found in particular to regulate the SHH-GL1 signaling in a m6A-dependent manner. The SHH-GLI pathway is mediated by the GLI family of proteins, whom act as markers of SHH activation, and by the protein Smo and PTCH1, but only the GL1 protein was observed to decrease after METTL3 depletion, together with its downstream targets CyclinD1 and c-Myc.

Colorectal Cancer

YTHDF1 of all the other YTH family protein, was found to be overexpressed in colorectal cancer tissues (CRC), the third most common cancer type (Nishizawa et al., 2018). Even in this case, the expression levels of YTHDF1 were related to negative cancer prognosis, with a higher expression in the most severe stages. Silencing of YTHDF1 inhibits cell proliferation and increased their sensitivity to chemotherapeutic drugs such as fluorouracil (5-FU) and oxaliplatin (L-OHP) compared to the control wild type cells. The expression of the oncogenic transcription factor c-Myc was also found to be correlated with the YTHDF1 expression, and that it was associated with the 5' of the transcription start site of YTHDF1.

This was then confirmed by the biological observation that upon silencing of c-Myc also YTHDF1 decreased its level of expression in a dose-dependent manner of transfection. The study did not pursue further in dissecting the role of YTHDF1 in m6A-dependent

transcription regulation, but surely suggested the m6A-reader as a potential therapeutic target.

A more recent study (Bai et al., 2019) went deeper in revealing the role of YTHDF1 in the development of CRC, focusing also on its role in the maintenance of the stem cell niche. YTHDF1 was found to be overexpressed in CRC by DNA copy number variation, increasing the tumorigenicity *in vitro* as already observed. YTHDF1 was then found to be associated with stemness markers and overexpressed in colonospheres, which are stemlike spheroid cells. Silencing of YTHDF1 decreased the level of expression of stem cell markers such as CD44, ALDH1, OCT4, Lgr5 and CD133 in colonospheres, causing conversely the increase of more enterocyte markers that drive the differentiation of the sphere towards a more epithelioid phenotype, when growth in differentiation-inducing conditions.YTHDF1 was also found to be correlated with the Wnt/$\boldsymbol{\beta}$-Catenin pathway, that is involved in cancer stem cells, and in particular two component of that signaling, WNT6 and FZD9, were identified as being its direct targets. In conclusion, YTHDF1 is involved in stem cell-like activity of CRC cells, and when downregulated colonospheres are left to differentiate, losing their self-renewal potential. The discovery highlights once again that YTHDF1 can be considered a candidate target for treating CRC.

Lung Cancer

In lung squamous cell carcinoma (LUSC), FTO has been identified as a prognostic factor after analysis of data present on cancer databases (Jiqin Liu et al., 2018).It was observed in particular that FTO was the only member of the methylation machinery to be dysregulated in LUSC, aberrantly decreasing the level of m6A methylation. Upon its silencing, cell proliferation and tumorigenicity were inhibited, while apoptosis of lung cancer cells was promoted. In particular, FTO was found to alter the m6A methylation of the Myeloid Zinc Finger Protein 1 (MZF1) transcript increasing its expression while decreasing the stability of its mRNA, causing the rise of an oncogenic phenotype as MZF1 abnormal expression contributes to cancer development.

METTL3 also has an oncogenic role in lung cancer (Lin et al., 2016), increasing the expression levels of EFGR and TAZ by associating with ribosomes and enhancing their

translation, independently from its methyltransferase activity, from METTL14 and from the reader proteins YTHDF1 and YTHDF2.

A more recent study highlighted the role of YTHDF1 in linking adaptation to hypoxic conditions and the progression of non-small cell lung cancer (NSCLC) (Y. Shi et al., 2019).In this study, it was found that YTHDF1, among other proteins related to adaptation to high altitudes hypoxic conditions, was less expressed in highland Tibetan animals than in lowlander animals, but amplified in NSCLC. The low expression level of YTHDF1 resulted to be an adaptation to hypoxic condition, as shown by the apoptosis decrease in normal human bronchial epithelium cells exposed *in vitro* to hypoxia. In NSCLC cells, silencing of YTHDF1 abrogates cell proliferation and colony formation, and was also found that many cell cycle regulators were also downregulated, as CDK2, CDK4 and Cyclin D1, and in particular reduced in the mRNA translating pool as YTHDF1 directly bounds their mRNAs. Silencing of YTHDF1 retarded also tumor formation *in vivo,* but unexpectedly low expression level of YTHDF1 were correlated with a poor clinical outcome in NSCLC patients, this because low level of expression of YTHDF1 cause resistance to chemotherapeutic treatment with cisplatin. This was explained by the fact that upon YTHDF1 knockdown, the transcription factor Nfr2, associated with the regulation of antioxidant processes, was upregulated together with its downstream responding factor AKR1C1, while the negative regulator of Nfr2, Keap1, was downregulated. Cisplatin treatment increase the ROS levels and cause the activation of p53, leading to cell death; the increased levels of Nfr2 and AKR1C1, antioxidant agents, in YTHDF1 knockdown cells antagonizes the drug mechanism of action causing resistance to treatment and a worse clinical outcome. This then is linked with the fact that YTHDF1 has low expression levels in highland cattle, which have a better antioxidant response in the hypoxic conditions caused by the altitude.

Other types of cancer

Since describing the role of the m6A modifiers in every type of cancer not only would not be easy but also too long, just some of the most studied and characterized have been briefly treated. To conclude, there are evidence of a YTHDF2 oncogenic role also in pancreatic cancer (J. Chen et al., 2017), with the protein being involved in two different

process, enhancing cell proliferation on one side and inhibiting migration on the other, two sides of the same biological phenomena, the so-called epithelial to mesenchymal transition (EMT). Silencing of YTHDF2 downregulates TGF-β/Smad signaling while increasing YAP expression, which is the main factor responsible for the activation of the EMT pathway, but there are no clear evidences of what is the molecular mechanism by which YTHDF2 could drive this transition, if by influencing the stability of some downstream transcript or else. Clear was instead the mechanism by which YTHDF1 was found to drive the progression of ovarian cancer (T. Liu et al., 2020), by binding to the mRNA of the EIF3 subunit EIF3C and enhancing its translation, so increasing the overall translation and promoting tumorigenesis.

In conclusion, there are a lot of discrepancies in what is the role not only of YTHDF1, but of all the other m6A modifiers in cancer development, meaning that their molecular function must be very well characterized in every type of cancer, being clearly cellular context-dependent, to adopt the better therapeutic strategy.

1.4.2 Stem cell differentiation

One of the biological functions of the m6A modification is to regulate stem cell differentiation. Human and Mouse Embryonic Stem Cells (hESC, mESC), the pluripotent cells originating directly from the blastocyst, fail to differentiate and exit the stage of pluripotency as a consequence of METTL3 knockdown, because the m6A decoration upon certain transcripts promoting self-renewal, like NANOG and SOX2, decrease their stability (Batista et al., 2014). METTL3 KO ESC cells resulted to be viable and self-renewing, with low levels of apoptosis, and proliferating more than wild type ESC. The injection of METTL3 KO ESC cells in nude mice resulted in the formation of teratomas mainly composed of poorly differentiated cells, compared to the ones generated from wild type cells, which tended to differentiate mostly in neuroectoderm (Batista et al., 2014). In contrast with these findings, in another study was observed that upon METTL3 or METTL14 knockdown the mESC colonies forming from the silenced cells were less proliferating and with a flatter phenotype (Y. Wang et al., 2014), and losing their ability to self-renew. Loss of m6A methylation in particular increased the interaction of the

transcripts with the RNA-binding protein HuR, that prevent microRNAs from binding to them, increasing their stability. This apparently insuperable obstacle was then explained by a following paper(Geula et al., 2015) in which was explained that the different outcome after METTL3 KO depended on the different ESC stage at which it was carried out, distinguishing between a na¨ıve molecular state of ESCs and a more “primed” state of epiblast stem cells (EpiSC). In naive stem cells, the increased concentration of the pluripotency transcripts due to METTL3 KO caused the impossibility to progress to differentiation, for which are needed low level of expression of those genes. On the contrary, for EpiSC METTL3 KO increased the level of lineage commitment factors causing the cells to undergo differentiation.

1.4.3 Nervous system

Since it is not the main object of this thesis, the role of m6A and its related proteins will not be deeply discussed, just pointing out some of the most important aspects. The brain tissue has the highest level of methylation compared to the others and has been observed in particular that the methylation signature changes during the different stages of brain and synaptic development. METTL14 KO in embryonic neural stem cells cause them to stop proliferating and start to prematurely differentiate (Geula et al., 2015). m6A methylation is responsible of the regulation of the cortical neurogenesis (Yoon et al., 2017), and METTL14 is involved in preventing the precocious expression of genes that can lead to differentiation towards a certain fate. YTHDF2 KO also negatively impacts neural stem cell progenitors (NSPC) in embryonic neocortex by inhibiting cell proliferation and differentiation. This was due to the fact that the depletion of YTHDF2, and consequently its mRNA clearance activity, caused the upregulation of its target mRNAs involved in the negative regulation of neural development (M. Li et al., 2018). FTO also is highly expressed in brain tissue, and it has a crucial role in regulating the dopaminergic system (Hess et al., 2013), in fact its loss impairs the signaling of two different group of dopaminergic neurons, DP2 and DP3. FTO also plays important roles in learning and memory, as different papers have investigated (Walters et al., 2017; Widagdo et al., 2016), and also YTHDF1 by promoting the translation of target transcripts involved in memory consolidation through long term potentiation (H. Shi et al., 2018). More recently, YTHDF1

has also been found to be involved in axon guidance, through the translational regulation of the Robo3.1 mRNA, encoding for a receptor involved in axon guidance, and in particular involved in switching axons from being attracted to being repulse from the floor plate (Zhuang et al., 2019).

1.5 High Throughput Screening

High Throughput Screening (HTS) is a method that provides a fast, miniaturized, automated way to analyze the activity of a large numbers of compounds, collected in so-called compound libraries, against biological targets. The purpose of HTS is to identify candidate molecules that can then be tested against their biological target in what are called secondary assays, to slowly get rid of the false positives and to finally select the candidate molecule that can then undergo a process of chemical optimization (to increase its selectivity and potency) to become a genuine lead for reaching clinical development. The drug discovery process takes a lot of time in its making, and before a candidate drug can reach the first step of clinical trial, many years can pass, generally from ten to fifteen years from the first identification of the candidate drug to the finished product. Success in drug discovery rely mostly on the goodness of the assay that is been adopted in the high throughput approach.

The suitability of the HTS is defined by a parameter called Z-factor (J.-H. Zhang, 1999). The formula of the Z-factor is: $1-3(\sigma_p+\sigma_n)/(\mu_p-\mu_n)$, where μ is the means, σ is the standard deviation, of both the positive (σ_p,μ_p) and negative control (σ_n,μ_n). The values of the Z-factor varies between 0 and 1, with values going from 0, indicating that the assay is not suitable for HTS, being too much overlapping between positive and negative controls, values between 0 and 0.5 indicating a marginal assay, values between 0.5 and 1 indicating a good and robust assay, and values identical to 1 indicating an ideal assay.

Choosing the right assay with the best read out is crucial for a good result. Detection methods must be reliable and at the same time amenable for miniaturization and high sensitivity. One of the most common method for detection that holds together all these characteristics is fluorescence (Fang et al., 2019). Fluorescence anisotropy, time-resolved fluorescent transfer (TR-FRET) are some of the most common examples, and still the

detection methods that are preferentially used also thanks to growing evolution of the sensitivity of the instruments that collect the readout signals.

1.6 RNA binding proteins as novel therapeutic targets in cancer

RBPs are aberrantly regulated in many types of diseases, particularly cancer. Their deregulation influences every step of cancer development, since they are responsible for the regulation of proliferation, migration, angiogenesis and escape from apoptosis of cancer cells through the regulation of different target coding and noncoding RNAs. For these reasons, in the last years, RBPs have started to be conceived as putative therapeutic targets for the development of drugs. To develop high throughput screenings ideal for identification of small molecules targeting RBPs, the common methods are based on measurement of the reduction of the RNA-RBP interaction or of the RNA target expression. RNA binding proteins can interact with their RNA targets with structured domains, that can be more than one for protein, or without any structured motif. RNA binding domain structures offer a good canonical “druggable target”, were the most common approach is to target enzymes, membrane proteins or receptors, because they often satisfied the concept of druggability, that includes the ability of the inhibitor to reach its target site, the characteristics of the binding sites itself, and the capacity to successfully disrupt the interaction of the domain with its natural ligand (Knapp, 2015). For these reasons, the best candidate to be considered amenable drug targets are binding sites located in pocket of the right dimension for containing a small molecule inhibitor, better with hydrophobic surfaces, and that shares with their binding site a weak interaction, like in the micromolar range, so that the drug can better compete with that interaction.

Many are the assays that have developed to target the RBPs-RNA interaction. Most of them are biochemical based, developed after a previous study of the interaction between protein and ligand at high resolution, through NMR, cryo-EM, or crystallography. The most common biochemical assay that are developed to be amenable for High Throughput Screening involved purification, labelling or immobilization of one of the two interactors, but some can also be label-free, as in the case of the Dynamic Mass Redistribution (DMR).

1.7 Epitranscriptome members as therapeutic targets

The breakthrough discovery that behind the development of many pathologies lies another level of regulation given by RNA modification lead to the consideration of epitranscriptomics regulatory proteins as potential therapeutic targets. A great focus has been given to the m6A modification, having discovered that upon its misregulation many biological events can be affected, as we already described in depth. FTO, of all the members of the m6A methylation machinery, has been the most studied member and the first one to be considered a therapeutic target. Structure-based *in silico* screening and biochemical analysis lead to the development of the first FTO inhibitor, the compound Rhein (B. Chen et al., 2012), that competitively bound to the active site of the demethylase, showing to be effective both on a protein level than in cells, but showed poor selectivity for the Alk family to which FTO belongs. Through a fluorescence polarization based assay, in which was tested the ability of a library of compounds to displace a ssRNA probe from FTO and ALKBH5, it was possible to discover meclofenamic acid (MA) as a specific FTO inhibitor over ALKBH5 (Huang et al., 2019). Another strategy, based on the identification of residues in the nucleotide-binding sites of the members of the Alk family of demethylases that determine their substrate specificity, lead to the identification of an FTO specific inhibitor, a fumarate-deriving compound simply identified with the number 12, which showed a 45 fold enhanced activity towards FTO compared to the generic inhibitor NOG (a catalytically inert amide analogue of 2OG), and 100 fold more selectivity with respect to ALKBH5 (Toh et al., 2015).

Also the oncogenic metabolite R-2-hydroxyglutarate (R-2HG), produced by mutant isocitrate dehydrogenase 1/2 (IDH1/2) enzymes, was found to inhibit FTO activity in leukemia R-2HG-sensitive cells, thus increasing the level of m6A methylation and indirectly decreasing the stability of MYC/CEBPA transcripts, exerting an oncosuppressor role (Su et al., 2018). Recurrent somatic mutations in IDH1 and IDH2 occur with high frequency in gliomas and secondary glioblastoma (GBM), but also in some cases of acute myeloid leukemia (AML) patients, causing the production of the oncometabolite R2HG. It was found that glioma and leukemia patients bearing the IDH1 mutation have a better tumor prognosis, confirming that R2HG has an anti-tumor activity in these cells due to its inhibition of FTO activity. Other inhibitors were developed and tested but resulting not to be

particularly efficient on cell viability (Svensen & Jaffrey, 2016), and in general none of these resulted to be applicable for clinical testing due to their poor selectivity and efficacy. Recently, the group who discovered MA as inhibitor of FTO developed a more potent and selective inhibitor adding some chemical modification to the MA structure with the help of rationale-based design, obtaining a molecule called FB23 and another derivative, called FB23-2, which displayed increased anti-tumor activity towards AML cells (Huang et al., 2019). The same year, Entacapone was identified as an FTO inhibitor by virtual screening and biochemical analysis (Peng et al., 2019), and following *in vivo* administration to mice, it was observed that it helped improve glucose tolerance, adipose thermogenesis and consequently body weight control. In that work, the mechanism of action was linked to the fact that the inhibition of FTO has an impact on the methylation of its target FOX1, that was already found to be associated with FTO in Non-alcoholic fatty liver disease (NAFLD) (Mizuno, 2018).

In a virtual screening, small molecules binding to the WTAP-METTL3-METTL14 complex were identified and further biochemically determined their binding kinetics and their effect on enzymes activity. Instead of having found inhibitors of the complex activity, the small molecules identified acted as activators instead (Selberg et al., 2019).The compounds showed to be more effective in increasing the cellular levels of m6A than MA, which was used as a positive control. These activators of the methylation complex resulted to be effective against diseases models in which the misregulation of the methylome requires m6A levels to be increased, as in glioblastoma or in AML, where already FTO inhibitors have been tested. For the moment any small molecule binding to the methylation complex and antagonizing its natural substrate SAM haven’t been identified yet, even if in the last years have been published papers showing in detail the development of assays amenable for HTS specifically developed to test molecules against the methyltransferases and the demethylases. For example, in (F. Li et al., 2016) a radioactivity-based assay has been developed to test the m6A modifications by METTL3 and ALKBH5, resulting suitable for testing the activity of small molecules, or in (Wiedmer et al., 2019), where an Homogeneous Time Resolved Fluorescence (HTRF) based enzyme assay has been developed to measure the activity of the writers proteins, the demethylases and the readers, and that can be easily adopted for HTS to find inhibitors of all the members of the methylation machinery.

My PhD project has been based on the set up of a High Throughput Screening Assay against the YTH domain, to identify and validate small molecules as potential candidate inhibitors, with also the aim of repurposing some already FDA approved drug to this new target. The aim of my work is entirely presented in the next chapter.

2.Hypothesis and Aim

As already described, dysregulation of the m6A methylation can be the driving cause of different pathologies, and cancer particularly. This can be caused by alteration in the level of expression of one of the methylation machinery members, mostly the writers and the erasers. Alteration in the level of expression of the readers does not have a direct impact on methylation but can influence translation and decay of target methylated mRNAs. For these reasons, in the last few years it is increased the focus on how to exploit the m6Amethylation machinery members as therapeutic targets. The focus has been put mostly on targeting the erasers, and in particular FTO; some attempts have also been made to target METTL3, founding molecules that increase its catalytic activity rather than inhibiting it, useful in the pathologies in which the m6A levels are decreased. Up till now instead, there have not been any known attempts to consider the YTH domain proteins as therapeutic targets, even if there are many hints pointing in that direction since the discovery of their oncogenic roles. The YTH domain, for its structural characteristics, could be easily exploited for designing a screening targeting its hydrophobic RNA-binding pocket, both *in silico*, with structural-based design, or *in vitro.* The aim of my PhD project it has been to set up a screening assay amenable for High Throughput, easy to perform and to analyze, to identify and validate small molecules interfering with its RNA-binding capacity. We decided to target the YTH domain, an RNA binding protein, because we thought that targeting METTL3 would be less easy to afford, being an enzyme with an high affinity for its substrate SAM, and because the total inhibition of its methyltransferase activity would bring some off target unpredictable effects also on non-cancer cells, altering as a consequence also the normal cellular functions. We based our efforts on the presence of the three well conserved tryptophan residues in the binding pocket, that lead

us to the development of a tryptophan quenching based assay. The candidate molecules then have been validated towards their target with different orthogonal biochemical assays, to be furthermore tested for their anticancer activity in a model in which at least one of the reader proteins plays a pivotal oncogenic role. We started by testing the anticancer activity on prostate cancer cells, in which YTHDF2 was already identified as an oncogene (J. Li et al., 2018). YTHDF2 regulates mRNA decay and for this reason we choose to test the effect of the treatments in comparison with silencing of the protein with RNA lifetime measurement after transcription inhibition with Actinomycin D, choosing some of the already published YTHDF2 mRNA targets (Xiao Wang et al., 2014). Then we decided to investigate the role of the cytoplasmic readers in a model that wasn't still been studied. For this reason, we choose to investigate the function of the cytoplasmic protein YTHDF1 in Neuroblastoma, due to prior analysis performed by a group in the Department of CIBIO collaborating with us on this project, in which the expression of this cytoplasmic reader, and not of the others, was significantly correlated with poor prognosis in Neuroblastoma patients. After characterizing the role of YTHDF1 in the development of Neuroblastoma, the aim of my PhD project was also to test the effect of treatment with the newly discovered drugs.

To sum up, during my PhD project I performed an High Throughput Screening to identify small molecules candidate inhibitors towards the YTH domain, I validate them from a biochemical and biological point of view, testing their function against different cancer models and in particular in Neuroblastoma, in which I also characterize for the first time the oncogenic role of one of the reader proteins, YTHDF1.

3.Results and Comments

3.1 Set up of a High Throughput Screening targeting the YTH domain.

As already mentioned in the introduction, my PhD project aimed to set up a screening amenable for High Throughput to find small molecules inhibitors of the YTH domain RNA binding ability. The screening assay was developed by exploiting the presence of three conserved tryptophan residues inside the hydrophobic binding pocket of the YTH domain, also responsible for the recognition of the m6A moiety. Tryptophan has an intrinsic fluorescence that can be used to monitor changes in the microenvironment of a protein, and in this case to measure the fluorescence quenching upon ligand binding. We started by purifying the YTH domain of the YTHDF1 reader, the structure annotated on the Protein Databank (PDB) as 4RCJ, that corresponds to the aa residues going from 365 to 554 (Figure 7A&B).

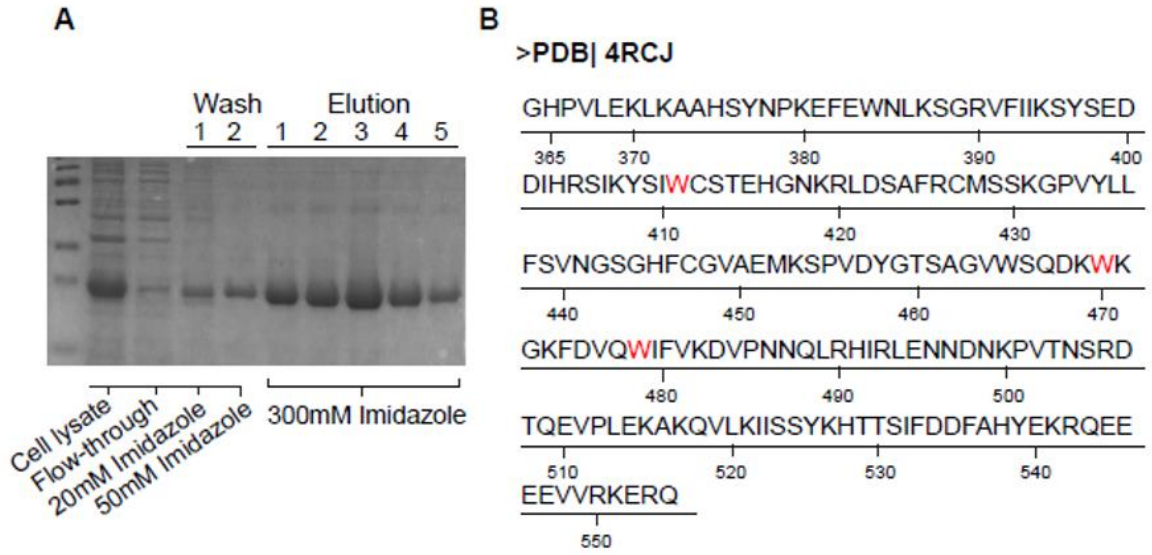

Figure 7. Purification of the 4RCJ structure of the YTH domain of YTHDF1 protein. (A) SDS-PAGE analysis of purification steps of the 4RCJ structure of the YTH domain. Washing steps have been carried out using increasing concentrations of Imidazole (20mM-50mM). The five elution fractions have been obtained using 300mM of Imidazole. **(B)** Amino Acid residues composing the 4RCJ structure of the YTH domain of YTHDF1 (365-554), taken from the Protein Data Bank (PDB).

We measured the intrinsic fluorescence of the protein and we started testing the feasibility of the quenching assay by tethering to the protein its natural ligands and their corresponding negative controls. We began using the N6-methyladenosine moiety alone and the unmethylated Adenosine, then also testing two RNA probes bearing two variants of the consensus sequence, both methylated and unmethylated. We obtained that quenching of the intrinsic fluorescence of the protein increased with increasing concentrations of N6-methyladenosine and increasing concentrations of the methylated RNA probes, for which we also calculated an IC50 in the micromolar, respectively 11,94μM for the 5'-CCGAm6ACUGUC-3' probe, and 5,245μM for the 5'-CCGGm6ACUGUC-3' probe, while the fluorescence was not affected by either rising concentrations of Adenosine neither by the unmethylated RNA probes (Figure 8A,B &C).

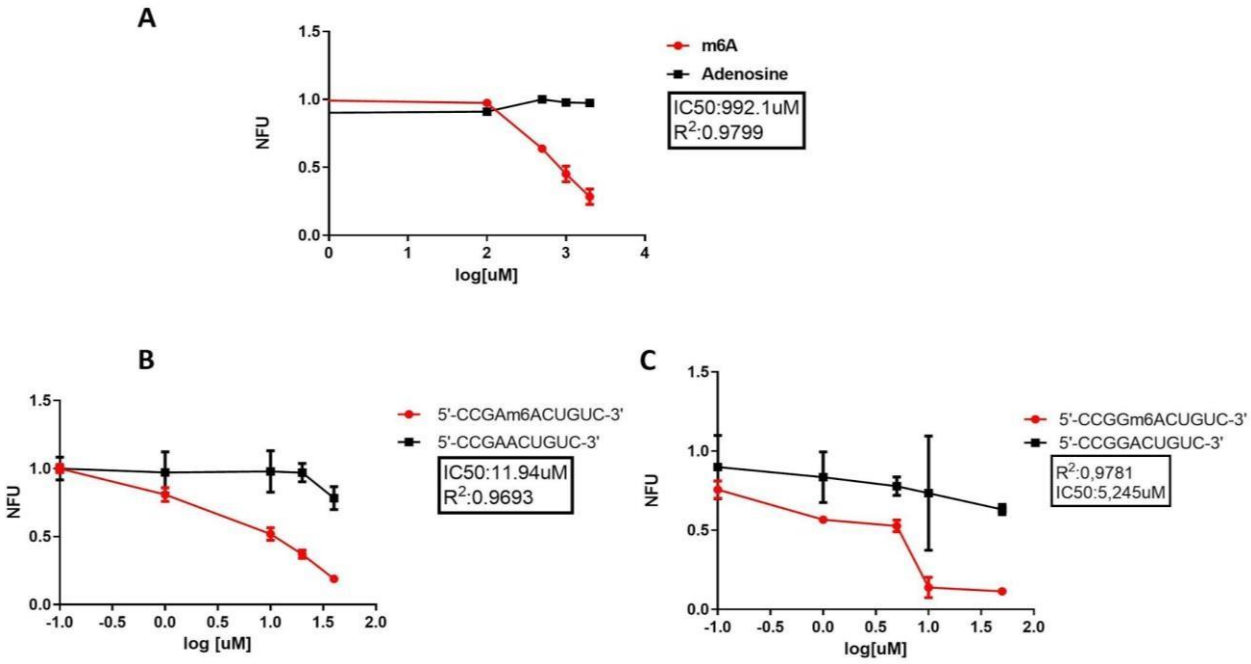

Figure 8. Binding specificity of YTH domain towards N6-methyladenosine. A) Dose dependent quenching of YTH domain fluorescence due to specific binding of N6-methyladenosine versus Adenosine as negative control. **B-C)** Binding specificity was also assessed through the binding of two methylated probes bearing two variants of the consensus sequence and the same unmethylated probes as negative control.

After we calculated the Z-factor of the assay to assess its robustness and its feasibility for

To further select the positive candidates, and to exclude that the quenching effect was due to some nonspecific interaction with the Tryptophan residues, we decided to test the quenching effect of the molecules against another protein with Tryptophan residues inside its catalytic pocket. As a negative control for the counter screening, we used the TEV protease, which has five Tryptophan residues in its catalytic domain. As in the primary screening, we added the small molecules directly to the protein in solution in 384 well black plates, and we measured the fluorescence intensity. We then calculated the ΔRFU between 4RCJ and the TEV protease, selecting all the compounds with the highest difference. In this way, we ended up picking just four molecules (Figure 9C&D).

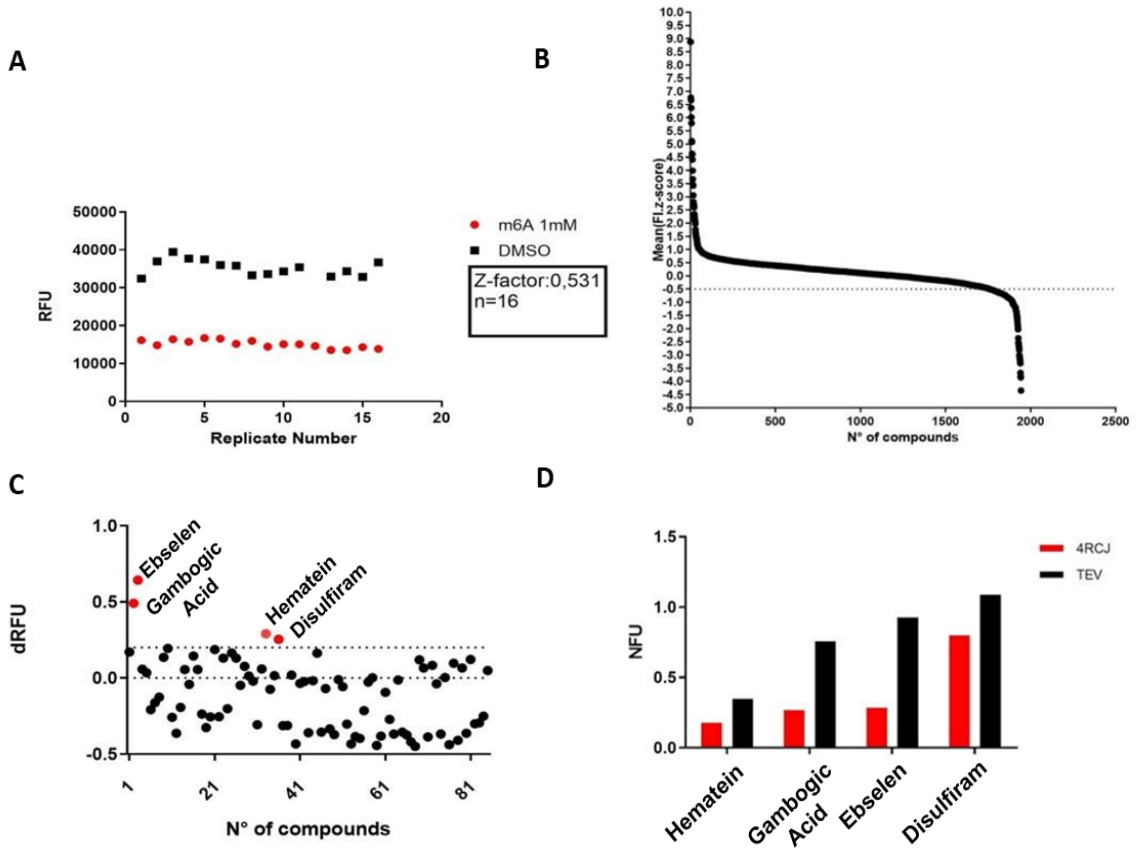

Figure 9. High Throughput Screening and counter screen. A) Calculation of the Z-factor for the quenching assay. Quenching effect of the m6A moiety against the YTH domain has been measured in sixteen replicates, with DMSO as a negative control. Z=0.531 is an indicator of a eccellent assay. **B)** Plot of progressive Z-score values of 2000 compounds according to their quenching effect on the YTH domain. **C)** Scatterplot of the candidate hits expressed as dRFU between

the YTH domain and the TEV protease. The ones highlighted in red are the candidate hits that showed a specific quenching effect toward the YTH domain. **D)**Only four compounds were selected as specifically binding to the YTH domain after the counter screening.

We tested the interference potential of the molecules with the RNA binding ability of the YTH domain by an RNA Electrophoretic Mobility Shift Assay. We found that one was able to disrupt the RNA binding capacity of the YTH domain starting from 1μM (Figure 10 A&B).

At the same time, we *in silico* screened the positive molecules to get rid of the potential PAINS.

PAINS, or Pan Assay Interference Compounds, are classes of molecules that share the same substructures and act promiscuously against different targets, appearing often as false positives in HTS approaches and are not at all to be considered optimizable or progressible as potential drug candidates (Baell et al., 2018). These kinds of molecules easily interact with many chemicals due to their structure and charge and are frequent false positive in screening campaigns. On this purpose we used two open source software, http://fafdrugs4.mti.univ-paris-diderot.fr/index.html (Lagorce et al., 2015) and http://advisor.bkslab.org/ (Irwin et al., 2015), the first one screening the molecules giving a summary of their chemical characteristics, if they followed the five Lipinski's rules and, most importantly, if they already have been reported as PAINS, while the other software screened the molecules and, based on their structures, could tell if they tend to form aggregates that make them not feasible as drugs. Thanks to these different approaches, we ended up selecting just one molecule, the organoselenium compound Ebselen, an already approved FDA drug with anticancer and anti-inflammatory properties that has also demonstrated to have antimicrobial properties (May et al., 2018).

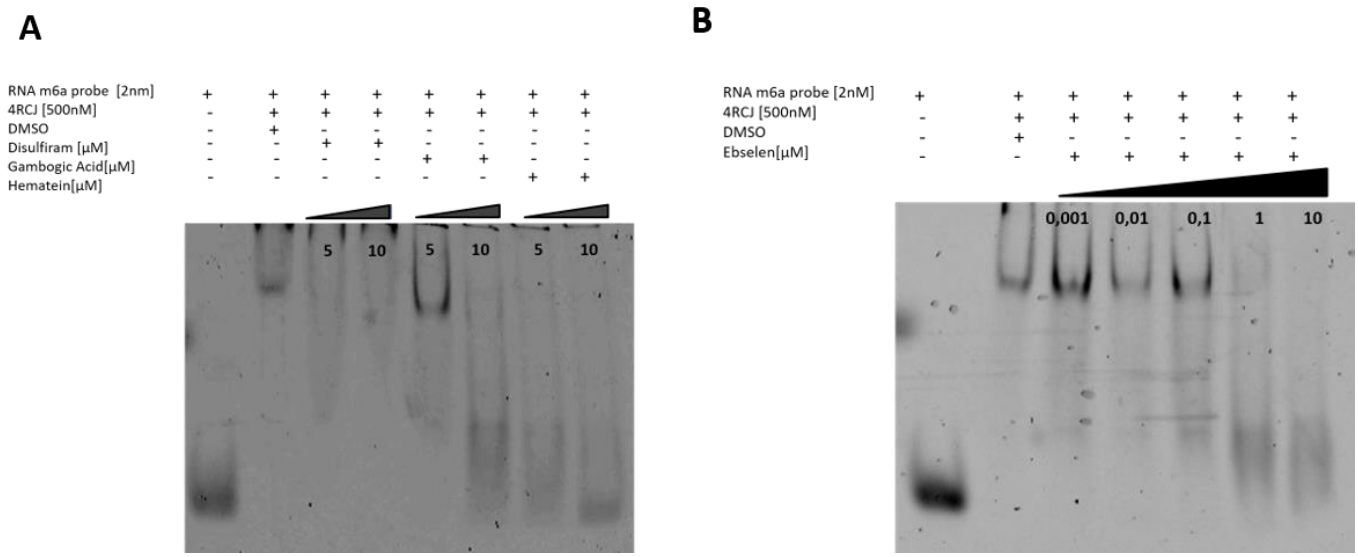

Figure 10. RNA Electrophoretic Mobility Shift Assay of the four candidate hits. A) REMSA showing disruption of YTH binding by the positive candidate hits, tested at 5µM and 10µM. **B)** REMSA showing disruption of YTH binding by the fourth and only candidate hit post i*n silico* screening, tested at different concentrations starting from 1nM to 10µM, which started to be effective at 1µM.

3.2. Characterization of YTH-Ebselen interaction

After we ensured that Ebselen has inhibitory activity towards the YTH domain, were further tested the YTH-Ebselen interaction with Dynamic Mass Distribution (DMR) assay. We obtained an EC50 at the equilibrium of 3,22µM (Figure 11B). We also evaluated the ability of Ebselen of inhibiting the formation of the RNA-complex with Alpha Screen® assay, in saturation binding conditions. Knowing that the Kd of interaction between the protein and the ssRNA is ~70nM, as we obtained with DMR, (Figure 11A) we fitted on AlphaScreen saturation curves the *K*i values, quantifying the inhibitory efficiency of Ebselen with different concentrations in the µM range (0-100 µM), obtaining a *K*i of ~4.8 µM (Figure 11C).

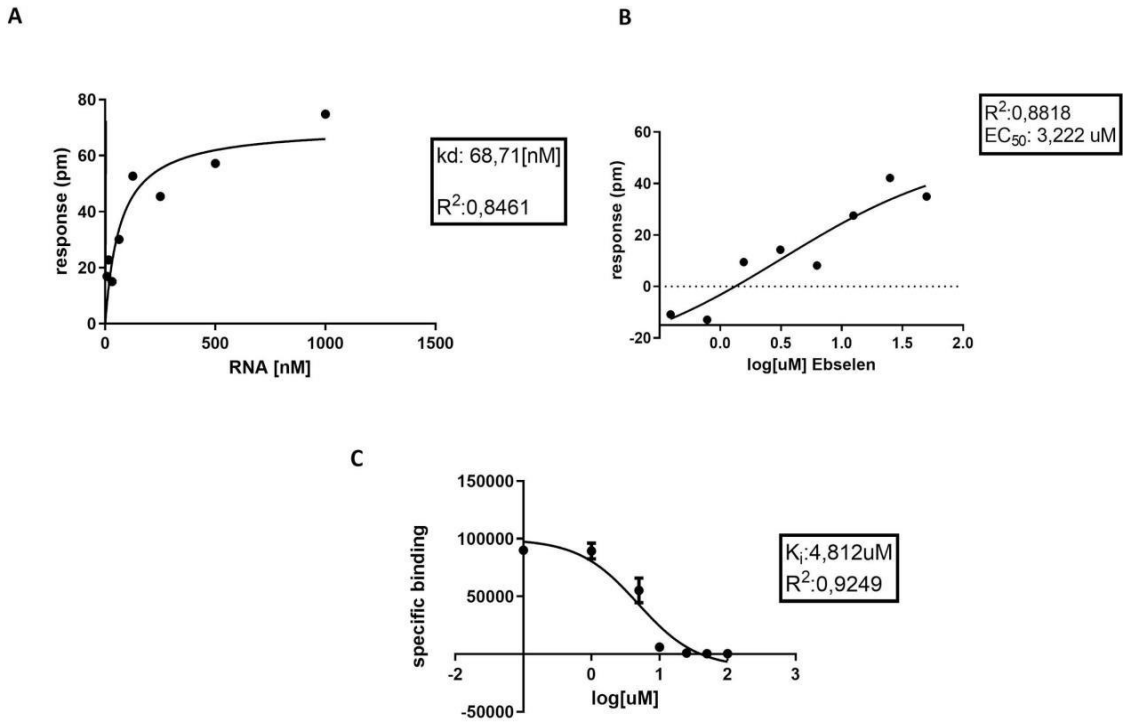

Figure 11. Ebselen interacts with the YTH domain *in vitro*. A) Determination of the kd of interaction between an m6ARNA probe wih the 4RCJ structure of the YTH domain calculated with the DMR. rYTH was immobilized to the wells with amino-coupled chemistry and different concentrations of RNA were added to the plate. Measurement were performed before adding the RNA, in order to define a baseline, and after the addition. Final response (pm) was obtained by subtracting to the last measurement the baseline. Signal for each well was obtained by subtracting the signal of a reference area with the protein coated to an uncoated one. R^2=0,8461 Kd=68,71nM. **B)** EC_{50} of interaction between the 4RCJ structure of the YTH domain and Ebselen calculated with DMR, following the same procedure of A) R^2=0,8818 EC_{50}=3,222 μM. **C)**Determination of the Ki of the Ebselen molecule with Alpha Screen® Assay, using nonlinear regression fits of the data according to 1-site fit Ki model: R^2=0,9249.The concentration (50 nM) and the Kd (70 nM) for the labeled Bi-TNF probe, calculated elsewhere with another assay, was kept constant.

After, since we hypothesized that the Ebselen interaction with the YTH domain could be due to formation of a covalent bond, since the compound is known to interact with thiols and form selenium sulfide bonds (Sakurai T. et al, 2006; Capper M. et al. 2017), we hypothesize that there could be a covalent interaction to a cysteine residue present in the binding pocket (C412). We so performed a mass spectrometry experiment in which we incubated the 4RCJ structure of the YTH domain in its native form with 50 μM of Ebselen, in a 1:10 ratio, and then we changed the buffer through desalting to get rid of the excess of unbound compound prior to subject the sample to MS by direct infusion. We found that the mass difference between the experimental sample and the native protein alone

corresponds to the mass of one Ebselen molecule, which has an average molecular mass of 274.18 Da (Figure 12A). As an additional control, we repeated the experiment by adding 1mM DTT in the incubation buffer, that then was removed through desalting. We obtained no significant difference between the experimental and the reference sample, meaning that in reducing condition the interaction between Ebselen and the YTH domain fails to happen because the covalent bond is erased by the reducing activity of DTT towards cysteine residues (Figure 12B).

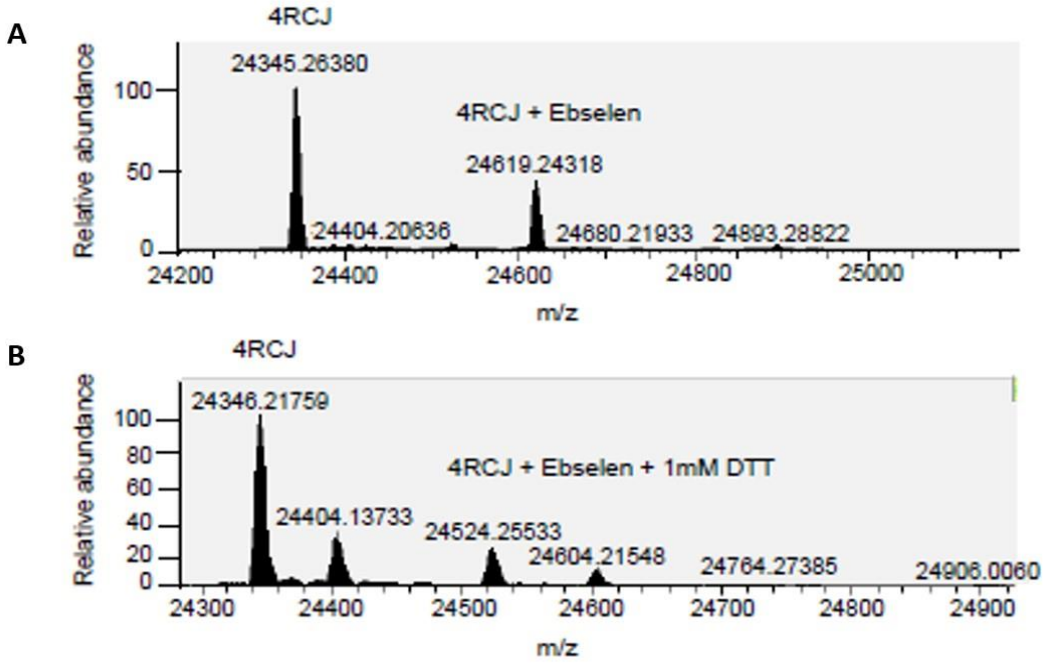

Figure 12. Ebselen binds covalently to the 4RCJ structure of the YTH domain. A) Mass spectra of the 4RCJ structure of the YTH domain alone and incubate with 50μM of Ebselen. In this case, its mass is increased by one time the mass of Ebselen, meaning that the small molecule is bound to the domain. **B)** Mass spectra of the 4RCJ structure of the YTH domain alone and incubate with 50μM of Ebselen in presence or abscence of 1mM of DTT. In this case, the mass of the complex corresponds to the protein alone, meaning that Ebselen has a covalent interaction with the domain that has been disrupted by DTT, which has broken sulfur-selenium bonds.

Ebselen has been already reported to bind cysteine-rich proteins including an RNA/DNA binding protein (Mukherjee et al., 2014). It has been suggested that Ebselen could function as cysteine modifier behaving as reversible or irreversible binder depending on concentration and incubation time. To further investigate the mechanism of YTH inhibition by Ebselen, and to prove the specificity of the interaction, we performed a NMR study, in collaboration with Marco Fragai and Linda Cerofolini at CERM in Florence. The protein was titrated with Ebselen, in the presence of β-mercaptoethanol (10 mM) as reductant, to

prevent the formation of the covalent bond and to investigate the possible presence of a reversible binding.

The titration was monitored by NMR to assess map with at atomic resolution the ligand binding site on the protein surface. Increasing amounts of the ligand [12.5, 25, 50, 100, 200 μM] were added to the protein solution during the NMR titration and 2D ^{1}H-^{15}N HSQC spectra were acquired (Figure 13). In the presence of sub-stoichiometric concentrations of the ligand (50 μM) a decrease in signal intensity is observed for some protein residues (K387, W411, T414, N418, K419, F425, C427, H445, D457, Y458, G459, W470, K471, F474, D475, Q477, F536, A537, see Figure 89A) as expected for a ligand with an affinity constant in low μM range, which is in an intermediate exchange regime on the NMR time scale. Few of these residues and some of their neighboring aminoacids (I402, S413, T414, N418, D422, Y458, W470, K471, D475), however, experience also a small chemical shift perturbation. All these selected residues are located in the pocket responsible for binding of methylated (m6A) RNA (Figure 13 C&D), indicating that the interaction occurs specifically in this hydrophobic pocket. We also observed that among the residues experiencing the largest decreases in signal intensity, two (W411 and W470) out of three of the tryptophan residues present inside thereof the binding pocket of the domain have been highlighted. Unfortunately, the assignment of the third tryptophan residue (W465) is missing, therefore, no information can be retrieved on this residue. The NMR results prove the specificity of

Ebselen for YTH and its micromolar affinity regardless of the selenium sulfide bonds.

These findings are also in agreement with the fluorescence data and explain the quenching of protein intrinsic fluorescence observed after interaction with Ebselen ligand.

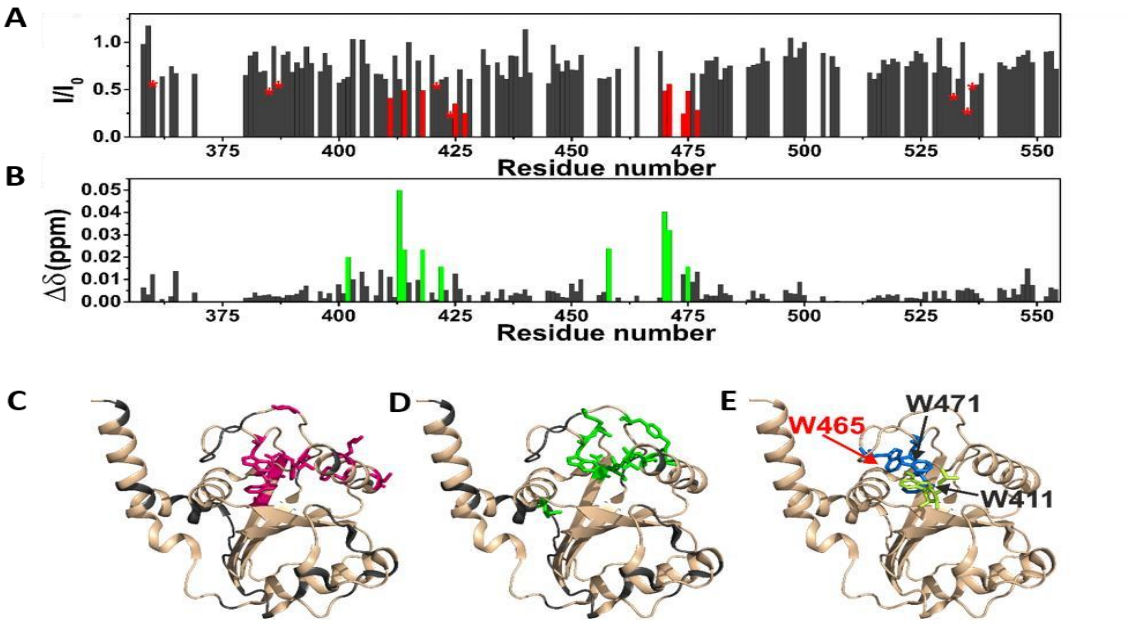

Figure 13. Ebselen specifically interacts with the hydrophobic pocket of the YTH domain. (A) Plot of the decreases in signal intensity of YTH domain (100 μM) in the presence of the ligand ebselen (50 μM); the residues exhibiting the largest decreases are highlighted in red. The stars indicate residues with a large decrease in signal intensity but overlapping in the NMR spectra. **(B)** Plot of the chemical shift perturbations (CSPs) of YTH domain (100 μM) in the presence of the ligand Ebselen (50 μM), evaluated according to the formula $\Delta\delta = \frac{1}{2}\sqrt{\Delta\delta_H^2 - \left(\frac{\Delta\delta_N}{5}\right)^2}$; the residues exhibiting the largest CSP are highlighted in green. **(C)** Cartoon representation of YTH domain (PDB code: 4RCJ) with highlighted in magenta the residues exhibiting the largest decreases in signal intensity; in grey the unassigned residues. **(D)** Cartoon representation of YTH domain (PDB code: 4RCJ) with highlighted in green the residues exhibiting the largest CSP; in grey the unassigned residues. **(E)** Cartoon representation of YTH domain (PDB code: 4RCJ) with the three tryptophan of the binding pocket highlighted in blue on the protein in complex with m6A molecule, displayed as yellow sticks. The tryptophan residue W465 was not assigned in the NMR spectra.

3.3 Ebselen affects viability and migration of cancer cells, and interferes with the RNA-binding ability of YTHDF2

To evaluate the biological activity and the anticancer properties of Ebselen, we firstly evaluated its toxicity in a dose dependent manner in different cancer cell lines. We decided to focus on the prostate cancer cell line PC-3. We chose PC-3 as model, because YTHDF2, one of the three cytoplasmic reader proteins, was involved in cancer development and correlated with poor prognosis of prostate cancer patients (Li J et al, 2017). We evaluated the toxicity of the molecule by treating cells with different concentrations (1,5, 12.5,25,50,100 and 200μM) for three different time points, 24h, 48h, and 72h.Half Maximal Inhibitory Concentration (IC50), alias the measurement at which a

compound has suppressed the 50% of biological activity,were evaluated for each time point as shown in Figure 14, with the toxicity of compound increasing with the increasing hours of treatment. Moreover, as YTHDF2 was indicated to impact the invasiveness of PCa cells in the aforementioned paper, we assessed if Ebselen was able to modulate these events by blocking the activity of YTHDF2. To evaluate the impact of the treatment of the invasion rate of the PC-3 cells, we performed an *in vitro* scratch assay treating cells for 24h and 48h with 25μM of Ebselen, using DMSO as a control. The scratch width separating the cells was measured and we were able to assess that after 48h of treatment Ebselen prevented cells to migrate and fill the wound area, compared to control. Even if informative, scratch assay has its limitations and should be complemented with orthogonal assays, and also here we have focused mostly on comparing the effect of the molecule on the migration of PC-3 cells, while still, we need to demonstrate YTHDF2-dependency, by its depletion or overexpression.

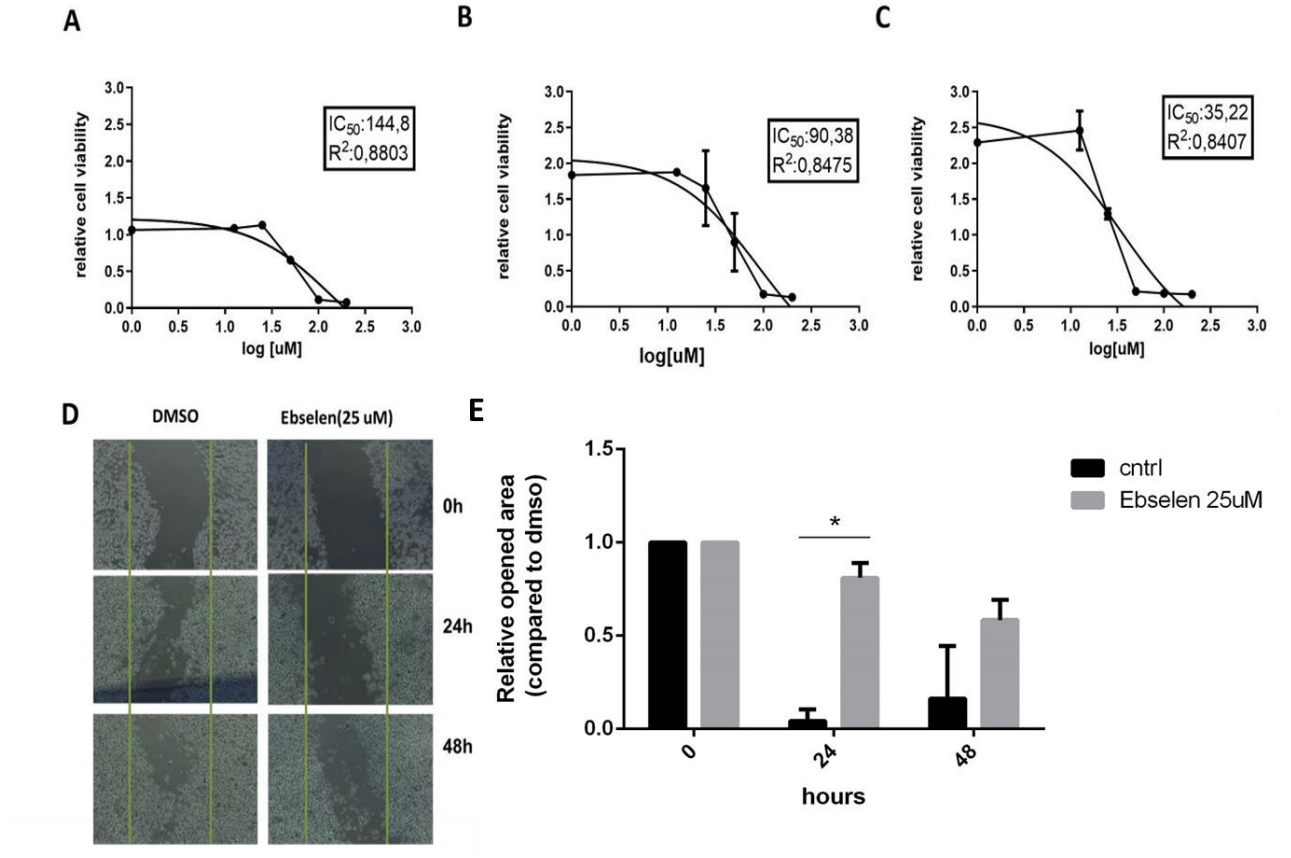

Figure 14. Ebselen affects PC-3 cells viability in a dose and time dependent manner, affecting also their migration rate. A) Cell viability was determined with OZblue kit after 24h of treatment with different Ebselen concentrations (1,5, 10, 25,50, 100 and 200μM), **B)** after 48h and **C)** 72h.Plotted bars are mean ± SD of a biological

duplicate, normalized to control (DMSO). Relative IC50 and R^2 were calculated by nonlinear regression curve fitting. **D-E)** Scratch assay in PC-3. Cells were treated with 25μM of Ebselen for 24h and 48h, and with DMSO as a control. Ebselen statistically slowed cell migration at 24h time point (*p* value:0.001497) compared to the other time points with paired t test between control and treated groups, and also at 48h time point albeit not significantly. The wound in **D)** was obtained with a 200μl tip, and the pictures were taken as a time lapse starting at time 0 were the scratch was first made. Residual open area at different time points was measured and analyzed with ImageJ software.

Since YTHDF2 is the cytoplasmic reader protein that is responsible for the turnover of target mRNAs, (Wang et al, 2014), we investigated the impact of Ebselen in interfering with its RNA-binding capacity and consequently with the regulation of the decay of some known targets that we picked from the RIP-seq analysis previously made in HeLa cells (Wang et al, 2014): the half-lives of CREBBP and SON genes in YTHDF2 depleted HeLa cells was measured and compared to control, finding out that they were increased. Since these mRNAs were taken from a RIP-seq made in a different cell model, we repeated the experiment maintaining the same conditions. We performed an RNA lifetime experiment treating HeLa cells with Actinomycin D for 0h, 1h, 3h. We compared the stability of CREBBP and SON mRNAs in cells transiently transfected for 72h with 100ng YTHDF2 siRNA (Figure 15C), cells transfected with scramble control siRNA and treated with 50μM of Ebselen or DMSO for 24h (Figure 15A&B). We obtained that, as expected, silencing of YTHDF2 increased the stability of the two mRNAs, while the treatment slightly increased it, although significantly only for CREBBP (Figure 15A).

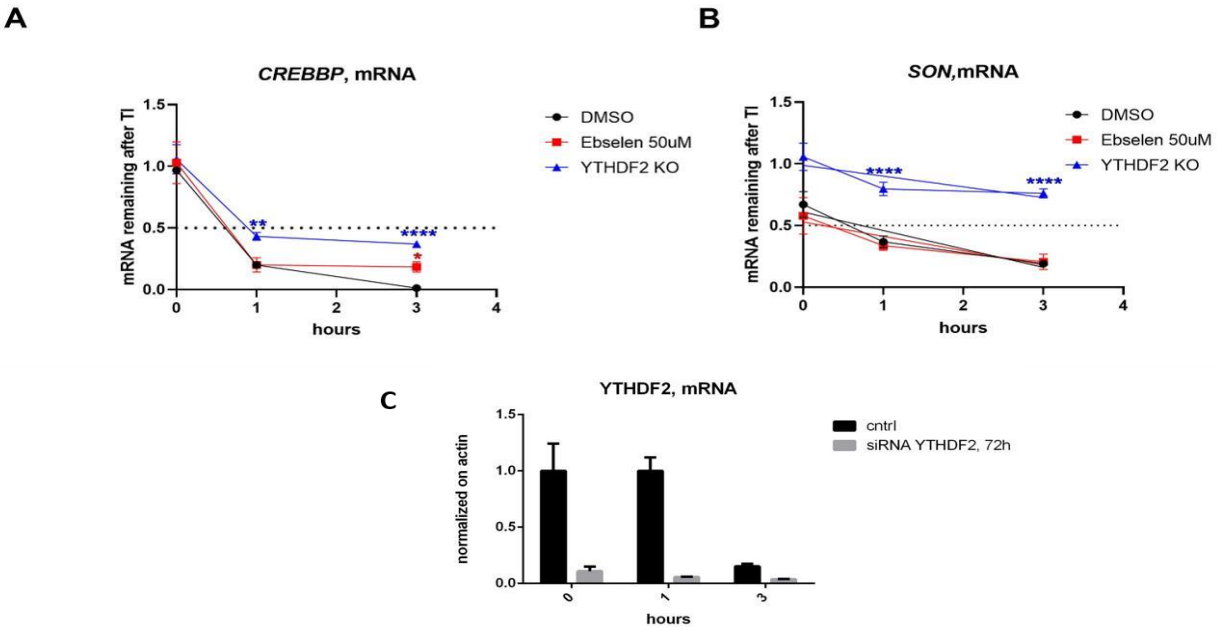

Figure 15. Effect of YTHDF2 silencing and Ebselen treatment on CREBBP and SON mRNA stability. A) mRNA remaining after Translation Inhibition (TI) after Actinomycin D chase was quantified with RT-PCR, using Actin as a control. CREEBP mRNA stability resulted to be enhanced by YTHDF2 silencing after 1h (p= 0,0022) and 3h of Actinomycin D treatment (p<0,0001), and slightly also by treatment with 50μM of Ebselen for 24h (p=0,0203), both conditions compared to DMSO control. **B)** SON mRNA stability resulted to be significantly enhanced only upon YTHDF2 silencing after 1h and 3h of Actinomycin D treatment (p=<0,0001). Data shown are means and SD of two biological replicates (n=2). **C)** Transient silencing of YTHDF2 with 100ng of siRNA after 72h of transfection was confirmed with RTPCR on the 0h time point samples.

After, to continue investigating the inhibitory activity of Ebselen toward the RNA-protein complex of the YTH domain, we performed an RNA Immunoprecipitation Assay in PC-3 cells, evaluating its activity towards YTHDF2 RNA binding capacity. We treated cells with a subtoxic dose of Ebselen (25μM) for 24h and with DMSO as control. After lysis of the cells and precipitation of RNA with both the YTHDF2 antibody and the relative IgG isotype as a control, we have performed Real Time Quantitative PCR (RT-PCR) to quantify the level of expression of the target mRNAs in each sample, and so to evaluate their depletion after treatment. We chose PEG10 and NOTCH2, because they were ranking as top 10 enriched genes in data taken from more than one PAR-CLIP on GEO (GSE63591, GSE49339, GSE86214), and were also interesting because they are both oncogenes (Xie et al., 2018; Xiu & Liu, 2019). We also choose CREBBP and SON, even if the latter did not result as significantly enriched in the YTHDF2-bound mRNA fractions, so we excluded it from the results. As shown in Figure 10, Ebselen treatment resulted to interfere with YTHDF2 and its targets, as suggested by the decrease of the mRNAs levels compared to control samples. The RNA immunoprecipitation has been normalized following the Percent Input Method, in which values obtained from the IP samples, both the IgG and the YTHDF2 fractions, are divided to the values obtained from the input, which is the 1% of RNA used in the RIP. All the values of the mRNA targets are also subtracted of the 18s values. In Figure 16, data are plotted as relative to the DMSO sample that we use as a control.

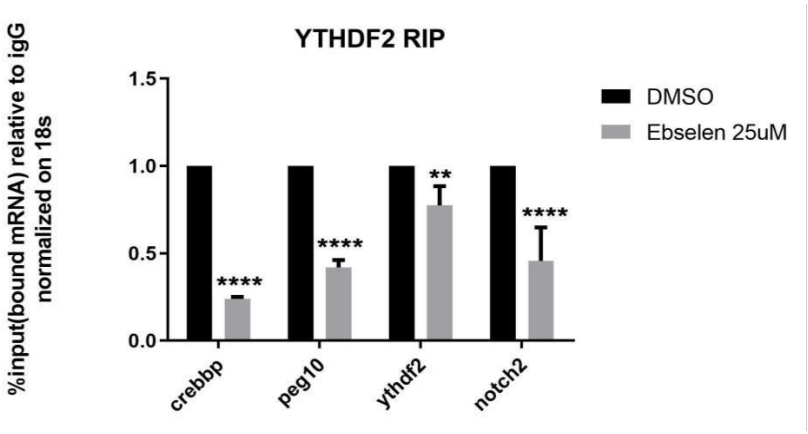

Figure 16. RNA Immunoprecipitation (RIP) of YTHDF2 after treatment with 25μM of Ebselen. RNA Immunoprecipitation Assay followed by RT-PCR. PC-3 were treated for 24h with DMSO (control) and 25μM of Ebselen. After cells were lysed and RNA precipitated with YTHDF2 antibody and the corresponding IgG isotype as negative control. Changes in the mRNA bound were quantified through RT-PCR, normalizing the values to 18s housekeeping and dividing the IgG and the YTHDF2 fraction values to the values obtained from the Input, that corresponds to the 1% of RNA used in the RIP. Data are plotted as relative of the DMSO sample, that is the control. Data are presented as means ± SD of a biological triplicate (**p=0.0015, ****p<0.0001, versus control).

3.4 YTHDF1 as a promising pharmacological target for Neuroblastoma

Thanks to preliminary data belonging to a group collaborating on the project aiming at drugging m6A in Neuroblastoma, we found that the expression levels of YTHDF1, and not of the other two cytoplasmic reader proteins, correlates with a worst prognosis in Neuroblastoma patients (Figure 17A,B&C),combined also with high levels of METTL14 (Figure 17D). For this reason we started focusing on the role of YTHDF1 in driving the development of this aggressive pediatric cancer, thanks also to the presence of pre-existing data sustaining the general role of m6A methylation in this particular model, still unstudied from an epitranscriptomic point of view.

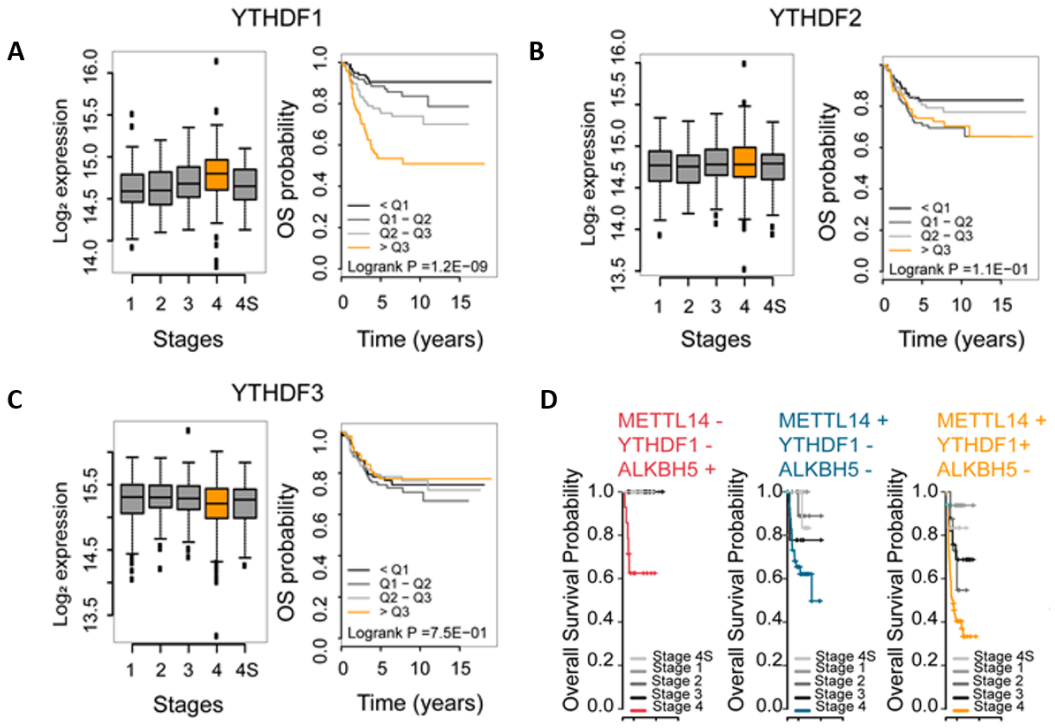

Figure 17. YTHDF1 expression correlates with worst prognosis in Neuroblastoma and is associated with METTL14 expression. A-C) RNA-seq expression of m6A "readers" in tumor samples from neuroblastoma patients (n=409), according to disease stages. Kaplan-Meyer curves showing overall survival (OS) probability of neuroblastoma patients with high expression of each factor. Number of total individuals n=409. Of the three YTHDFs proteins, only YTHDF1 high expression levels are associated with aggressive stage and increased mortality**. D)** In low expressing ALKBH5 samples, there is a combined high expression of METTL14 and YTHDF1 that identify patients with a worst prognosis than with METTL14 alone. All these data were analyzed by Dr. Erik Dassi, from The RNA Regulatory Networks Laboratory at DeCIBIO.

We initially characterized the expression level of this gene in various Neuroblastoma cell lines, both at the protein and mRNA level. We found that SK-N-DZ and CHP-134 lines were the ones with the highest expression levels of the YTHDF1 protein, while SK-N-BE(2) and SK-N-AS were the ones with the lowest level (Figure 18A). At the mRNA level, it was confirmed that CHP-134 is the neuroblastoma cell line with the highest level of YTHDF1 expression, while in the others there was no significant difference and all showed to have low levels of mRNA with respect to CHP-134 (Figure 18B).

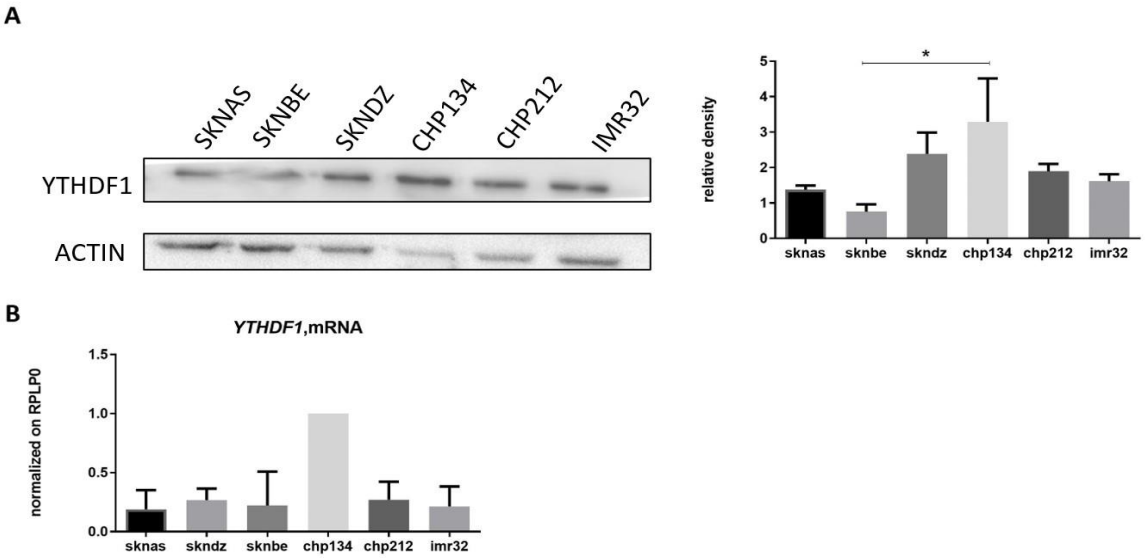

Figure 18. Quantification of YTHDF1 level of expression. A) Western blot and its quantification showing the level of expression of the YTHDF1 protein in six different Neuroblastoma cell lines. **B)** Quantification of mRNA expression of YTHDF1 by qRT-PCR in six different Neuroblastoma cell lines. CHP-134 is the Neuroblastoma cell line with the highest levels of YTHDF1, both on a protein and on a mRNA level.

To functionally study the effect of YTHDF1 on the development of neuroblastoma, we proceed in generating two stably overexpressing cell lines, choosing SK-N-AS and SK-NBE(2) because of their low endogenous level of protein and for their easiness in manipulation. We infected both lines with a pLenti CRISPR v2 vector containing the fulllength sequence of YTHDF1, we selected the positive pool of cells with Puromycin for two weeks and after assessing the presence of the overexpression with Western Blot, we started performing the phenotype experiments (Figure 19A) . Firstly, we evaluated the effect of the overexpression on cells proliferation compared to the WT lines. To do so, we used a Real Time Cell Analyzer (RTCA DP Analyzer, Roche), for which we needed to seed cells in an E-16 plate®, containing at the bottom of its wells gold microelectrodes that real-time monitors cell status, including number of cells, their shape/size and attachment. We seeded 5000 cells in quadruplicate for each conditions (WT and YTHDF1 OE) for both SKN-AS and SK-N-BE(2) and we let them grow for 144h, while their impedance was evaluated every 15min. We so observed that both the overexpressing lines, SK-NA-S and SK-N-BE(2), have an increased rate of proliferation compared to their corresponding control (Figure 19B). This experiment and the generation of the overexpressing lines was

carried out with the collaboration of Giulia Montuori of the laboratory of Translational Genomics (PI, prof Quattrone A.) of the DeCIBIO.

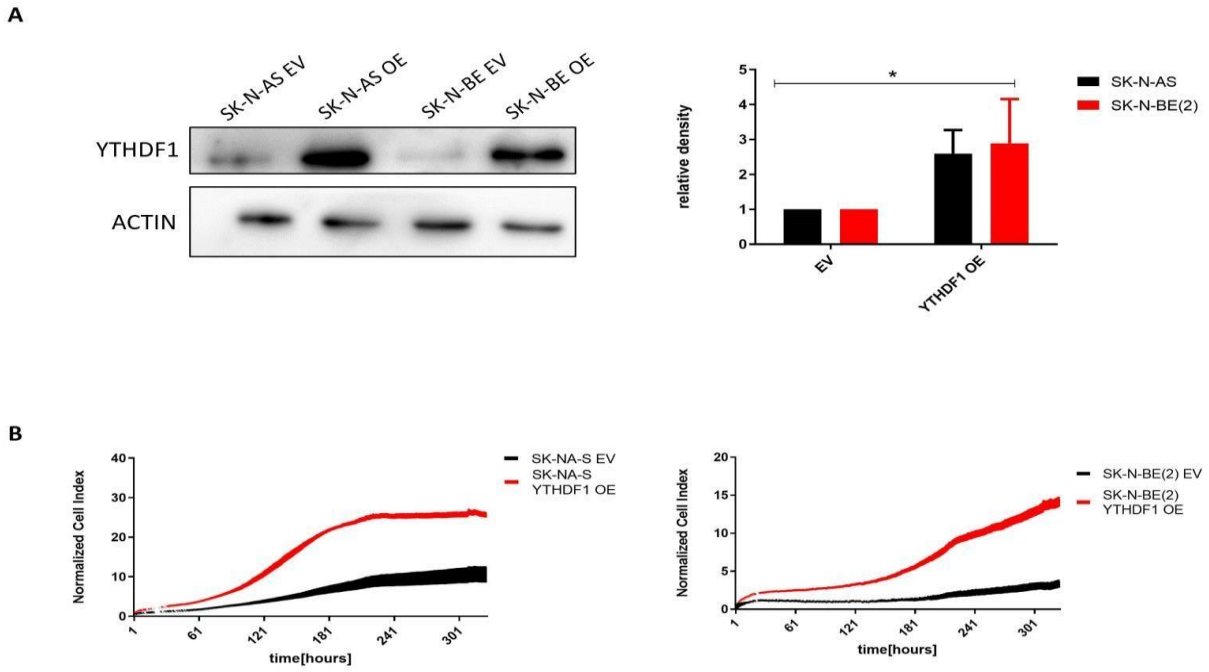

Figure 19. Generation of Neuroblastoma stably overexpressing YTHDF1 cell lines and Real Time proliferation assay. A) Western Blot and quantification confirming the stable overexpression of YTHDF1 in both SK-NAS and SK-NBE(2) after Puromycin selection for two weeks. **B)** Real time proliferation assay on the overexpressing YTHDF1 lines compared to their control wt. For both SK-N-AS and SK-N-BE(2) the overexpression of YTHDF1 enhances the proliferation rate compared to control. These experiments were performed with the collaboration of Giulia Montuori from the Laboratory of Translational Genomics at the Department of CIBIO.

After, we generated spheroids to investigate the effect of the overexpression on 3D cell cultures, as these have many advantages over monolayer cultures, as representing the best avascular *in vitro* tumor models (Ivanov et al., 2014). Most importantly, they resulted to be a more reliable model for preclinical drug screening, since they have showed often to have reduced sensitivity to certain drug treatments (Lv et al., 2017), with respect to monolayer cultures. To generate spheroids, we grew cells seeded at the lowest density in Ultra low attachment 96 plates, embedding them in medium containing low percentage of Matrigel. We incubated for 24h, and then we monitored their growth every three days, for twelve days in total, acquiring images with a Leica DM IL Led Microscope (5x magnification). We analyzed images with ImageJ, quantifying the dimensions of the spheroids with a macro designed and published in (Ivanov et al., 2014). SK-N-AS

generated very well round-shaped spheroids that could be easily analyzed already after three days of growth, while SK-N-BE(2) did not generate round-shaped spheroids, but more like very wide three dimensional cellular aggregoids, of which structures could be appreciated only starting after six days of growth. For this reason, the analysis of the images taken from the spheroids in culture differs between the two cell lines. We observed that, for both SK-N-AS and SK-N-BE(2), spheroids generated from the overexpressing cell lines had grown bigger than controls starting from the same number of cells (Figure 19A&B). That means that overexpression of YTHDF1 enhances Neuroblastoma cells proliferation and consequently also spheroids growth. Then we decided to use the spheroids generated to perform an invasion assay on Matrigel, but we used only the SK-N-AS lines because their shape made them easier to handle during the transfer to another support. We growth spheroids for nine to twelve days on ultra-low attachment 96 plates and then we transferred them manually, with the help of a 200µl pipet tip, into the wells of a normal flat bottom 96 plate, to after embed them in Matrigel covered with complete medium acting as a chemoattractant. We then took images every three days, starting from t=0, for six days in total, acquiring them with a 2x magnification, and analyzed the area of invasiveness with ImageJ. Even in this case, we observed that the overexpression of YTHDF1 enhanced the invasion rate in both the lines (Figure 19C). We then proceed in analyzing the frequencies of Tumor Initiating Cells (TICs) for both lines comparing wt to overexpression, performing a Limiting Dilution Assay (LDA). TICs constitutes a small subpopulation of cells that can sustain alone the maintenance of tumor proliferation, starting from a very low number of cells. For this aim, we seeded cells in 96 well format at a very low density, even lesser than the one we used for spheroid generations, but a bit more than the single cell culture that is required for clonal selection, obtaining to have a density of around ten cells/well. We left them growing for three/four weeks, and then counted all the wells that showed to have formed colonies inside them. Since the statistical significance of an LDA experiment relies on the fact that the active units per well must be distributed following a Poisson distribution, we used the ELDA software (http://bioinf.wehi.edu.au/software/elda/), developed and explained in (Hu & Smyth, 2009), to analyze the data obtained. We observed that the overexpressing cells have a higher frequency of TICs, that are plotted as % of the frequency (Figure 20D).

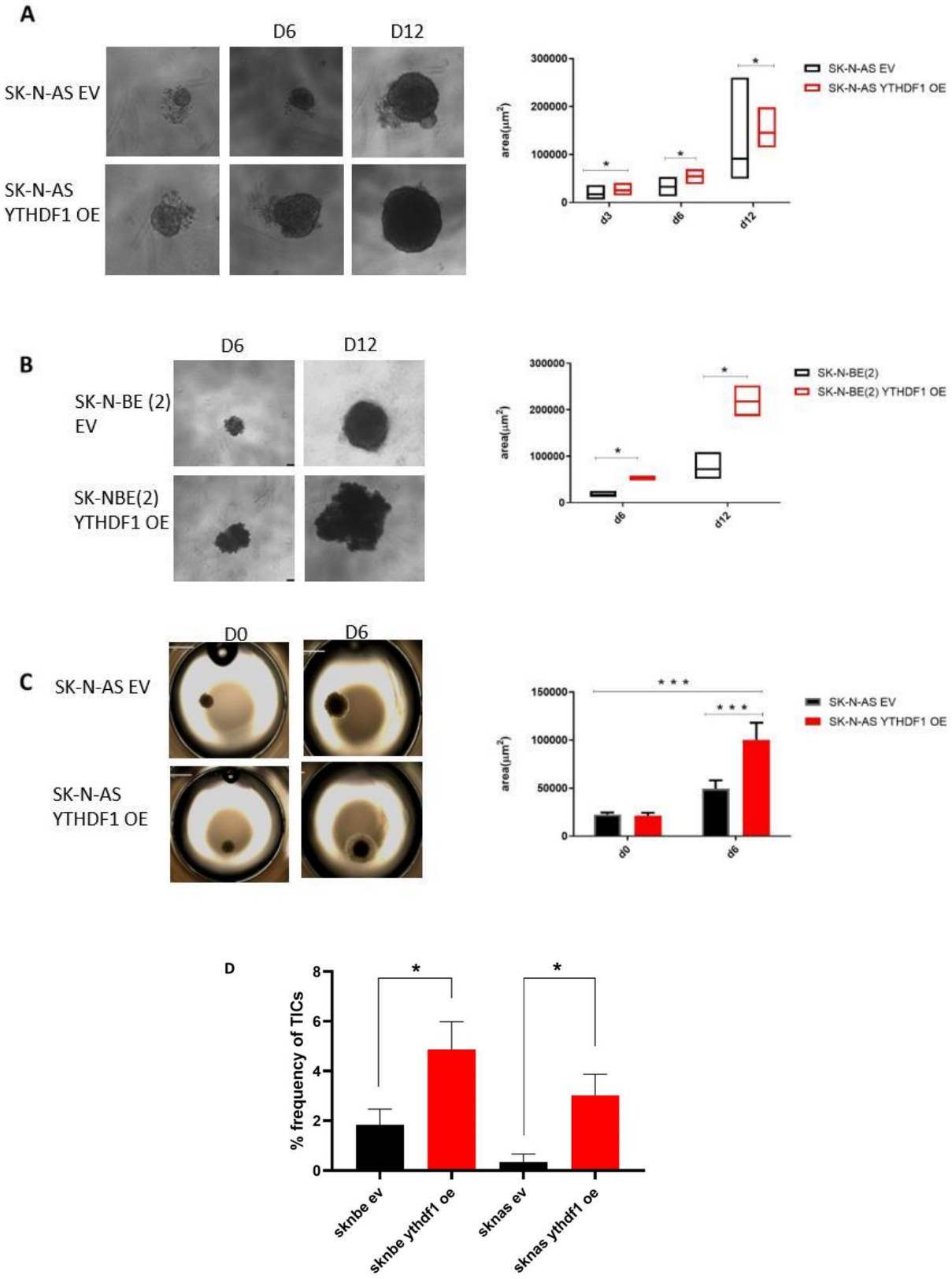

Figure 20. YTHDF1 overexpression enhances tumor-sphere forming ability of Neuroblastoma cells and their invasion ability. A) Spheroids generated from SK-N-AS cells, monitored every three days for twelve days. The line stably overexpressing YTHDF1 generated bigger spheroids. **B)** Spheroids generated from SK-N-BE(2) cells, monitored for twelve days. The structure of the aggregoids could be analysed only after six days of growth. In this case also the line

overexpressing YTHDF1 generated bigger spheroids. **C)** Invasion assay on Matrigel with spheroids generated from SKN-AS and SK-N-AS YTHDF1 OE cell lines. The invasion ability has been monitored for six days. The overexpression of YTHDF1 enhances the invasion ability of SK-N-AS compared to the control line. **D)** Results from the Limiting Dilution Assay plotted as frequency of the TICs (Tumor Initiating Cells). Both the overexpressing cell lines showed to have a higher frequency of TICs, as calculated with the software ELDA.

We then decided to analyze if the overexpression of YTHDF1 could influence the cell cycle progression of SK-N-AS and SK-N-BE(2). For this reason, we fixed and stained cells from monolayer cultures with PI staining, and we analyzed them with Flow Cytometry. We observed that the overexpression of YTHDF1 increased the percentage of cells in phase G1, significantly only for what concerns SK-N-AS (Figure 21 A&B).

We concluded that YTHDF1 overexpression enhances Neuroblastoma cells proliferation, as the overexpressing cells have a higher frequency of TICs and an increased percentage of cells belonging to the G1 subpopulation, at least for SK-N-AS, and increases also their tumor-sphere forming ability and their invasion ability. Still we lack some experiment to fully characterize the role of YTHDF1 that would be really informative, cause some of them are still ongoing, such as the generation of a stably silenced YTHDF1 line. For this aim we started infecting CHP-134, the Neuroblastoma cell line that showed to have the highest level of YTHDF1 expression, with a pLenti CRISPR v2 vector containing the sgRNA guide to obtain the KO of the gene. Selection CHP-134 with Puromycin has revealed to be difficult since this cell line tend to easily detach from flask and undergo apoptosis, so it took a bit of time to find the right concentration of antibiotics that can select positive infected cells without making them die, and that is the reason why we still struggling a bit to obtain a perfectly stably silenced cell line. Despite this, we decided to carry on with testing our lead compound Ebselen on the models that we have, since the results that we obtained until now suggested a strong relevant role of YTHDF1 in the maintenance of Neuroblastoma aggressiveness, making it possible to consider it as a new pharmacological target for this disease.

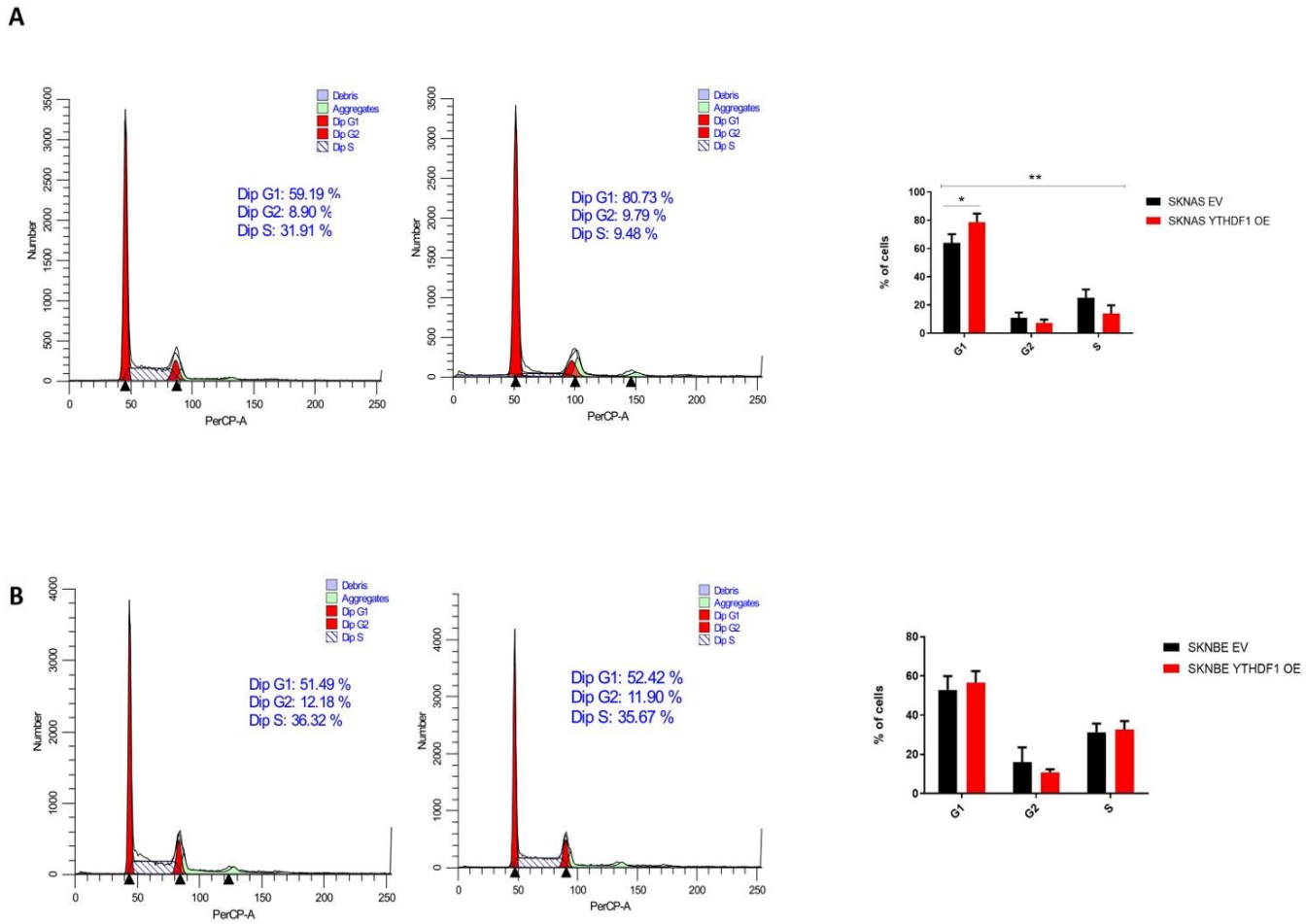

Figure 21. Cell cycle analysis of SK-N-AS and SK-N-BE(2) wt and YTHDF1 OE lines. A) Flow cytometry diagram of SK-N-AS EV and SK-N-AS YTHDF1 OE stained with propidium iodide (PI). The percentage of cells indicated in blue in the diagram refers to a single experiment, while the percentage in the graph on the right refers to three biological replicates. SK-N-AS YTHDF1 OE cells have an increase percentage of cells in the G1 subpopulation, and a decreased percentage in G2 compared to the control line. **B)** Flow cytometry diagram of SK-N-BE(2) EV and SK-N-BE (2) YTHDF1 OE stained with propidium iodide (PI). The percentage of cells indicated in blue in the diagram refers to a single experiment, while the percentage in the graph on the right refers to three biological replicates. In this case there is no significant differences in the distribution of cells in the different subpopulations.

3.5 Ebselen affects the tumor-sphere forming ability and the invasion rate of Neuroblastoma cells

We first assessed the toxicity of the compound on Neuroblastoma cell lines, treating them for 24h with different concentrations of Ebselen (1,6.25, 12.5, 25, 50 and 100μM) and using DMSO as a control.IC50 for each line was calculated after fitting the curves with

non-linear regression with the Graph Pad Prism software (Figure 22). The compound did not show high toxicity on these cells, with IC50 values all in a high micromolar range.

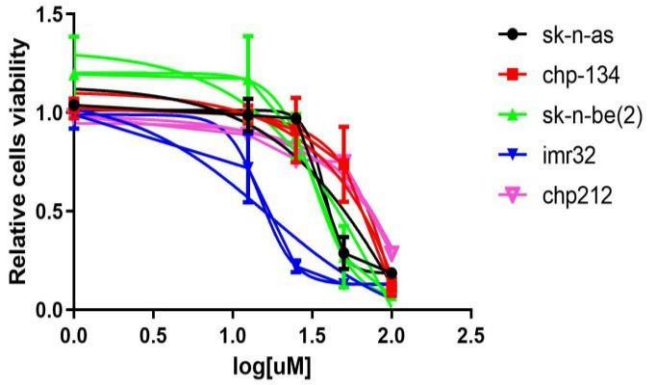

	SK-N-AS	CHP-134	SK-N-BE(2)	IMR32	CHP212
R^2	0,9880	0,9410	0,9467	0,9711	0,9584
IC50	37,87	~ 3236	32,90	15,07	~ 68734

Figure 22. Ebselen toxicity on Neuroblastoma cell lines. Cell viability was determined with OZblue kit after 24h of treatment with different Ebselen concentrations (1, 6.25, 12.5, 25, 50 and 100μM). Plotted bars are mean ± SD of a biological duplicate, normalized to control (DMSO). Relative IC50 and R^2 were calculated by non-linear regression curve fitting. Ebselen affect the viability of Neuroblastoma cells differentially for each line, with an IC50 in the micromolar range for SK-N-AS, SK-N-BE(2) and IMR32 and with very high values, in the millimolar range for CHP-134 and CHP212, meaning that for this lines it does not have any toxic effect.

After this, we decided to test the compound ability on the tumor-sphere forming ability of our overexpressing cell lines, knowing that probably the toxic effect would be even less compared to the one observed on monolayer cultures. We seeded cells to generate spheroids and soon after embedding them in medium containing Matrigel, we added the treatment after 24h and let them grow for three days prior to analyze their shape and size, starting to acquire images at t=0. We tested three different concentration of Ebselen, 12,5-25 and 50μM, and we compared their effect to DMSO control. We observed that Ebselen affected the tumor-sphere forming ability of SK-N-AS control line starting from 50μM, while it showed no effect on the SK-N-AS YTHDF1 OE generated spheroids, which appear also to be bigger than the control ones, as expected (Figure 23A&B). After 72h of treatment, we supplemented the medium of the spheroids with 1 mg/mL calcein-AM dye that once metabolized by viable cells becomes fluorescent. After 30 minutes, brightfield and

fluorescent spheroid photographs were automatically captured by Operetta imaging system (PerkinElmer) using a 10x objective. The intensity of calcein staining was calculated in the rim and in the center of the spheroids and plotted as the ratio between calcein area and spheroids area, as shown in Figure 15. Calcein staining confirmed that spheroids formation is affected starting from 50μM of Ebselen, while spheroids generated by overexpressing SK-NAS are not affected at all (Figure 24C&D).

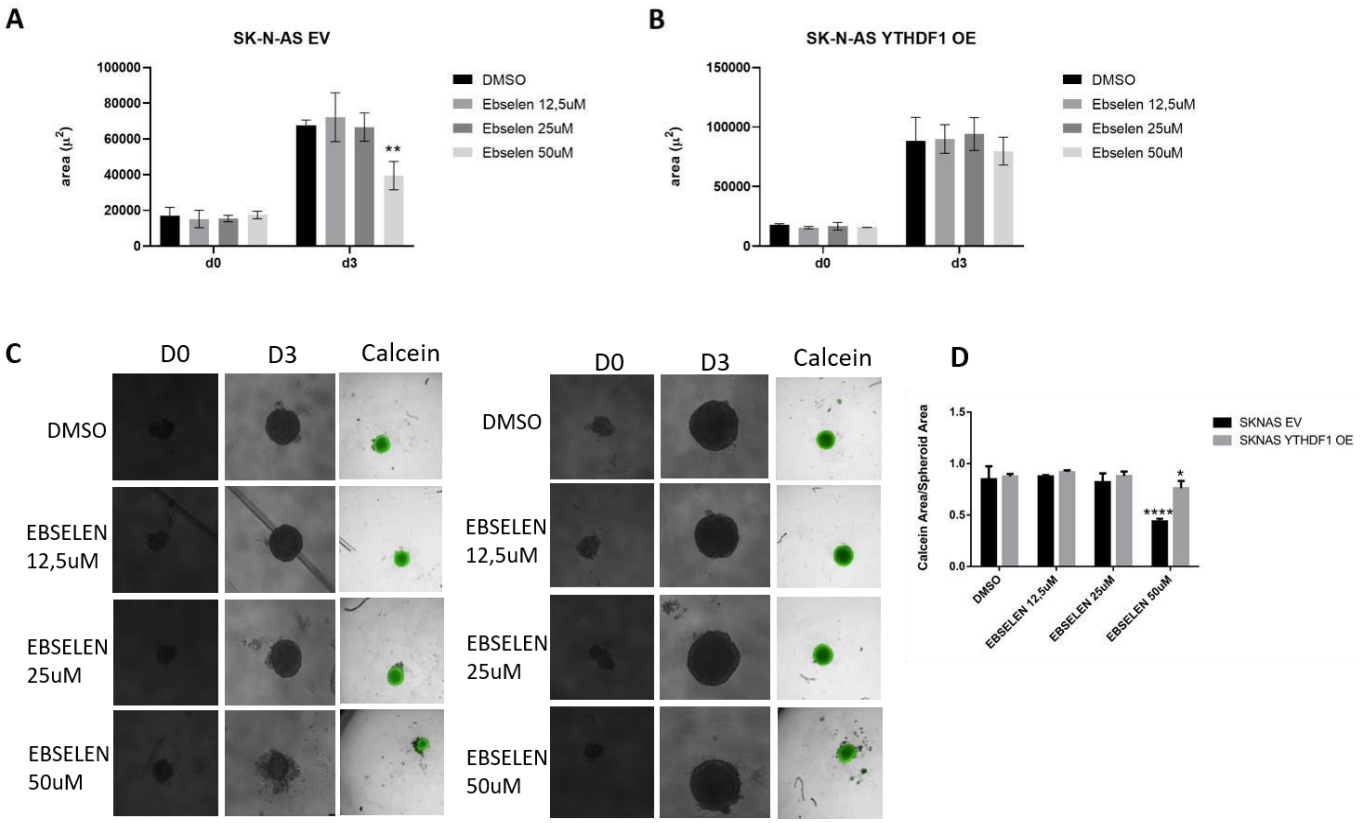

Figure 23. Ebselen affects the tumor-sphere forming ability of SK-N-AS at high doses. A) SK-N-AS EV spheroids were treated with three different concentrations of Ebselen (12.5-25-50μM) after 24h of seeding, for 72h, using DMSO as a control. Only at 50μM Ebselen affects the tumor-sphere forming ability of SK-N-AS EV (p=0,0084). **B)** SK-N-AS YTHDF1 OE spheroids were treated in the same way as SK-N-AS EV described in **A).** In this case, Ebselen did not show any significant effect on their tumor-sphere forming ability. **C)** Images of SK-N-AS EV and YTHDF1 OE spheroids taken before and after treatment, and the respective Calcein staining. **D)**Quantification of Calcein staining, plotted as the ratio between Calcein Area and Spheroid Area. The difference in the quantity of the staining is significant only for SK-NA-S EV treated with 50μM of Ebselen, as expected.

We also exploited the effect of Ebselen treatment on the invasion ability of SK-N-AS EV and YTHDF1 OE spheroids. We transferred spheroids growth for ten to twelve days from ultra-low attachment plates to flat bottom 96 well plates, we embedded them in Matrigel

and covered them in complete medium supplemented with DMSO or 25µM of Ebselen. We let them expand for six days, acquiring images starting from t=0 with a 2X objective. We then measured the area of invasiveness with ImageJ, and we observed that the treatment slightly impaired the invasion rate of the SK-N-AS EV spheroids, albeit not significantly, while it did not have any effect on the overexpressing YTHDF1 spheroids (Figure 24A,B&C).In both the spheroids treatments and the invasion assays the overexpression played a protective role that counteracted the efficacy of the compound.

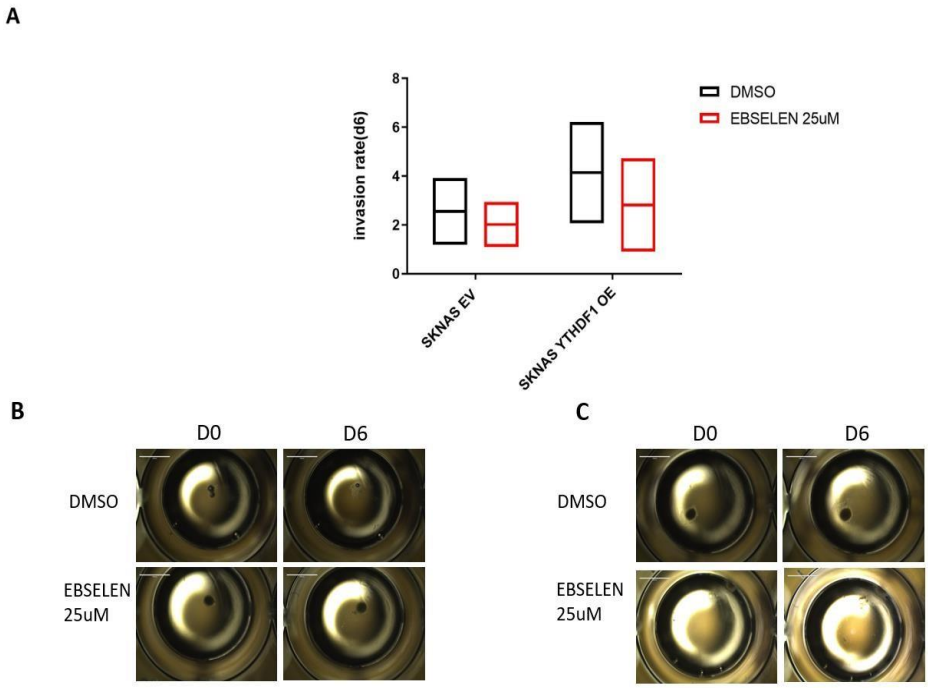

Figure 24. Effect of Ebselen treatment on the invasion rate of SK-N-AS EV and YTHDF1 OE spheroids. A) Quantification of the area of invasiveness over the course of 6 days; means n = 2 independent experiments. The effect of Ebselen treatment slightly impaired the invasion rate of both SK-N-AS EV and YTHDF1 OE spheroids, albeit not significantly. The invasion rate of YTHDF1 OE is still higher than the control line. **B)** Images of the area of invasiveness of SK-N-AS EV spheroids taken at t=0 and t=6, of both the DMSO and the treatment conditions. **C)** Images of the area of invasiveness of SK-N-AS YTHDF1 OE spheroids taken at t=0 and t=6.

To better understand if this was due to the highest levels of YTHDF1, we also generated spheroids from CHP-134 cells, the cell line with the highest endogenous level of protein, as shown in Figure 18, we firstly analyzed their shape and size and then we added the treatment with the three concentrations of Ebselen after 24h from seeding, for 72h. We acquired images starting at t=0 and after 72h of treatments. We observed that, as expected, treatment with the same concentrations of Ebselen did not show any effect on

the tumor-sphere forming ability of CHP-134, accordingly also with the IC50 calculated in Figure 22, that resulted to be in the high millimolar range.

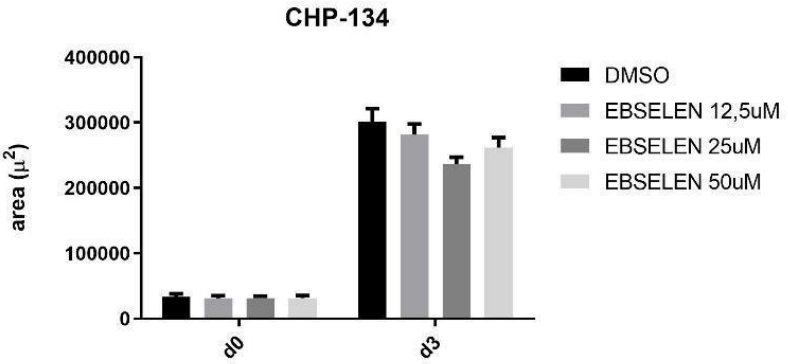

Figure 25. Effect of Ebselen treatments on CHP-134 spheroids. CHP-134 spheroids were treated after 24h from seeding with three different Ebselen concentrations (12,5-25-50μM). Treatments did not affect the tumor-sphere forming capacity of this cell line, as observed for the SK-N-AS YTHDF1 OE line, having a high endogenous level of YTHDF1.

3.6 Ebselen treatment on Drosophila resembles the *ythdf -/-* model phenotype

Thanks to the collaboration with Alessia Soldano, current member of the laboratory of Translational Genomics at the department of CIBIO, it has been possible to test the effect of the molecule *in vivo*, on Drosophila. According to the experimental design, two concentrations of drug and DMSO as control were administered to the Drosophila larvae mixing it with the water used to prepare the lyophilized food. We used 50 and 100μM of Ebselen and used DMSO alone as a control, having for each condition a final concentration of DMSO not above the 0,25% to avoid toxicity effects. Drosophila larvae were left reaching maturity, but treatment was added again prior to their entering the pupal stages, in which they would not be able anymore to feed themselves. The total duration of their life cycle before reaching adulthood lasted ten days, during which, apart from the pupal stages, the flies were able to feed and swallow the drugs at the same time. Their brain were then extracted and dissected, to observe the drug effect on the development of their brain, since as previously observed by Alessia Soldano (unpublished data), the KO

model of the only ortholog cytoplasmic protein of YTHDF1, that here we will refer to as *ytdhf-/-*, showed a visible impairment in brain development. In particular, she found that the two mushrooms bodies are fused together in the KO model, while in the wt they are normally in close proximity as sharing a lot of synaptic connections, but not fused in a single body at all. Mushroom bodies are brain structures present in insects that are responsible for olfactory learning and memory, and for this reason very dense in neuronal processes. After dissecting the brains of adult flies treated with the different concentrations of drug, we found that there was a high penetrance of the same phenotype as the *ythdf-/-* model, with the fusion at the level of the mushroom bodies. Curiously, the highest penetrance of the phenotype was observed for the flies treated with 50µM, while flies treated with higher concentrations of Ebselen showed with less frequency this phenotype. A low penetrance of the same phenotype was also found in the DMSO control, but we concluded that was due to some random mutation occurred during the larvae development. Our hypothesis was that most of the young larvae did not survive to the highest concentrations of treatment and failed to reach adulthood, so the ones that survived were the ones that showed mild defects in brain development or were not affected by the treatment at all. In conclusion, this experiment is to be considered a starting point to further investigate whether the biological effect of Ebselen is dependent on *ythdf*, given the fact that the treatment and the gene silencing shared the same phenotype.

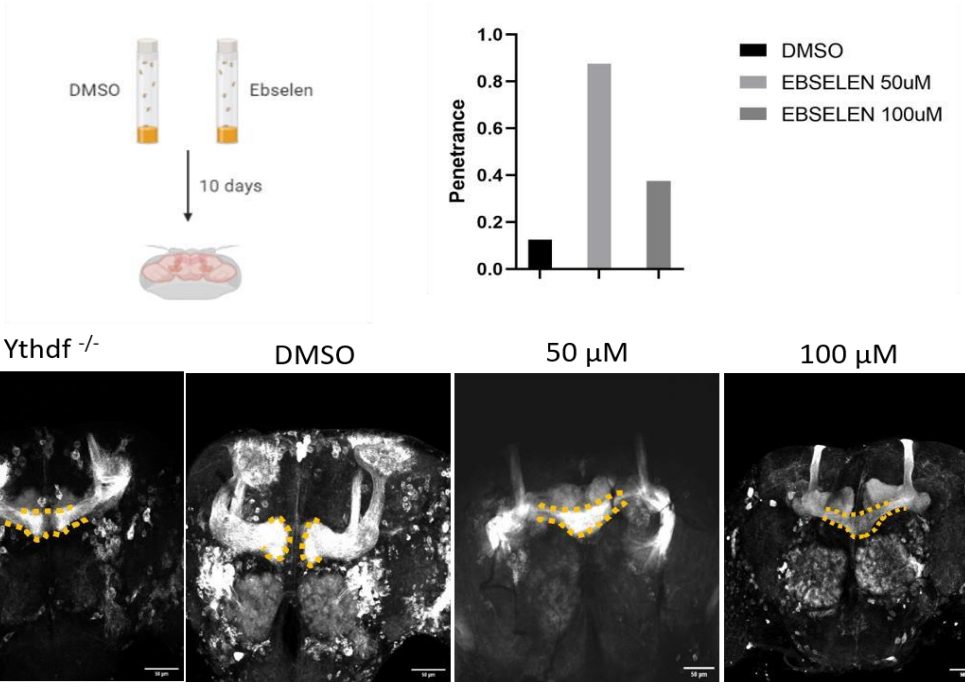

Figure 26. Effect of Ebselen treatment on Drosophila brain development. Drosophila larvae were treated with two concentrations of drugs, 50 and 100μM, that were administered through the water used prepare the lyophilized food. They then were left growing and reaching adulthood following their normal life cycle for ten days, after which adults were collected and their brain dissected for further analysis. It was possible to observe that the treatment with Ebselen caused an impairment in brain development, causing the fusion of the two mushroom bodies, with a phenotype identical to the one previously observed in the ythdf-/- model. The penetrance of the fusion phenotype, as indicated in the graph, is higher in the 50μM Ebselen treated flies than the 100μM Ebselen treated flies.

3.7 Ebselen analogues

Ebselen showed to have a covalent interaction with the YTH domain, forming a selenium sulfide bond with a Cys residue in the hydrophobic pocket. Covalent drugs usually shared a strong interaction with their target, so stronger potency and a longer duration of their biological effect. This kind of interaction could also lead to higher toxicity caused by difficulties in disassociation from off-target bindings. Ebselen, though being a covalent drug, did not show a very strong interaction with the YTH domain, at least not under the micromolar range, neither a high toxicity even if we cannot exclude off-target bindings. We decided to test some other molecules sharing the same scaffold of Ebselen, to maintain the structure that fitted well in the hydrophobic pocket but at the same time avoiding the covalent binding. We choose to test the oxidized analogue of Ebselen, Ebselen oxide, in which the selenium is occupied by a double bond with an Oxygen atom, and other two not commercially available analogues, Benzisothiazolone, in which the selenium atom was substituted with a sulfur atom and the phenyl ring was eliminated and substituted with a hydrogen atom, and N-Phenylphthalimidine in which the selenium compound was substituted with a simple carbon atom. We firstly tested their ability to interact with the YTH domain with the fluorescence quenching assay, using a series of micromolar concentrations (0-12.5-25-50-100-200μM). Only Ebselen Oxide showed to quench the fluorescence of the protein at each concentration, with a little less efficacy than Ebselen, while the other two had no effect at all. We continued testing the capability of Ebselen Oxide to inhibit the YTH domain binding ability, so we performed a REMSA using two concentration of compound (5 and 10μM) comparing it with Ebselen, and we observed that it was identically able to disrupt the protein-RNA complex formation. We then performed Alpha Screen® assay to evaluate the ability of Ebselen Oxide to inhibit the formation of the

RNA-complex in saturation binding conditions. Knowing already the Kd of interaction between the protein and the ssRNA that we calculated elsewhere, we fitted on AlphaScreen saturation curves the *K*i values, quantifying the inhibitory efficiency of Ebselen Oxide with different concentrations in the μM range (0-100 μM), obtaining a *K*i of ~11,56 μM, which is still in the micromolar range but a little bit higher than the one observed for Ebselen. We also repeated the mass spectrometry experiment that we have done with the protein incubated with 50μM Ebselen in presence or in absence of 1mM DTT, to understand if the interaction between the two molecules was due to covalent binding. We hypothesize that since Ebselen Oxide has the selenium atom occupied in a double bond with an oxygen atom, there could not be a covalent interaction with the protein. We observed instead the same outcome as for the Ebselen, that in the presence of DTT the interaction with the protein disappeared, meaning that the molecule lost its oxidized state and it is probably reduced by the buffer of the reaction. The fact that the molecule is less efficient in inhibiting the YTH domain could mean that in solution it exists in both the oxidized form and the reduced form, that is the one responsible for the stronger interaction with the domain, but to ensure this further analysis would be needed.

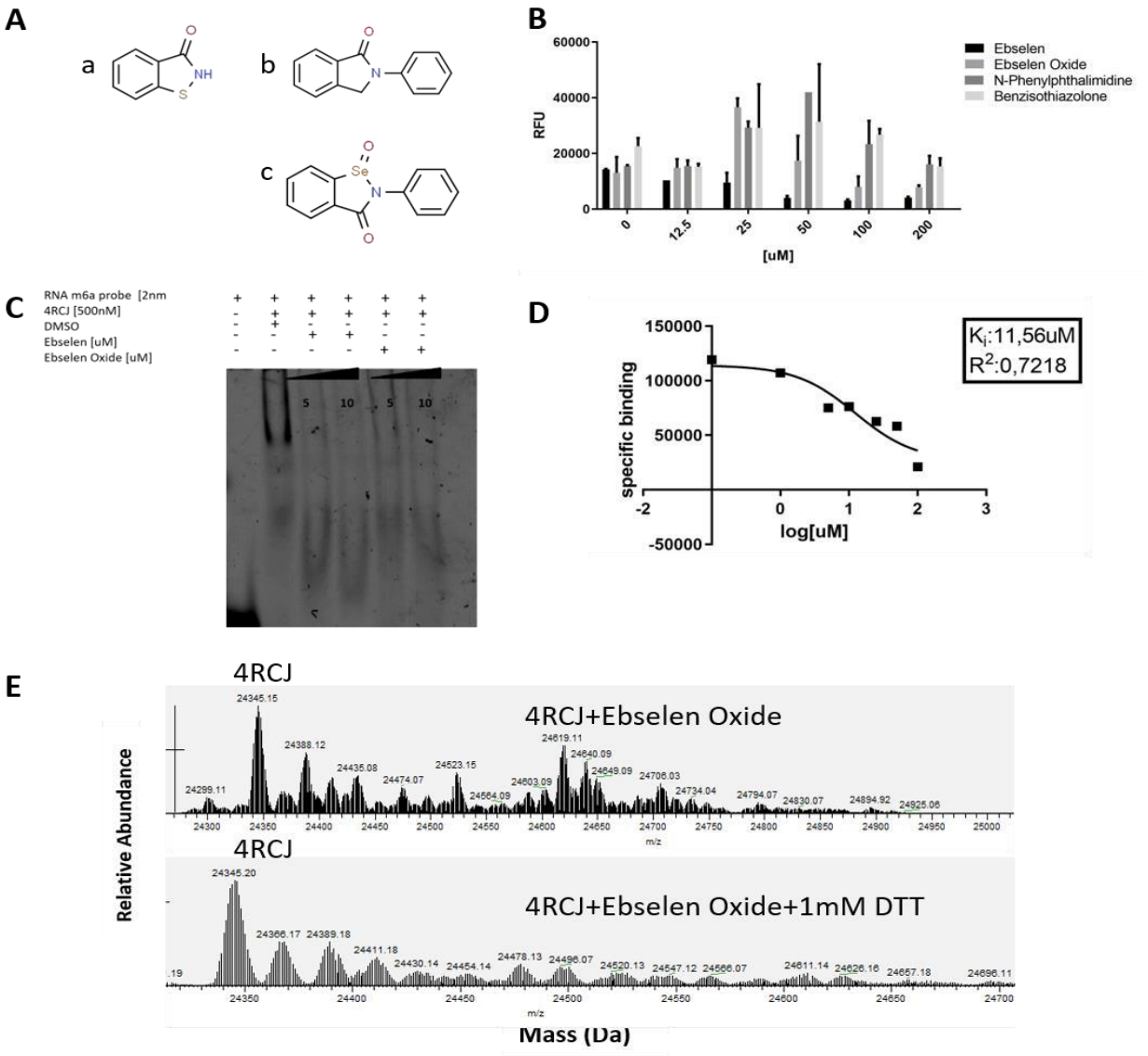

Figure 27. Testing Ebselen analogues. A) Chemical structures of the Ebselen analogues tested. a)Benzisothiazolone, b)N-Phenylphthalimidine and c)Ebselen Oxide. **B)** Tryptophan fluorescence quenching assay to test the efficacy of the analogues in binding the YTH domain, using five different concentrations (0-12.5-25-50-100-200μM). Only Ebselen Oxide resulted to interact with the YTH domain, even if with slight less efficacy than Ebselen. **C)** REMSA assay confronting Ebselen and Ebselen Oxide at 5 and 10μM efficacy in disrupting the RNA-protein complex. **D)** Determination of the Ki of the Ebselen Oxide molecule with Alpha Screen® Assay, using nonlinear regression fits of the data according to 1-site fit Ki model: R^2=0,7218.The concentration (50 nM) and the Kd (70 nM) for the labeled Bi-TNF probe, calculated elsewhere with another assay, was kept constant. **E)** Mass spectra of the 4RCJ structure of the YTH domain alone and incubate with 50μM of Ebselen Oxide in presence or absence of 1mM of DTT. In this case, the mass of the complex corresponds to the one of the protein alone, meaning that Ebselen Oxide double oxygen bond is reduced in solution and shows to have indeed a covalent interaction with the domain that otherwise has been disrupted by DTT.

We then evaluated the toxicity of Ebselen Oxide by treating PC-3 cells with different concentrations (1,6.125,12.5, 25,50, 100 and 200μM) for two different time points, 24h and

48h. IC50 were evaluated for each time point as shown in Figure 21, with the toxicity of compound increasing with the increasing hours of treatment. Ebselen Oxide showed to be a little more toxic on these cells with IC50 always in the high micromolar range but lower than the ones showed by Ebselen on the same cell line (Figure 14).

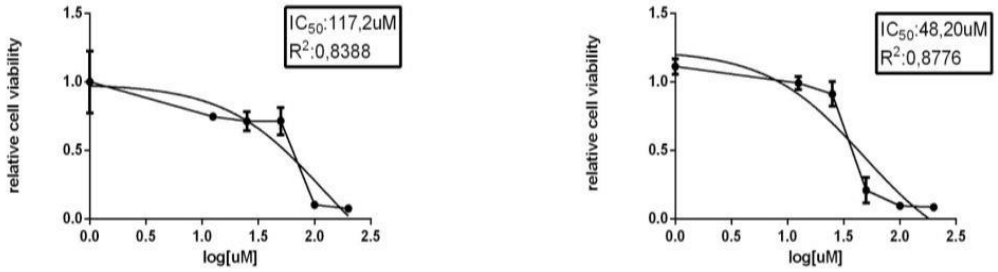

Figure 28. Ebselen Oxide toxicity on PC-3 cells. Cell viability was determined with OZblue kit after 24h and 48h of treatment with six different Ebselen concentrations (1, 6.125, 12.5, 25, 50,100 and 200μM.Plotted bars are mean ± SD of a biological duplicate, normalized to control (DMSO). Relative IC50 and R^2 were calculated by nonlinear regression curve fitting. Ebselen Oxide resulted to be toxic for PC-3 cells always in the high micromolar range, but with IC50 slightly lower for both the 24h and 48h time point with respect to Ebselen, as observed in Figure 13.

4.Discussion and Future Aims

Regulation of gene expression happens at different levels in Eukaryotes. Some of them can be unwritten, and not hereditary, such as epigenomic regulation of gene expression. Recently the new discovered field of epitranscriptomic brought the focus on another layer of gene expression regulation, an eventually even more dynamical and reversible, given by RNA modifications upon coding and noncoding RNAs. Only recently, it has been started to investigate the role of these modifications on gene expression, also because the technology to identify, quantify and map them was being developed in the last decade. RNA modifications, as I already said in the Introduction section of this thesis, brought with them a lot of new protein classes working on RNA called writers, erasers, readers that

work together to add, remove and recognize them, and are starting also to be linked to cancer development. For this reason, there is a growing interest in starting to consider them as potential therapeutic targets. In this thesis, I focused on the N6-methyladenosine methylation, and on the role exerted by its eukaryotic cytoplasmic readers, the YTHDFs family of proteins, in cancer development, with a particular focus on Neuroblastoma, which is a model in which the epitranscriptomic roles are still unknown, with the aim of targeting its RNA-binding ability to stop the progression of the tumor.

Here we showed the first attempt to design and perform a High Throughput Screening targeting the YTH domain, the RNA binding domain conserved in the family of readers of the m6A modification bearing the same name. We figured that the YTH domain was the perfect target to exploit, between all the other methylation machinery members, for its being an RBP and not an enzyme, like the writers and the erasers, targeting which could generate a major and unpredictable post-transcriptional effect that could result in more severe side effects. Indeed, there is in literature just one example of a screening carried out targeting the writer protein METTL3 (Seidelberg, 2019), that resulted in the finding of small molecule enhancing its methylation activity rather than inhibiting it. The YTH domain gave us also the possibility to use a simple and fast technique to screen a complete library of compounds, Tryptophan fluorescence quenching, having three very well conserved tryptophan residues in its hydrophobic pocket. We started by testing if it was amenable for HTS, by checking the quenching effect of N6-methyladenosine and methylated RNA probes on the fluorescence of the domain, obtaining a specific effect of the modified molecule compared to the unmodified ones, Adenosine and unmethylated probes (Figure 8). These observations gave us the confidence to calculate the Z factor of the assay and go straight to the HTS, for which we tested a library of 2000 compounds. First, we sorted out more than 100 potential positive hits, but after secondary screening and other intense filtering, we were left with just one candidate molecule. Ebselen, the molecule that became our candidate hit, it is a synthetic organoselenium compound with known anti-oxidant, anti-inflammatory and also showing an efficient antibacterial action (Marshall et al., 2019). But Ebselen it has also been approved for clinical trial for the treatment of Hypo/Mania (https://clinicaltrials.gov/ct2/show/NCT03013400) as a lithium like drug, and has been in clinical trial also for stroke (Yamaguchi et al., 1998).

We were able to describe for the first time the inhibitory activity of a small molecule towards the YTH domain with several biochemical assays, obtaining dose-response curves of interaction and also identifying the residues inside the binding pocket that are involved in the interaction with the compound through NMR (Fig. 12). We were also able to identify that the interaction between the YTH domain and Ebselen it is covalent (Fig. 13). The full nature of this interaction is anyway still to fully understand, since this molecule has already been reported to be a cysteine modifier, causing reversible or irreversible modification based on incubation time and concentration (Mukherjee et al., 2014).

Repeating the mass spectrometry experiment using different concentrations of compound would be necessary to uncover the exact means by which the inhibition mechanism happens, and also performing a mutagenesis experiment targeting the only Cys residue present in the hydrophobic pocket to analyze how the interaction could be affected.

We, for the first time, assessed the anticancer activity of the compound in a model in which the oncogenic function of one of the cytoplasmic readers was already been documented (Li et al., 2018). In PCa cells, YTHDF2 was observed to be overexpressed and consequently after its silencing, they observed that the clonogenicity and the invasion ability of the tumor were impaired. We tested the effect of the compound on PC-3 cells and found that is mildly toxic, with toxicity increasing according to the time of treatment, with an IC50 of 35.22μM after 72h of treatment with different concentrations (Fig. 14), and it affected cell migration. We also check its effect on modulating the mRNA targets of YTHDF2, evaluating their level of expression after 24h treatment with RNA immunoprecipitation. We choose CREBBP, PEG10 and NOTCH2 that were known to be YTHDF2 targets (Wang et al. 2014), even if still not checked in PCa cells, and we observed for the first time that all of them were enriched in the YTHDF2 fractions, so they were to be considered bona fide targets of the protein also in this cancer model, and most importantly that the treatment impaired the interaction of the protein with them (Fig. 16). Being YTHDF2 the reader that is involved in the regulation of mRNA decay, we tested the half-life of CREBBP and SON mRNAs, that were already been used in literature for the same purpose (Du et al., 2016; Wang et al., 2014). There is still no direct evidence of the involvement of these particular mRNAs in the development of PCa, but both PEG10 and NOTCH2 have recognized oncogenic roles (Xie et al., 2018; Xiu & Liu, 2019).

We found that Ebselen treatment increased CREBBP stability (Fig. 15) even if not as strong as the YTHDF2 silencing. The modulation of these target mRNAs by Ebselen treatment was a proof of concept of its capability of targeting specifically the YTH domain, but at the same time raised a question about its protein specificity, since in the cell there are in total five different YTH containing proteins, sharing high percentage of similarity, which is possibly another reason why there are still not attempts to target this domain, even if it is not the only family of proteins that share a domain used as a target for drug discovery, as learned by the bromodomain-containing histone modifiers proteins (Cochran et al., 2019). Since we cannot exclude that the treatment affects also the other readers, we should focus on looking at the most expressed or the one playing a critical role among the others on the model that we are studying in that moment; the idea to overcome this matter is to modify the molecule, after SAR analysis, taking into account also the residues that lies out of the pocket but that slightly differentiate the five proteins from one another. Still, we can consider ours the first successful attempt to characterize a small molecule interacting with the YTH domain, that has also a mild inhibitory activity towards it, that can be considered a starting point to develop other screenings in the future.

After this, we started to investigate the role of YTHDF1, another cytoplasmic reader, in the development of Neuroblastoma. Neuroblastoma (NB) is the most common extracranial solid tumor in early childhood, and it is a very unusual tumor characterized by a substantial heterogeneity of manifestation: from a very aggressive disease to completely spontaneous regression. This peculiar characteristic, coupled with a robust quantitative imbalance in the transcriptome, suggests the involvement of post-transcriptional modification in NB development and progression. Thanks to preliminary correlation data derived from a bioinformatic analysis of patients, performed by Erik Dassi from the Department of CIBIO, collaborating also on this project that involves more than one work group, it was clear that YTHDF1, and not the other YTH domain family proteins, correlated with poor prognosis in NB patients (Figure 17). We demonstrated the involvement of YTHDF1 in sustaining NB aggressiveness generating two stably overexpressing cell lines, that showed to be higher in proliferation, generate bigger spheroids that had also a higher rate of invasiveness compared to the control (Fig.22-23). We then tested the effect of Ebselen treatment, and fpund that it affected only the wt cell lines, while the overexpressing ones showed a sort of resistance towards it (Fig 23). We hypothesized that, since the interaction with the domain

is covalent, this happens till all the disposable Ebselen titrates the protein, saturating it and preventing its binding with RNA, so the same concentration of drug used for the control line was not sufficient in the overexpressing line, in which the protein expression level is higher. To understand if this mechanism could correlate with the expression levels of YTHDF1, we generated and treated spheroids from a NB cell line that we observed as being the one with the highest endogenous level of YTHDF1 (Fig. 18), obtaining that, in fact, the spheroids were not affected by none of the concentrations of Ebselen tested.

We also tested our compound in a *in vivo* model, the fruit fly Drosophila Melanogaster, in which the m6A methylation has been described to be involved in brain development and sex determination (Haussmann et al., 2016; Lence et al., 2016).

We performed this experiment in collaboration with Alessia Soldano, from the laboratory of Translational Genomics at the Department of CIBIO, who administered the drug to the larvae and dissected and analyzed the brain of the adults. She previously observed, in a fly model KO for YTHDF1, that the ablation of the protein caused a fusion at the level of the mushroom bodies, that are normally in close proximity sharing lot of synaptic connections but indeed separated (Akalal et al., 2006).We hypothesized that the highest dosage could have been lethal to the larvae, and thus less of them survived and reach adulthood showing the brain impairment, while with 50µM we observed a higher number of individuals sharing that phenotype cause it was less toxic for the young flies. The fact that the phenotype observed in the KO and in the treatment was the same it was an indication of the specificity of the molecule towards its target, but indeed it was not intended to exploit the therapeutic role of the drug on Drosophila as an *in vivo* model, but just as a proof of concept that the drug is working against the YTH domain. To fully understand how the targeting of YTH lead to the observed phenotype further experiments would be needed, in particular aiming at the characterization of the mRNAs displaced from the protein that play pivotal roles in brain development; to test the therapeutic efficacy of the drug on Drosophila we would have needed instead a model mimicking the development of Neuroblastoma, but actually the only available is one that bears mutation in the ALK gene, which encodes for a neuronal receptor tyrosine kinase, that is implicated in many other cancers. For this reason, it cannot be considered a specific model for NB. Since this was

not our main purpose, we did not pursue further on this way and left it aside, to explore it deeper in the future.

Since we had in mind to design more efficient molecules targeting the YTH domain deriving from Ebselen, after having obtained a crystal structure of the YTH domain together with the drug as a starting point for further structural-based design, while waiting to obtain this tool we started testing some already commercially available analogue of Ebselen. We tested Benzisothiazolone, N-Phenylphthalimidine, and Ebselen Oxide, obtaining that just the latter successfully quenched the fluorescence of the protein (Fig. 27). We further characterized the interaction of the oxidized version of Ebselen with the YTH domain, discovering that also this molecule, unexpectedly, interacted with it through a covalent bond (Fig. 27). This is probably because, even if the selenium atom is involved in a double bond with an oxygen atom, the ambient of the reaction is able to reduce selenium anyway. Probably Ebselen oxide in solution is at the equilibrium with its reduced version, explaining both why the molecule appears to have a covalent bond with the domain despite the oxygen and why it is less effective compared to Ebselen alone. We did not further characterize both biochemically and biologically the effect of this molecule because we were searching for a more potent analogue, possibly not interacting covalently with the YTH domain, and this molecule did not answer to our requests.

Our future plans indeed comprise the repetition of a High Throughput Screening using another approach, HTR-FRET, always targeting the domain, that is based still on a fluorescence approach but much more sensible and with less background, similar to the one presented in (Wiedmer et al., 2019).

In this case, our aim is to transform the YTH domain and a methylated RNA probe in a FRET pair, by coupling the protein with an anti-His antibody conjugated with the Eu3+ fluorophore, and the RNA probe with the corresponding acceptor fluorophore of the Eu3+ molecule through a biotin-streptavidin interaction. In this way, if a molecule succeeded in displacing the RNA probe from the protein, there would be no FRET signal to collect. This assay, even if more complicated than the fluorescence quenching one that we already performed, is anyway still cheaper than other approaches and as the pros to generate a low number of false positive and to require very low concentrations of reagents, due to its high sensitivity.

The screening that I presented in this thesis represents anyway the first attempt ever made to target directly the YTH domain; the candidate hit Ebselen, although being a covalent drug and having other recognized cellular targets, worked against the YTH domain, as showed by the biochemical and cellular assays. It is not the most potent inhibitor that we could possibly obtained, but it is indeed a promising starting point, even for eventually design more specific analogues from its chemical scaffold.

For the first time to our knowledge, in this thesis, we linked epitranscriptomic regulation to Neuroblastoma development, focusing on the role exerted by the YTHDF1 cytoplasmic reader. Being part of a wider project done in collaboration with the laboratory of Translational Genomics at the Department of CIBIO, that investigated the role of also the other main members of the methylation machinery, the ongoing experiments that we are currently following are not directly related to the reader protein. We are in fact validating data deriving from mi-CLIP of CHP-212 ALKBH5 overexpressing cells, compared to wild type, from which we obtained a series of targets that are differentially methylated between the two samples. Our aim is to validate this data though m6A-immunoprecipitation, to observe if the targets are effectively less methylated in the ALKBH5 overexpressing samples. Apart from this, we are also validating with mRNA half-life measurement following Actinomycin D treatment data deriving from a SLAM-Seq experiment done on CHP-212 METTL14 overexpressing cells. Our aim is to prove that the overexpression of METTL14 caused the decrease in the stability of target mRNAs identified in the previous experiment after bioinformatic analysis (Data not shown). Taking together all this different experiments, we are aiming at fully characterized the role played by m6A methylation in the progression of Neuroblastoma, focusing on all the actors of the play, from the writers to the readers, for the first time in this model of solid intracranial pediatric tumor that still lack a full comprehension of its development and, most importantly, an efficient therapeutic strategy.

5.Conclusions

Through this thesis, we set up a High Throughput Screening Assay to identify a novel inhibitor of the YTH domain and we fully characterized its biochemical and biological activity.

In particular, we analyzed its interaction with the domain identifying the residues inside the binding pocket that are involved with NMR, performed by our collaborators M. Fragai and L. Cerofolini in Florence at CERM, and we determined dose-response curves and constant of inhibition using different orthogonal biochemical approaches. We found that the interaction between our hit, the organoselenium compound Ebselen, and the YTH domain has a covalent nature and this led us to interpret our dose response curves as saturation binding curves, derived from the protein titration with increasing doses of the molecule. We also tested the activity of some already commercially available analogues of our main candidate hit, not finding any molecule particularly interesting to continue to exploit. We tested the biological activity of our compound on its ability to displace known mRNA targets from being bound to the cytoplasmic reader YTHDF2 with RNA immunoprecipitation assays, and also checked the effect on the same transcript stability, comparing the compound efficacy to the transient silencing of the protein.

We then investigated the oncogenic role of the YTHDF1 cytoplasmic reader in the development of the pediatric tumor Neuroblastoma, a model in which currently is not known the involvement of any of the m6A methylation machinery members. Since it is a tumor caused by very different genetic alterations none of which has resulted to be sufficient for its development, we hypothesize that there could be an additional epitranscriptomic regulation. Thanks also to preliminary data produced by our collaborators at the Department of CIBIO from the laboratory of Translational Genomics, it has been possible to correlate the expression levels of YTHDF1 with poor prognosis in Neuroblastoma patients, giving us the right to start investigating the function of the protein in this model. We demonstrated that YTHDF1 overexpression cause an increase in proliferation and in the percentage of cells belonging to the G0/G1 subpopulation during

cell cycle, while contributing to the generation of spheroids of greatest dimensions and with a higher invasion rate in Matrigel. We then proceed in treating these cells with Ebselen, founding that the treatment impairs, even if at high micromolar doses, spheroids generation only in the control lines, while the overexpressing cells resulted to be more resistant to it, also for what concerns the inhibition of their invasion rates. Last but not least, we also generated some promising proof of concept data *in vivo,* administering the drug to Drosophila larvae and checking the effect on their brain development afterwards, obtaining that the individuals treated with the medium dosage (50μM) showed a high penetrance of a fused mushroom bodies phenotype that is also been observed (unpublished data) in the ythdf ortholog knockout model, but further experiment would be needed to better understand the mechanism of action that cause this kind of alteration in the brain of flies.

Taking all these data together, I have presented for the first time a screening approach against the YTH domain, repurposed an already FDA approved drug, Ebselen, as a novel inhibitor of its RNA-binding activity and with anti-cancer properties, that would be needed to be further tested for *in vivo* analysis and other therapeutic implications.

6.Material and Methods

6.1 Experimental methodology for High Throughput Screening

The YTH domain is composed of a hydrophobic pocket in which the methylation on the adenosine inside the consensus sequence is sandwiched between two tryptophan residues and perpendicular to a third one. This three tryptophan residues are very well conserved among the different proteins of the family, and since tryptophan can emit a fluorescence signal that can be collected at 330nm, with an excitation wavelength of 280nm, this constitute a good condition to set up a label-free assay to test the binding of potential inhibitor towards the RNA binding pocket, just by measuring the quenching of the intrinsic fluorescence gave by tryptophan. To set up the assay, we decided to use the YTH domain of the YTHDF1 protein, registered on PDB as 4RCJ, comprised of the amino acids 365-554.After purification, we tested the natural ligand of the domain to validate the goodness of the assay. After calculating a robust Z factor, we set up the conditions for the High Throughput Screening.

6.2 Expression and purification of recombinant YTHDF1 YTH domain

The 4RCJ (PDB) construct of the human YTHDF1 YTH domain (amino acids 365-554), inserted in a pET28a-MHL vector (Addgene plasmid # 64654) and fused with a 6x His Tag at the N-terminal, was expressed in BL21(DE3) E.Coli strain cultured in LB medium at 37°C till OD=0.5, and then shifted at 18°C O/N after induction with 0.5mM mM IPTG. After the bacteria were harvested by centrifugation (5000 rpm for 30min at 4°C) and the bacterial pellets were lysed with lysis buffer containing 20mM Hepes (pH 7.5), 300mM NaCl and supplemented with protease inhibitors. The lysates were then sonicated with 6 pulses of 30sec followed by 30 sec of pause, keeping the suspension in ice. The clarified lysates were then centrifuged to remove the precipitates (15000 rpm for 30min at 4°C). The protein was purified using an Ni-chelating resin (Quiagen©) after three steps of

imidazole elution (20mM, 50mM, 300mM), and dialyzed O/N in a buffer containing 20mM Hepes (pH 7.5),150mM NaCl and 5mM bME but lacking imidazole. The recombinant protein was analyzed with Coomassie blue staining after SDS-PAGE of all the purification steps. The concentration was determined with both the Bradford assay method and through the extinction coefficient calculation (C=A/e*L, assuming L=1cm).

6.3 Fluorescence spectroscopy and binding assay

For the tryptophan quenching experiment, black 384 well plates were coated with the protein alone in a final concentration of 5uM, and with the protein incubated with different concentrations of Adenosine (Sigma-Aldrich), N6-methyladenosine (Selleckchem) and two RNA probes containing two variants of the consensus sequence, methylated and unmethylated(5'-CCGGm6ACUGUC-3'/5'-CCGGACUGUC-3';5-'CCGAm6ACUGUC-3'/5'CCGAACUGUC-3, Dharmacon), diluted in a buffer assay containing 20 mM Hepes (pH
7.5), 150mM NaCl and 10%Glycerol.Fluorescence was measured using a Tecan Infinite® 200 Microplate reader(Tecan Group Ltd), setting as emission wavelength 288 nm and collecting the emission data at 330 nm.

6.4 High Throughput Screening and counter screening

The Z Factor of the fluorescence quenching assay was calculated by tethering 1mM of N6methyladenosine sixteen times with the protein (5uM), and measuring its quenching effect upon binding, with the formula: $Z=1-3(\sigma_p+\sigma_n)/(\mu_p-\mu_n)$, where σ is the standard deviation, μ is the mean, and ($_p$) and ($_n$) are positive and negative controls, respectively. In this way, it was obtained a Z Factor=0,53, which is a value that indicate that the assay is quite robust and amenable for High Throughput. The High Throughput Screening was performed by coating, through automatic liquid handling with the Freedom EVO® (Tecan), black 384well plates with the protein diluted in a buffer assay containing 20mM Tris (pH 7.5), 150mM NaCl and 10%Glycerol, in a final concentration of 5uM, and then by adding the library of compounds at a final concentration of 10uM. The fluorescence of the plates was measured immediately after compounds addition. The library used was the Spectrum Collection (Microsource Discovery System, Inc.), composed of 2560 compounds, of whom the 60% are clinically used drugs, 25% natural products and 15% other bioactive

components. The Z-score was calculated as (X-μ_p)/σ_p, were X is the fluorescence intensity of the protein. Candidate molecules were considered all the ones that were under the threshold of Z=0,5, while all the ones over that value were discarded.

For the counter screening, the candidate molecules were tested against the TEV protein, to test if the quenching effect observed was due to specific interaction with the YTH domain, and not due to nonspecific interaction with the tryptophan residues. For these reason, TEV protease was choose because it has also tryptophan residues in its catalytic site, and was already disposable in lab in great amounts. The counterscreen was carried out by coating black 384-well plates with 5uM of protein, and then adding the compounds at 10uM. Measurement of fluorescence were carried out as for the HTS. Together with the counterscreen, the candidate molecules were in silico filtered to sort out potential PAINS, Pan Assay Interfering molecules, namely compounds that often result as false positive in HTS, due to their peculiar structures,and molecules with poor druggability, mostly the ones not respecting Lipinski's five rules (Lipinski et al., 2001). The In silico filtering was performed by analyzing the candidate hits with the http://fafdrugs4.mti.univ-parisdiderot.fr/index.html (Lagorce et al., 2015) free source software for PAINS detection and the http://advisor.bkslab.org/ (Irwin et al., 2015) free source software for aggregation prone molecules detection. Following this procedure, basically every candidate molecule except one survived to this filtering, the organoselenium compound Ebselen.

6.5 RNA Electrophoretic Mobility Shift Assay (REMSA)

Prior to perform the competitive REMSA to test the ability of the candidate hits to interfere with the RNA binding ability of the 4RCJ structure of the YTH domain, we determine the right concentration of RNA probe to use, tethering against a fixed concentration of protein (500nM), choosing the lowest concentration at which binding was still detectable (2nM). We also tested the specificity of the binding using a negative RNA probe as a control, bearing the unmethylated adenosine in the consensus sequence. Competitive REMSA was then performed by incubating 500nM of 4RCJ with various concentrations of Ebselen (0.1uM-10uM) and 2uM 5'- IRDYE-700 conjugated RNA probe (Metabion), 5'CCGAm6ACUGUC-3, in a buffer containing 20mM Hepes(pH 7.5), 50mM KCL, 0,5ug BSA, 0,25% Glycerol, in a final volume of 20ul. The reaction was loaded on a 6% polyacrylamide gel with 0,5% glycerol. Run was performed in 0.5X TBE buffer at 80V and

4°C for forty minutes, then switching at 100V for twenty minutes. Free and complexed RNA probes were detected with Odyssey® CLx Imaging System (Licor Biosciences) using the infrared filters.

6.6 Dynamic Mass Redistribution (DMR)

Dynamic Mass Redistribution (DMR) is a label-free assay that permits the detection *in vitro* of the interaction between two interactors, basically using light to measure the ligand induced changes of mass of the molecules inside the wells of a SBS- 384 black plate, that has at its bottom optical biosensors and attachment surface chemistry. As material binds to the surface of the sensors, the wavelength of the light reflected by the biosensors is changed, and this change is directly proportional to the amount of material bound.

Prior to proceed to testing the Ebselen interaction with the protein, some optimizations were needed to determine the right concentration and pH condition of the buffer assay that allows the protein to be anchored at the wells of the 384 plate, and for this reason the interaction with a methylated RNA probe, 5'-CCGAm6ACUGUC-3', was tested.

For protein immobilization, three dilutions of the 4RCJ construct of the YTHDF1 YTH domain (25 µg/mL, 50 µg/mL and 75 µg/mL) in 20 mM Sodium Acetate buffer at different pH (5, 6, 7, 8) were prepared.15ul of protein were added to the label-free 384 plate (EnSpire-LFB, 384-well with amine coupling, Perkin Elmer), that then was centrifuged at 800 rpm for 1min. After this step, the plate was sealed and incubated O/N at 4°C, to allow the seeding and the immobilization of the protein by amine-coupling chemistry. The day after, plate was washed 4 times using 25 µL assay buffer (HEPES 25 mM pH 8, 3 mM MgCl2, 100 mM NaCl, 8% Glycerol, 0.05% BSA, 0.05% Tween20). After the last washing step, a total volume of 20µL was left in the plate, and the plate was again centrifuged at 800 rpm for 1min, and then incubated for at least 3h at RT prior the binding assay, to help the soaking of the protein in the assay buffer. While the plate is incubating, the preparation of the ssRNA dilutions was carried out in the same buffer in which the protein was left soaking. The concentrations were, starting from: 3µM-1µM-300nM-100nM-30nM10nM-1nM. Prior to adding the ssRNA dilutions to the plate, after the 3h incubation, it is needed to make the baseline measurement, with the Ensight Multimode Plate Reader

(Perkin Elmer). After loading the RNA dilutions, the plate is loaded into the instrument for the final measurements, that will last for 1h and will be taken one every 30sec. For the detection of the interaction of the compound with the protein, the 4RCJ construct of the YTHDF1 YTH domain was immobilized to the plate in a final volume of 15ul/well of a 50ug/ml solution in 20mM sodium acetate buffer, pH 6, that resulted from the previous experiment to be the optimal condition for immobilization. The plate was equilibrated with the same assay buffer as in the previous experiment, and different concentration of Ebselen diluted in the same buffer were added to the plate (100µM-30µM-10µM-3µM1µM-300nM-100nM-30nM) and the interaction between the molecule and the protein was monitored during 1h at room temperature, acquiring the analysis with the Ensight Multimode Plate Reader (Perkin Elmer). Both the protein and the compound, in both experiments, were dispensed to the plates by the pipetting head of the Tecan EVO 200. The data were fitted with One-Site Binding Fit model in the GraphPad Prism® software, to obtain an estimated affinity constant (Kd) for the RNA probe and an estimated EC50 for Ebselen.

6.7 Alphascreen® Assay

The Amplified Luminescent Proximity Homogeneous Assay (ALPHA Assay) was performed in white 384-well Optiplates (Perkin Elmer) in a final volume of 25µL, and it was first optimized by titrating both the protein and the biotinylated RNA probe (5'-Bi-CCGAm6ACUGUC-3', Dharmacon) to find the appropriate right protein:RNA ratio. Both were tested in a nanomolar range, with a series of concentrations for 4RCJ (0-250nM) incubated with different concentrations of RNA (25-100nM) in a buffer assay containing 25 mM HEPES (pH 7.5), 100 mM NaCl, 0.1% BSA using the AlphaScreen Histidine (Nichel Chelate) detection kit (PerkinElmer). Anti-His Acceptor beads (PerkinElmer) (20 µg/ml final concentration) were added and the reaction was placed in the dark at room temperature for 30 min. Then streptavidin-Donor beads (20 µg/ml final concentration) were added and reaction was incubated at room temperature for 1h to reach equilibrium. Fluorescence signals were detected with an Enspire Multimode Plate reader (Perkin Elmer). For the competitive assay, different concentration of Ebselen (0-100µM) were mixed with 50nM RNA-probe and 50nM of 4RCJ, in the experimental condition of saturation binding. The

equilibrium dissociation constant (K_i) of Ebselen was determined from nonlinear regression fits of the data according to 1-site fit Ki model in GraphPad Prism®, by keeping constant the concentration (50 nM) of the RNA probe and its Kd calculated with the DMR (70nM), and assuming that the binding was reversible and at equilibrium.

6.8 Mass Spectrometry

Protein sample (in Hepes/NaCl and glycerol) treated with 50uM of Ebselen or untreated was subjected to desalting and buffer exchange by Zeba™ Spin Desalting Columns, 7K MWCO, 2 mL (Thermo Fisher Scientific) in 20 mM Ammonium acetate (pH 6.8), to remove salt and unbound molecule. The final concentration of the protein after desalting was determined with BCA. For the direct infusion, 50 µl of sample (9 µM) was diluted 1:1 in ACN with 0.1% formic acid and injected at 5µl/min. Spectra were acquired with an Orbitrap mass spectrometer with a resolution of 120k, and the protein deconvolution and the monoisotopic mass extraction were performed by the Thermo Xtract Algorithm. Desalting, protein quantification and direct infusion were performed by the Mass Spectrometry Facility of the Department of CIBIO, by Dr. Romina Belli and Dr. Daniele Peroni.

6.9 NMR

NMR experiment was performed by our collaborators in Florence at CERM, Marco Fragai and Linda Cerofolini.

The binding region of the m6A RNA probe (5'-CCGAm6ACUGUC-3') and of Ebselen on the 4RCJ structure of the YTH domain of the YTHDF1 protein has been investigated by monitoring the effects in the 2D 1H-15N HSQC solution NMR spectrum of the 15N isotopically enriched protein upon the addition of increasing amounts of RNA/compound. The spectra were acquired on a Bruker Avance 950 MHz NMR spectrometer at 298 K on a buffered solution [20 mM Tris, pH 7.5, 150 mM NaCl, 250 mM LiCl, 80 mM KCl, 10 mM βME, 0.5 mM EDTA, 0.1 % NaN3, protease inhibitors] of the protein at the concentration of 100 µM.

The protein assignment was obtained from the analysis of triple resonance NMR spectra (3D HNCA, 3D CBCA(CO)NH, 3D HNCACB, 3D HNCO, 3D HN(CA)CO) acquired on a NMR DRX spectrometer operating at 500 MHz. The assignment was helped also by the analysis of 2D C-detected experiments (2D CBCACO, 2D CACO, 2D CON) acquired on a Bruker Avance NMR spectrometer operating at 700 MHz 1H Larmor frequency, equipped with a cryogenically cooled probe optimized for 13C sensitivity (TCI, S/N 1500:1, on the ASTM standard sample). The large signal overlap in the 2D 1H-15N HSQC and the loss of the signals in the 3D NMR experiments, because of unfavorable relaxation phenomena, prevented the complete resonance assignment. Only the 70% of the protein sequence could be assigned. Increasing amounts of the m6A-RNA fragment [10, 20, 40, 100, 150 μM], and also increasing amounts of Ebselen [12.5, 25, 50, 100, 200 μM] were added to the protein solution during the NMR titration.

6.10 Cell lines

SK-N-AS (ECACC, 94092302), SK-N-BE(2) (ECACC, 95011815),HeLa(ATCC CCL-2), HEK293T (ATCC) cell lines were cultured in Dulbecco's Modified Eagle Medium (DMEM, Corning, 15-017-CVR) supplemented with 10% FBS (Corning, 35-079-CV), 1% LGlutamine (Corning, 25-005-CI), 1% Penicillin/Streptomycin (Gibco, 15140-122). CHP-212 (ATCC, CRL-2273) cell line was cultured in 1:1 ratio of Minimum Essential Medium (MEM,
Gibco,11095-080) and Ham's F12 (Euroclone, ECB7302L) supplemented with 10% FBS (Corning, 35-079-CV), 1% L-Glutamine (Corning, 25-005-CI) 1% Penicillin/Streptomycin (Gibco, 15140-122),1% Non-essential Aminoacids (Euroclone, ECB3064D). PC-3 (ATCC CRL-1435), CHP-134 (ECACC 06122002) cell lines were cultured in RPMI-1640 (ThermoFisher Scientific, 31870) supplemented with 10% FBS (Corning, 35-079-CV), 1% L-Glutamine (Corning, 25-005-CI) and 1% Penicillin/Streptomycin (Gibco, 15140-122). For genetically engineered cell lines overexpressing YTHDF1, lentiviral particles were prepared in HEK293T cells as previously described (Shi et al., 2004). We used a lentivirus plasmid in which the complete sequence of YTHDF1 was already been inserted by Dr.

Luigi Pasini previously working in the Laboratory of Translational Genomics at the Department of CIBIO.

Neuroblastoma cell lines were seeded 24h before transduction and incubated with lentivirus and 5mg/mL polybrene (Hexadimethrine bromide, M&C Gene Technology) in serum-free medium and kept at 37°C with 5% CO2 for 6h. Cultures were then replaced with complete medium and selected with 0.5µg of puromycin after 48h of transduction. The experiment was performed in collaboration with Giulia Montuori at DeCIBIO.

6.11 Cell viability assays

Cells were seeded and treated in 96 plate for 24h,48h and 72h. Viability was assessed with OZBlue assay, that was added at 10% the culture media volume to cells, that were further incubated at 37°C, until color signal developing was observed. Fluorescence was then determined (excitation 560nm and emission 590 nm) by a Tecan microplate reader. Cell survival was calculated with respect to control (DMSO), and IC50 values were determined by fitting with GraphPad Prism software.

6.12 Wound Healing Assay

When cells seeded in 6 well plate reached 80%-90% confluency, a scratch upon the cell monolayer is created using a p200 pipette tip. The plate is then washed once, to get rid of the detached cells, and medium replaced with the one containing the drug, respectively 25µM of Ebselen and DMSO. Cells were treated for 48h and images of the same field were taken at time 0 and at 24h and 48h using a Leica DM IL Led microscope with 5x magnification. Area of the open wounds were then measured with ImageJ software.

6.13 Spheroids assembly and treatments

For spheroids generation from SK-N-AS, SK-N-BE and the relative YTHDF1 OE lines, and from CHP-134 cells, cells were counted and seeded at a density of 1000 cells/well in a 96 well Clear Round Bottom Ultra-Low Attachment Microplate (ULA) Corning®. After 15 min of incubation at RT, to let cells seed at the bottom of the wells, the plate was centrifuged

for 5min at 1600 rpm at 4°C. The plate was then covered and kept in an incubator (37°C, 5% CO2, 95% humidity) for at least three days before imaging. Images were collected with a Leica DM IL Led Microscope (5x magnification) every three days, for twelve days, and analyzed with a macro of ImageJ published in Ivanov et al. 2014. For treatments, spheroids were generated as described before, and the treatment was added in the medium after seeding. We tested three different concentrations of Ebselen, 12,5μM-25μM50μM, and images were acquired after six days and analyzed with the macro of ImageJ mentioned before. Spheroids were then stained with Calcein and analyzed with the Operetta® High Content Imaging System to determine the intensity of the dye signal, to measure the impact of the drug on spheroids viability.

6.14 Invasion Assay

Cells were grown in a 96-well Clear Round Bottom Ultra-Low Attachment Microplate (Corning®) as 3D-spheroids and embedded in Cultrex® Reduced Growth Factor Basement Membrane Matrix, Type 2 (BME 2, Trevigen) in presence or absence of Ebselen (25uM) (Santa Cruz Biotechnology®). The invasion ability was evaluated every three days and the area of invasiveness was calculated as previously described (E.B. Berens, 2015) with ImageJ.

6.15 Real Time Proliferation Assay

Neuroblastoma cell lines proliferation ability was evaluated with the Real Time Cell Analyzer (RTCA DP Analyzer, Roche) according to the manufacturer's instructions. 5000 cells were seeded in a E-16 Plate (Acea Bioscience Inc.) in four technical replicates. E-16 Plates are embedded at their bottom with golden microelectrodes that monitor cell status, comprising their number, shape/size and attachment. Cells impedance was evaluated every 15 minutes for 144h and Cell Index values (CI) were acquired by the RTCA Software (V1.2) for subsequently normalization and analysis. Cells impedance refers to their interfering with the current flowing between the electrodes, due to their attachment to the wells. This parameter is plotted and referred to as Cell Index (CI), that grows with increasing cell proliferation and reaches its plateau when cells reaches the 100% confluence. The continuous acquisition made possible the generation of real time curves and the monitoring of different conditions at the same time.

6.16 Flow Cytometric Analysis

DNA content of neuroblastoma cell lines was evaluated using the nucleic acid stain Propidium Iodide (abcam) followed by flow cytometry analysis. Cells were harvested and fixed in 66% ethanol for 2 to 16 hours at 4°C and treated for 30 min at 37°C with 20x PI + 200x RNase. Propidium Iodide fluorescence intensity was collected on a flow cytometer and 488 nM laser excitation and data were analysed by FlowJo™ v10.6.1 software (FlowJo LLC).

6.17 RNA Immunoprecipitation Assay (RIP)

Five million cells were used for each RIP experiments followed by RT-PCR according to the protocol published by Keene et al 2006, without cross-linking steps and using 1-15µg of YTHDF2 antibody (Proteintech, 24744-1-AP) or same amount of rabbit normal IgG isotype (negative control, Cell Signaling,2729S). Cells were harvested after 24h of treatment with 25µM of Ebselen and DMSO as a control and lysed with 20 mM Tris–HCl at pH 7.5, 100 mM KCl, 5 mM MgCl2, and 0.5% NP-40 for 10 min on ice and centrifuged at 15 000 × g for 10 min at 4°C. Lysates were then incubated with dynabead A/G (Thermo Fisher, 10001D/10003D) for preclearing 1h at 4°C, while a 80% of Dynabeads A and 20% of Dynabeads G each samples were incubated at RT for 1h with YTHDF2 or rabbit isotype IgG for Ab coating. After the preclearing steps and the coating, lysates were splitted between YTHDF2 and IgG coated beads, while 1-5% of lysate was stored as input, and incubated O/N at 4°C. Finally, samples have been washed with NT2 buffer for 5 times, 5 minutes each at 4°C. TRIzol reagent was then added directly to the beads for RNA extraction following the protocol described before. After RNA extraction, samples were processed for RT-PCR, that was performed after cDNA synthesis following the kit manufacturer's instructions (Thermo Scientific, K1612), using Universal SYBR Master Mix (KAPA Biosystems, KR03089) on CFX 96/384 Thermal Cyclers. Ct values for YTHDF2 and IgG IP was subtracted from the Ct value of the housekeeping gene 18s to yield the ΔCt value. For each condition, the ΔCt value of IgG and YTHDF2 was evaluated in triplicate. Normalization of the values was then carried out following the Percent Input Method, in which values from IgG and YTHDF2 IPs were calculated as %Input of the adjusted Input values. Adjusted Input corresponds to the Input ΔCt subtracted of the log2

of the input dilution factor, in this case 100, so 6,64. YTHDF2 and IgG fractions were calculated as %Input by subtracting to the Adjusted Input values their ΔCt values. YTHDF2 IP values were then normalized on IgG.

6.18 Total RNA extraction and qRT-PCR

Total RNA has been extracted with TRIzol reagent followed by chloroform precipitation and by DNAse I treatment for 10min at 37°C. cDNA synthesis was carried out following manufacturer's instructions of the cDNA synthesis kit (Thermo Fisher), using 1μg of RNA template and an equimolar mix of random and oligo-dT primers. qRT-PCR conditions were the following: 3min at 95°C, followed by 39 cycles of 15 sec at 95°C alternating with 60°C for 15 sec. Melting curve analysis was performed in every reaction to confirm the presence of a single amplicon. All qPCR experiments were performed in triplicates and normalized on 18s or Actin internal controls according to the conditions. The following table recapitulates all the primers used for the qRT-PCR reactions.

Table 1. List of Primers used for all the experiments.

Human	**Sequence**	
gene	**Forward (5'-3')**	**Reverse (3'-5')**
SON	CATCATCCCTTTAAACTCAGTG	TCTTCACCATTTTTCTCCAC
CREBBP	AACATGTCACTCAGGAC	AATATTCATCCCTGCTGTTG
PEG10	CTGAGGAGAACAGCGGAGAAG	GTCCTCGCGTGAAATAAGCG
NOTCH2	GTGGATACAGATGCGAGTGTG	GGGGCCTACTCTGTGAAGA
YTHDF1	CCAGAGAACAAAAGGACAA	TTTGACTGTCCAGTAAGGTAG
YTHDF2	GTCCATTACTAGTAACATCG	TGTCAGATTCCTACTTACCC

RNA 18S	GCAGCTAGGAATAATGGAATAG	TGGCAAATGCTTTCGCTCTG
RPLP0	CATTCTCGCTTCCTGGAG	CTTGACCTTTTCAGCAAGTGG

6.19 RNA stability experiments with Actinomycin D

2*10⁵ HeLa cells were seeded in 24 well plate and transfected with 100ng of YTHDF2 siRNA (Sigma Aldrich) and same amount of control siRNA (Santa Cruz Biotechnology) for 72h using Lipofectamine (Thermo Fisher) following manufacturer's instructions, and the well transfected with the control siRNA were also treated for 24h with DMSO and 25μM of Ebselen. Cells were then treated with 5μg/ml of Actinomycin D to shut off translation according to the following time points: 0h-1h-3h. Cells were then harvested immediately after the last time point, following RNA extraction according to TRIzol reagent protocol.
Decay curves were plotted on Graph Pad Prism® software using linear regression fit.

6.20 Statistical analysis

Statistical analysis Experiments were performed in number of biological replicates indicated in all experiments described in the Results section. t-tests were used to calculate final p-values, without assuming variances to be equal (Welch's t-test). Pvalue<0.05,<0.01,<0.001 and <0.0001 were indicated with *, **, ***, **** symbols, respectively.

REFERENCES

Akalal, D.-B. G., Wilson, C. F., Zong, L., Tanaka, N. K., Ito, K., & Davis, R. L. (2006). Roles for Drosophila mushroom body neurons in olfactory learning and memory. *Learning & Memory*, *13*(5), 659–668. https://doi.org/10.1101/lm.221206

Alarcón, C. R., Goodarzi, H., Lee, H., Liu, X., Tavazoie, S., & Tavazoie, S. F. (2015). HNRNPA2B1 Is a Mediator of m6A-Dependent Nuclear RNA Processing Events. *Cell*, *162*(6), 1299–1308. https://doi.org/10.1016/j.cell.2015.08.011

Anders, M., Chelysheva, I., Goebel, I., Trenkner, T., Zhou, J., Mao, Y., Verzini, S., Qian, S.-B., & Ignatova, Z. (2018). Dynamic m ^{6} A methylation facilitates mRNA triaging to stress granules. *Life Science Alliance*, *1*(4), e201800113. https://doi.org/10.26508/lsa.201800113

Baell JB, Nissink JWM. Seven Year Itch: Pan-Assay Interference Compounds (PAINS) in 2017-Utility and Limitations. *ACS Chem Biol*. 2018;13(1):36-44. doi:10.1021/acschembio.7b00903

Bai, Y., Yang, C., Wu, R., Huang, L., Song, S., Li, W., Yan, P., Lin, C., Li, D., & Zhang, Y. (2019). YTHDF1 Regulates Tumorigenicity and Cancer Stem Cell-Like Activity in Human Colorectal Carcinoma. *Frontiers in Oncology*, *9*. https://doi.org/10.3389/fonc.2019.00332

Barbieri, I., Tzelepis, K., Pandolfini, L., Shi, J., Millán-Zambrano, G., Robson, S. C., Aspris, D., Migliori, V., Bannister, A. J., Han, N., de Braekeleer, E., Ponstingl, H., Hendrick, A., Vakoc, C. R., Vassiliou, G. S., & Kouzarides, T. (2017). Promoter-bound METTL3 maintains myeloid leukaemia by m6A-dependent translation control. *Nature*, *552*(7683), 126–131. https://doi.org/10.1038/nature24678

Batista, P. J., Molinie, B., Wang, J., Qu, K., Zhang, J., Li, L., Bouley, D. M., Lujan, E., Haddad, B., Daneshvar, K., Carter, A. C., Flynn, R. A., Zhou, C., Lim, K.-S., Dedon, P., Wernig, M., Mullen, A. C., Xing, Y., Giallourakis, C. C., & Chang, H. Y. (2014). m6A RNA Modification Controls Cell Fate Transition in Mammalian Embryonic Stem Cells. *Cell Stem Cell*, *15*(6), 707–719. https://doi.org/10.1016/j.stem.2014.09.019

Bokar, J. A., Shambaugh, M. E., Polayes, D., Matera, A. G., & Rottman, F. M. (1997). Purification and cDNA cloning of the AdoMet-binding subunit of the human mRNA (N6adenosine)-methyltransferase. *RNA (New York, N.Y.)*, *3*(11), 1233–1247.

Bujnicki, J. M., Feder, M., Radlinska, M., & Blumenthal, R. M. (2002). Structure Prediction and Phylogenetic Analysis of a Functionally Diverse Family of Proteins Homologous to the MTA70 Subunit of the Human mRNA:m6A Methyltransferase. *Journal of Molecular Evolution*, *55*(4), 431–444. https://doi.org/10.1007/s00239-002-2339-8

Cai, J., Yang, F., Zhan, H., Situ, J., Li, W., Mao, Y., & Luo, Y. (2019). RNA m6A Methyltransferase METTL3 Promotes The Growth Of Prostate Cancer By Regulating Hedgehog Pathway. *OncoTargets and Therapy*, *Volume 12*, 9143–9152. https://doi.org/10.2147/OTT.S226796

Chen, B., Ye, F., Yu, L., Jia, G., Huang, X., Zhang, X., Peng, S., Chen, K., Wang, M., Gong, S., Zhang, R., Yin, J., Li, H., Yang, Y., Liu, H., Zhang, J., Zhang, H., Zhang, A., Jiang, H., … Yang, C.-G. (2012). Development of Cell-Active *N* ^{6} -Methyladenosine RNA Demethylase FTO Inhibitor. *Journal of the American Chemical Society*, *134*(43), 17963–17971. https://doi.org/10.1021/ja3064149

Chen, J., Sun, Y., Xu, X., Wang, D., He, J., Zhou, H., Lu, Y., Zeng, J., Du, F., Gong, A., & Xu, M. (2017). YTH domain family 2 orchestrates epithelial-mesenchymal transition/proliferation dichotomy in pancreatic cancer cells. *Cell Cycle*, *16*(23), 2259–2271. https://doi.org/10.1080/15384101.2017.1380125

Chen, M., Wei, L., Law, C.-T., Tsang, F. H.-C., Shen, J., Cheng, C. L.-H., Tsang, L.-H., Ho, D. W.-H., Chiu, D. K.-C., Lee, J. M.-F., Wong, C. C.-L., Ng, I. O.-L., & Wong, C.-M. (2018). RNA N6-methyladenosine methyltransferase-like 3 promotes liver cancer progression through YTHDF2-dependent posttranscriptional silencing of SOCS2. *Hepatology*, *67*(6), 2254–2270. https://doi.org/10.1002/hep.29683

Cochran, A.G., Conery, A.R. & Sims, R.J. Bromodomains: a new target class for drug development. *Nat Rev Drug Discov* **18,** 609–628 (2019). https://doi.org/10.1038/s41573019-0030-7

Cui, Q., Shi, H., Ye, P., Li, L., Qu, Q., Sun, G., Sun, G., Lu, Z., Huang, Y., Yang, C.-G., Riggs, A. D., He, C., & Shi, Y. (2017). m 6 A RNA Methylation Regulates the Self-Renewal and Tumorigenesis of Glioblastoma Stem Cells. *Cell Reports*, *18*(11), 2622–2634. https://doi.org/10.1016/j.celrep.2017.02.059

Desrosiers, R., Friderici, K., & Rottman, F. (1974a). Identification of Methylated Nucleosides in Messenger RNA from Novikoff Hepatoma Cells. *Proceedings of the National Academy of Sciences*, *71*(10), 3971–3975. https://doi.org/10.1073/pnas.71.10.3971

Dominissini, D., Moshitch-Moshkovitz, S., Schwartz, S., Salmon-Divon, M., Ungar, L., Osenberg, S., Cesarkas, K., Jacob-Hirsch, J., Amariglio, N., Kupiec, M., Sorek, R., & Rechavi, G. (2012). Topology of the human and mouse m6A RNA methylomes revealed by m6A-seq. *Nature*, *485*(7397), 201–206. https://doi.org/10.1038/nature11112

Dominissini, D., Nachtergaele, S., Moshitch-Moshkovitz, S., Peer, E., Kol, N., Ben-Haim, M. S., Dai, Q., di Segni, A., Salmon-Divon, M., Clark, W. C., Zheng, G., Pan, T., Solomon, O., Eyal, E., Hershkovitz, V., Han, D., Doré, L. C., Amariglio, N., Rechavi, G., & He, C. (2016). The dynamic N1-methyladenosine methylome in eukaryotic messenger RNA. *Nature*, *530*(7591), 441–446. https://doi.org/10.1038/nature16998

Du, H., Zhao, Y., He, J., Zhang, Y., Xi, H., Liu, M., Ma, J., & Wu, L. (2016). YTHDF2 destabilizes m6A-containing RNA through direct recruitment of the CCR4–NOT deadenylase complex. *Nature Communications*, *7*(1), 12626. https://doi.org/10.1038/ncomms12626

Fang, X., Zheng, Y., Duan, Y., Liu, Y., & Zhong, W. (2019). Recent Advances in Design of Fluorescence-Based Assays for High-Throughput Screening. *Analytical Chemistry*, *91*(1), 482–504. https://doi.org/10.1021/acs.analchem.8b05303

Geula, S., Moshitch-Moshkovitz, S., Dominissini, D., Mansour, A. A., Kol, N., Salmon-Divon, M., Hershkovitz, V., Peer, E., Mor, N., Manor, Y. S., Ben-Haim, M. S., Eyal, E., Yunger, S., Pinto, Y., Jaitin, D. A., Viukov, S., Rais, Y., Krupalnik, V., Chomsky, E., … Hanna, J. H. (2015). m ^{6} A mRNA methylation facilitates resolution of naïve pluripotency toward differentiation. *Science*, *347*(6225), 1002–1006. https://doi.org/10.1126/science.1261417

Gokhale, N. S., McIntyre, A. B. R., McFadden, M. J., Roder, A. E., Kennedy, E. M., Gandara, J.

A., Hopcraft, S. E., Quicke, K. M., Vazquez, C., Willer, J., Ilkayeva, O. R., Law, B. A., Holley, C. L., Garcia-Blanco, M. A., Evans, M. J., Suthar, M. S., Bradrick, S. S., Mason, C. E., & Horner, S. M. (2016). N6 -Methyladenosine in Flaviviridae Viral RNA Genomes Regulates Infection. *Cell Host & Microbe*, *20*(5), 654–665. https://doi.org/10.1016/j.chom.2016.09.015

Haussmann, I. U., Bodi, Z., Sanchez-Moran, E., Mongan, N. P., Archer, N., Fray, R. G., & Soller, M. (2016). m6A potentiates Sxl alternative pre-mRNA splicing for robust Drosophila sex determination. *Nature*, *540*(7632), 301–304. https://doi.org/10.1038/nature20577

Hazra D, Chapat C, Graille M. (2019) m⁶A mRNA Destiny: Chained to the rhYTHm by the YTH-Containing Proteins. *Genes (Basel)*. 10(1):49. doi:10.3390/genes10010049

Hess, M. E., Hess, S., Meyer, K. D., Verhagen, L. A. W., Koch, L., Brönneke, H. S., Dietrich, M. O., Jordan, S. D., Saletore, Y., Elemento, O., Belgardt, B. F., Franz, T., Horvath, T. L., Rüther, U., Jaffrey, S. R., Kloppenburg, P., & Brüning, J. C. (2013). The fat mass and obesity associated gene (Fto) regulates activity of the dopaminergic midbrain circuitry. *Nature Neuroscience*, *16*(8), 1042–1048. https://doi.org/10.1038/nn.3449

Hou, J., Zhang, H., Liu, J., Zhao, Z., Wang, J., Lu, Z., Hu, B., Zhou, J., Zhao, Z., Feng, M., Zhang, H., Shen, B., Huang, X., Sun, B., He, C., & Xia, Q. (2019). YTHDF2 reduction fuels inflammation and vascular abnormalization in hepatocellular carcinoma. *Molecular Cancer*, *18*(1), 163. https://doi.org/10.1186/s12943-019-1082-3

Hsu, P. J., Zhu, Y., Ma, H., Guo, Y., Shi, X., Liu, Y., Qi, M., Lu, Z., Shi, H., Wang, J., Cheng, Y., Luo, G., Dai, Q., Liu, M., Guo, X., Sha, J., Shen, B., & He, C. (2017). Ythdc2 is an N6methyladenosine binding protein that regulates mammalian spermatogenesis. *Cell Research*, *27*(9), 1115–1127. https://doi.org/10.1038/cr.2017.99

Hu, Y., & Smyth, G. K. (2009). ELDA: Extreme limiting dilution analysis for comparing depleted and enriched populations in stem cell and other assays. *Journal of Immunological Methods*, *347*(1–2), 70–78. https://doi.org/10.1016/j.jim.2009.06.008

Huang, Y., Su, R., Sheng, Y., Dong, L., Dong, Z., Xu, H., Ni, T., Zhang, Z. S., Zhang, T., Li, C., Han, L., Zhu, Z., Lian, F., Wei, J., Deng, Q., Wang, Y., Wunderlich, M., Gao, Z., Pan, G.,

… Yang, C.-G. (2019). Small-Molecule Targeting of Oncogenic FTO Demethylase in Acute Myeloid Leukemia. *Cancer Cell*, *35*(4), 677-691.e10. https://doi.org/10.1016/j.ccell.2019.03.006

Hussain, S., Sajini, A. A., Blanco, S., Dietmann, S., Lombard, P., Sugimoto, Y., Paramor, M., Gleeson, J. G., Odom, D. T., Ule, J., & Frye, M. (2013). NSun2-Mediated Cytosine-5 Methylation of Vault Noncoding RNA Determines Its Processing into Regulatory Small RNAs. *Cell Reports*, *4*(2), 255–261. https://doi.org/10.1016/j.celrep.2013.06.029

Imai, Y., Matsuo, N., Ogawa, S., Tohyama, M., & Takagi, T. (1998). Cloning of a gene, YT521, for a novel RNA splicing-related protein induced by hypoxia/reoxygenation. *Molecular Brain Research*, *53*(1–2), 33–40. https://doi.org/10.1016/S0169-328X(97)00262-3

Irwin, J. J., Duan, D., Torosyan, H., Doak, A. K., Ziebart, K. T., Sterling, T., Tumanian, G., & Shoichet, B. K. (2015). An Aggregation Advisor for Ligand Discovery. *Journal of Medicinal Chemistry*, *58*(17), 7076–7087. https://doi.org/10.1021/acs.jmedchem.5b01105

Ivanov, D. P., Parker, T. L., Walker, D. A., Alexander, C., Ashford, M. B., Gellert, P. R., & Garnett, M. C. (2014). Multiplexing Spheroid Volume, Resazurin and Acid Phosphatase Viability Assays for High-Throughput Screening of Tumour Spheroids and Stem Cell Neurospheres. *PLoS ONE*, *9*(8), e103817. https://doi.org/10.1371/journal.pone.0103817

Iwanami, Y., & Brown, G. M. (1968). Methylated bases of ribosomal ribonucleic acid from HeLa cells. *Archives of Biochemistry and Biophysics*, *126*(1), 8–15. https://doi.org/10.1016/00039861(68)90553-5

Jia, G., Fu, Y., & He, C. (2013). Reversible RNA adenosine methylation in biological regulation. *Trends in Genetics*, *29*(2), 108–115. https://doi.org/10.1016/j.tig.2012.11.003

Jia, G., Fu, Y., Zhao, X., Dai, Q., Zheng, G., Yang, Y., Yi, C., Lindahl, T., Pan, T., Yang, Y.-G., & He, C. (2011a). N6-Methyladenosine in nuclear RNA is a major substrate of the obesityassociated FTO. *Nature Chemical Biology*, *7*(12), 885–887. https://doi.org/10.1038/nchembio.687

Jia, G., Fu, Y., Zhao, X., Dai, Q., Zheng, G., Yang, Y., Yi, C., Lindahl, T., Pan, T., Yang, Y.-G.,

& He, C. (2011b). N6-Methyladenosine in nuclear RNA is a major substrate of the obesityassociated FTO. *Nature Chemical Biology*, *7*(12), 885–887. https://doi.org/10.1038/nchembio.687

Kang, H.-J., Jeong, S.-J., Kim, K.-N., Baek, I.-J., Chang, M., Kang, C.-M., Park, Y.-S., & Yun, C.-W. (2014). A novel protein, Pho92, has a conserved YTH domain and regulates phosphate metabolism by decreasing the mRNA stability of PHO4 in Saccharomyces cerevisiae. *Biochemical Journal*, *457*(3), 391–400. https://doi.org/10.1042/BJ20130862

Kasowitz, S. D., Ma, J., Anderson, S. J., Leu, N. A., Xu, Y., Gregory, B. D., Schultz, R. M., & Wang, P. J. (2018). Nuclear m6A reader YTHDC1 regulates alternative polyadenylation and splicing during mouse oocyte development. *PLOS Genetics*, *14*(5), e1007412. https://doi.org/10.1371/journal.pgen.1007412

Kennedy, E. M., Bogerd, H. P., Kornepati, A. V. R., Kang, D., Ghoshal, D., Marshall, J. B., Poling, B. C., Tsai, K., Gokhale, N. S., Horner, S. M., & Cullen, B. R. (2016). Posttranscriptional m 6 A Editing of HIV-1 mRNAs Enhances Viral Gene Expression. *Cell Host & Microbe*, *19*(5), 675–685. https://doi.org/10.1016/j.chom.2016.04.002

Knapp, S. (2015). *Emerging Target Families: Intractable Targets* (pp. 43–58). https://doi.org/10.1007/164_2015_28

Knuckles P,Lence T., Hausmann I.U., et al.(2018). Zc3h13/Flacc is required for adenosine methylation by bridging the mRNA-binding factor Rbm15/Spenito to the m^{6}A machinery component Wtap/Fl(2)d. *Genes Dev*. 2018;32(5-6):415-429. doi:10.1101/gad.309146.117

Kretschmer, J., Rao, H., Hackert, P., Sloan, K. E., Höbartner, C., & Bohnsack, M. T. (2018). The m ^{6} A reader protein YTHDC2 interacts with the small ribosomal subunit and the 5′–3′ exoribonuclease XRN1. *RNA*, *24*(10), 1339–1350. https://doi.org/10.1261/rna.064238.117

Krug, R. M., Morgan, M. A., & Shatkin, A. J. (1976). Influenza viral mRNA contains internal N6methyladenosine and 5'-terminal 7-methylguanosine in cap structures. *Journal of Virology*, *20*(1), 45–53. https://pubmed.ncbi.nlm.nih.gov/1086370

Lagorce, D., Sperandio, O., Baell, J. B., Miteva, M. A., & Villoutreix, B. O. (2015). FAF-Drugs3: a web server for compound property calculation and chemical library design. *Nucleic Acids Research*, *43*(W1), W200–W207. https://doi.org/10.1093/nar/gkv353

Lence, T., Akhtar, J., Bayer, M., Schmid, K., Spindler, L., Ho, C. H., Kreim, N., AndradeNavarro, M. A., Poeck, B., Helm, M., & Roignant, J.-Y. (2016). m6A modulates neuronal functions and sex determination in Drosophila. *Nature*, *540*(7632), 242–247. https://doi.org/10.1038/nature20568

Li, F., Kennedy, S., Hajian, T., Gibson, E., Seitova, A., Xu, C., Arrowsmith, C. H., & Vedadi, M. (2016). A Radioactivity-Based Assay for Screening Human m ^{6} A-RNA Methyltransferase, METTL3-METTL14 Complex, and Demethylase ALKBH5. *Journal of Biomolecular Screening*, *21*(3), 290–297. https://doi.org/10.1177/1087057115623264

Li, J., Meng, S., Xu, M., Wang, S., He, L., Xu, X., Wang, X., & Xie, L. (2018). Downregulation of N6-methyladenosine binding YTHDF2 protein mediated by miR-493-3p suppresses prostate cancer by elevating N6-methyladenosine levels. *Oncotarget*, *9*(3). https://doi.org/10.18632/oncotarget.23365

Li, M., Zhao, X., Wang, W., Shi, H., Pan, Q., Lu, Z., Perez, S. P., Suganthan, R., He, C., Bjørås, M., & Klungland, A. (2018). Ythdf2-mediated m6A mRNA clearance modulates neural development in mice. *Genome Biology*, *19*(1), 69. https://doi.org/10.1186/s13059018-1436-y

Li, S., & Mason, C. E. (2014). The Pivotal Regulatory Landscape of RNA Modifications. *Annual Review of Genomics and Human Genetics*, *15*(1), 127–150. https://doi.org/10.1146/annurev-genom-090413-025405

Lichinchi, G., Zhao, B. S., Wu, Y., Lu, Z., Qin, Y., He, C., & Rana, T. M. (2016). Dynamics of Human and Viral RNA Methylation during Zika Virus Infection. *Cell Host & Microbe*, *20*(5), 666–673. https://doi.org/10.1016/j.chom.2016.10.002

Lin, S., Choe, J., Du, P., Triboulet, R., & Gregory, R. I. (2016). The m 6 A Methyltransferase METTL3 Promotes Translation in Human Cancer Cells. *Molecular Cell*, *62*(3), 335–345. https://doi.org/10.1016/j.molcel.2016.03.021

Linder, B., Grozhik, A. v, Olarerin-George, A. O., Meydan, C., Mason, C. E., & Jaffrey, S. R. (2015). Single-nucleotide-resolution mapping of m6A and m6Am throughout the transcriptome. *Nature Methods*, *12*(8), 767–772. https://doi.org/10.1038/nmeth.3453

Lipinski, C. A., Lombardo, F., Dominy, B. W., & Feeney, P. J. (2001). Experimental and computational approaches to estimate solubility and permeability in drug discovery and development settings 1PII of original article: S0169-409X(96)00423-1. The article was originally published in Advanced Drug Delivery Reviews 23 (1997) 3–25. 1. *Advanced Drug Delivery Reviews*, *46*(1–3), 3–26. https://doi.org/10.1016/S0169-409X(00)00129-0

Liu, Jianzhao, Yue, Y., Han, D., Wang, X., Fu, Y., Zhang, L., Jia, G., Yu, M., Lu, Z., Deng, X., Dai, Q., Chen, W., & He, C. (2014a). A METTL3–METTL14 complex mediates mammalian nuclear RNA N6-adenosine methylation. *Nature Chemical Biology*, *10*(2), 93–95. https://doi.org/10.1038/nchembio.1432

Liu, Jianzhao, Yue, Y., Han, D., Wang, X., Fu, Y., Zhang, L., Jia, G., Yu, M., Lu, Z., Deng, X., Dai, Q., Chen, W., & He, C. (2014b). A METTL3–METTL14 complex mediates mammalian nuclear RNA N6-adenosine methylation. *Nature Chemical Biology*, *10*(2), 93–95. https://doi.org/10.1038/nchembio.1432

Liu, Jiqin, Ren, D., Du, Z., Wang, H., Zhang, H., & Jin, Y. (2018). m 6 A demethylase FTO facilitates tumor progression in lung squamous cell carcinoma by regulating MZF1 expression. *Biochemical and Biophysical Research Communications*, *502*(4), 456–464. https://doi.org/10.1016/j.bbrc.2018.05.175

Liu, T., Wei, Q., Jin, J., Luo, Q., Liu, Y., Yang, Y., Cheng, C., Li, L., Pi, J., Si, Y., Xiao, H., Li, L., Rao, S., Wang, F., Yu, J., Yu, J., Zou, D., & Yi, P. (2020). The m6A reader YTHDF1 promotes ovarian cancer progression via augmenting EIF3C translation. *Nucleic Acids Research*, *48*(7), 3816–3831. https://doi.org/10.1093/nar/gkaa048

Lv, D., Hu, Z., Lu, L., Lu, H., & Xu, X. (2017). Three-dimensional cell culture: A powerful tool in tumor research and drug discovery (Review). *Oncology Letters*. https://doi.org/10.3892/ol.2017.7134

Luo, S., & Tong, L. (2014). Molecular basis for the recognition of methylated adenines in RNA by the eukaryotic YTH domain. *Proceedings of the National Academy of Sciences*, *111*(38), 13834–13839. https://doi.org/10.1073/pnas.1412742111

Ma, J., Yang, F., Zhou, C., Liu, F., Yuan, J., Wang, F., Wang, T., Xu, Q., Zhou, W., & Sun, S. (2017). METTL14 suppresses the metastatic potential of hepatocellular carcinoma by modulating N^6-methyladenosine-dependent primary MicroRNA processing. *Hepatology*, *65*(2), 529–543. https://doi.org/10.1002/hep.28885

Mao, Y., Dong, L., Liu, X.-M., Guo, J., Ma, H., Shen, B., & Qian, S.-B. (2019). m6A in mRNA coding regions promotes translation via the RNA helicase-containing YTHDC2. *Nature Communications*, *10*(1), 5332. https://doi.org/10.1038/s41467-019-13317-9

Marshall, A. C., Kidd, S. E., Lamont-Friedrich, S. J., Arentz, G., Hoffmann, P., Coad, B. R., & Bruning, J. B. (2019). Structure, Mechanism, and Inhibition of *Aspergillus fumigatus* Thioredoxin Reductase. *Antimicrobial Agents and Chemotherapy*, *63*(3). https://doi.org/10.1128/AAC.02281-18

May, H. C., Yu, J.-J., Guentzel, M. N., Chambers, J. P., Cap, A. P., & Arulanandam, B. P. (2018). Repurposing Auranofin, Ebselen, and PX-12 as Antimicrobial Agents Targeting the Thioredoxin System. *Frontiers in Microbiology*, *9*. https://doi.org/10.3389/fmicb.2018.00336

Mauer, J., Luo, X., Blanjoie, A., Jiao, X., Grozhik, A. v., Patil, D. P., Linder, B., Pickering, B. F., Vasseur, J.-J., Chen, Q., Gross, S. S., Elemento, O., Debart, F., Kiledjian, M., & Jaffrey, S. R. (2017). Reversible methylation of m6Am in the 5′ cap controls mRNA stability. *Nature*, *541*(7637), 371–375. https://doi.org/10.1038/nature21022

Meyer, K. D., Patil, D. P., Zhou, J., Zinoviev, A., Skabkin, M. A., Elemento, O., Pestova, T. V., Qian, S.-B., & Jaffrey, S. R. (2015). 5′ UTR m6A Promotes Cap-Independent Translation. *Cell*, *163*(4), 999–1010. https://doi.org/10.1016/j.cell.2015.10.012

Meyer, K. D., Saletore, Y., Zumbo, P., Elemento, O., Mason, C. E., & Jaffrey, S. R. (2012).

Comprehensive Analysis of mRNA Methylation Reveals Enrichment in 3′ UTRs and near Stop Codons. *Cell*, *149*(7), 1635–1646. https://doi.org/10.1016/j.cell.2012.05.003

Mizuno, T. (2018). Fat Mass and Obesity Associated (FTO) Gene and Hepatic Glucose and Lipid Metabolism. *Nutrients*, *10*(11), 1600. https://doi.org/10.3390/nu10111600

Mukherjee, S., Weiner, W. S., Schroeder, C. E., Simpson, D. S., Hanson, A. M., Sweeney, N. L., Marvin, R. K., Ndjomou, J., Kolli, R., Isailovic, D., Schoenen, F. J., & Frick, D. N. (2014). Ebselen Inhibits Hepatitis C Virus NS3 Helicase Binding to Nucleic Acid and Prevents Viral Replication. *ACS Chemical Biology*, *9*(10), 2393–2403. https://doi.org/10.1021/cb500512z

Nishizawa, Y., Konno, M., Asai, A., Koseki, J., Kawamoto, K., Miyoshi, N., Takahashi, H., Nishida, N., Haraguchi, N., Sakai, D., Kudo, T., Hata, T., Matsuda, C., Mizushima, T., Satoh, T., Doki, Y., Mori, M., & Ishii, H. (2018). Oncogene c-Myc promotes epitranscriptome m6A reader YTHDF1 expression in colorectal cancer. *Oncotarget*, *9*(7). https://doi.org/10.18632/oncotarget.23554

Niu, Yamei, Zhao, X., Wu, Y.-S., Li, M.-M., Wang, X.-J., & Yang, Y.-G. (2013). N6-methyladenosine (m6A) in RNA: An Old Modification with A Novel Epigenetic Function. *Genomics, Proteomics & Bioinformatics*, *11*(1), 8–17. https://doi.org/10.1016/j.gpb.2012.12.002

Niu, Yi, Lin, Z., Wan, A., Chen, H., Liang, H., Sun, L., Wang, Y., Li, X., Xiong, X., Wei, B., Wu, X., & Wan, G. (2019). RNA N6-methyladenosine demethylase FTO promotes breast tumor progression through inhibiting BNIP3. *Molecular Cancer*, *18*(1), 46. https://doi.org/10.1186/s12943-019-1004-4

Patil, D. P., Chen, C.-K., Pickering, B. F., Chow, A., Jackson, C., Guttman, M., & Jaffrey, S. R. (2016). m6A RNA methylation promotes XIST-mediated transcriptional repression. *Nature*, *537*(7620), 369–373. https://doi.org/10.1038/nature19342

Peng, S., Xiao, W., Ju, D., Sun, B., Hou, N., Liu, Q., Wang, Y., Zhao, H., Gao, C., Zhang, S., Cao, R., Li, P., Huang, H., Ma, Y., Wang, Y., Lai, W., Ma, Z., Zhang, W., Huang, S., … Huang, N. (2019). Identification of entacapone as a chemical inhibitor of FTO mediating metabolic regulation through FOXO1. *Science Translational Medicine*, *11*(488), eaau7116. https://doi.org/10.1126/scitranslmed.aau7116

Perry, R. P., & Kelley, D. E. (1974). Existence of methylated messenger RNA in mouse L cells. *Cell*, *1*(1), 37–42. https://doi.org/10.1016/0092-8674(74)90153-6

Ping, X.-L., Sun, B.-F., Wang, L., Xiao, W., Yang, X., Wang, W.-J., Adhikari, S., Shi, Y., Lv, Y., Chen, Y.-S., Zhao, X., Li, A., Yang, Y., Dahal, U., Lou, X.-M., Liu, X., Huang, J., Yuan, W.P., Zhu, X.-F., … Yang, Y.-G. (2014). Mammalian WTAP is a regulatory subunit of the RNA N6-methyladenosine methyltransferase. *Cell Research*, *24*(2), 177–189. https://doi.org/10.1038/cr.2014.3

Roundtree, I. A., Luo, G.-Z., Zhang, Z., Wang, X., Zhou, T., Cui, Y., Sha, J., Huang, X., Guerrero, L., Xie, P., He, E., Shen, B., & He, C. (2017). YTHDC1 mediates nuclear export of N6-methyladenosine methylated mRNAs. *ELife*, *6*. https://doi.org/10.7554/eLife.31311

Schwartz, S., Agarwala, S. D., Mumbach, M. R., Jovanovic, M., Mertins, P., Shishkin, A., Tabach, Y., Mikkelsen, T. S., Satija, R., Ruvkun, G., Carr, S. A., Lander, E. S., Fink, G. R., & Regev, A. (2013). High-Resolution Mapping Reveals a Conserved, Widespread, Dynamic mRNA Methylation Program in Yeast Meiosis. *Cell*, *155*(6), 1409–1421. https://doi.org/10.1016/j.cell.2013.10.047

Schwartz, S., Mumbach, M. R., Jovanovic, M., Wang, T., Maciag, K., Bushkin, G. G., Mertins, P., Ter-Ovanesyan, D., Habib, N., Cacchiarelli, D., Sanjana, N. E., Freinkman, E., Pacold, M. E., Satija, R., Mikkelsen, T. S., Hacohen, N., Zhang, F., Carr, S. A., Lander, E. S., & Regev, A. (2014). Perturbation of m6A Writers Reveals Two Distinct Classes of mRNA Methylation at Internal and 5′ Sites. *Cell Reports*, *8*(1), 284–296. https://doi.org/10.1016/j.celrep.2014.05.048

Selberg, S., Blokhina, D., Aatonen, M., Koivisto, P., Siltanen, A., Mervaala, E., Kankuri, E., & Karelson, M. (2019). Discovery of Small Molecules that Activate RNA Methylation through Cooperative Binding to the METTL3-14-WTAP Complex Active Site. *Cell Reports*, *26*(13), 3762-3771.e5. https://doi.org/10.1016/j.celrep.2019.02.100

Shi, H., Zhang, X., Weng, Y.-L., Lu, Z., Liu, Y., Lu, Z., Li, J., Hao, P., Zhang, Y., Zhang, F., Wu, Y., Delgado, J. Y., Su, Y., Patel, M. J., Cao, X., Shen, B., Huang, X., Ming, G., Zhuang, X., … Zhou, T. (2018). m6A facilitates hippocampus-dependent learning and memory through YTHDF1. *Nature*, *563*(7730), 249–253. https://doi.org/10.1038/s41586-018-0666-1

Shi, Y., Fan, S., Wu, M., Zuo, Z., Li, X., Jiang, L., Shen, Q., Xu, P., Zeng, L., Zhou, Y., Huang, Y., Yang, Z., Zhou, J., Gao, J., Zhou, H., Xu, S., Ji, H., Shi, P., Wu, D.-D., … Chen, Y. (2019). YTHDF1 links hypoxia adaptation and non-small cell lung cancer progression. *Nature Communications*, *10*(1), 4892. https://doi.org/10.1038/s41467-019-12801-6

Stoilov, P., Rafalska, I., & Stamm, S. (2002). YTH: a new domain in nuclear proteins. *Trends in Biochemical Sciences*, *27*(10), 495–497. https://doi.org/10.1016/S0968-0004(02)02189-8

Su, R., Dong, L., Li, C., Nachtergaele, S., Wunderlich, M., Qing, Y., Deng, X., Wang, Y., Weng, X., Hu, C., Yu, M., Skibbe, J., Dai, Q., Zou, D., Wu, T., Yu, K., Weng, H., Huang, H., Ferchen, K., … Chen, J. (2018). R-2HG Exhibits Anti-tumor Activity by Targeting FTO/m6A/MYC/CEBPA Signaling. *Cell*, *172*(1–2), 90-105.e23. https://doi.org/10.1016/j.cell.2017.11.031

Svensen, N., & Jaffrey, S. R. (2016). Fluorescent RNA Aptamers as a Tool to Study RNAModifying Enzymes. *Cell Chemical Biology*, *23*(3), 415–425. https://doi.org/10.1016/j.chembiol.2015.11.018

Tanabe, A., Tanikawa, K., Tsunetomi, M., Takai, K., Ikeda, H., Konno, J., Torigoe, T., Maeda, H., Kutomi, G., Okita, K., Mori, M., & Sahara, H. (2016). RNA helicase YTHDC2 promotes cancer metastasis via the enhancement of the efficiency by which HIF-1α mRNA is translated. *Cancer Letters*, *376*(1), 34–42. https://doi.org/10.1016/j.canlet.2016.02.022

Theler, D., Dominguez, C., Blatter, M., Boudet, J., & Allain, F. H.-T. (2014). Solution structure of the YTH domain in complex with N6-methyladenosine RNA: a reader of methylated RNA. *Nucleic Acids Research*, *42*(22), 13911–13919. https://doi.org/10.1093/nar/gku1116

Tirumuru, N., Zhao, B. S., Lu, W., Lu, Z., He, C., & Wu, L. (2016). N6-methyladenosine of HIV1 RNA regulates viral infection and HIV-1 Gag protein expression. *ELife*, *5*. https://doi.org/10.7554/eLife.15528

Toh, J. D. W., Sun, L., Lau, L. Z. M., Tan, J., Low, J. J. A., Tang, C. W. Q., Cheong, E. J. Y., Tan, M. J. H., Chen, Y., Hong, W., Gao, Y.-G., & Woon, E. C. Y. (2015). A strategy based on nucleotide specificity leads to a subfamily-selective and cell-active inhibitor of N^6 methyladenosine demethylase FTO. *Chemical Science*, *6*(1), 112–122. https://doi.org/10.1039/C4SC02554G

Visvanathan, A., Patil, V., Arora, A., Hegde, A. S., Arivazhagan, A., Santosh, V., & Somasundaram, K. (2018). Essential role of METTL3-mediated m6A modification in glioma stem-like cells maintenance and radioresistance. *Oncogene*, *37*(4), 522–533. https://doi.org/10.1038/onc.2017.351

Vu L.P., Cheng Y, Kharas MG. The Biology of m6A RNA Methylation in Normal and Malignant Hematopoiesis. Cancer Discov. 2019;9(1):25-33. doi:10.1158/2159-8290.CD-18-0959

Vu, L. P., Pickering, B. F., Cheng, Y., Zaccara, S., Nguyen, D., Minuesa, G., Chou, T., Chow, A., Saletore, Y., MacKay, M., Schulman, J., Famulare, C., Patel, M., Klimek, V. M., Garrett-Bakelman, F. E., Melnick, A., Carroll, M., Mason, C. E., Jaffrey, S. R., & Kharas, M. G. (2017). The N6-methyladenosine (m6A)-forming enzyme METTL3 controls myeloid differentiation of normal hematopoietic and leukemia cells. *Nature Medicine*, *23*(11), 1369–1376. https://doi.org/10.1038/nm.4416

Walters, B. J., Mercaldo, V., Gillon, C. J., Yip, M., Neve, R. L., Boyce, F. M., Frankland, P. W., & Josselyn, S. A. (2017). The Role of The RNA Demethylase FTO (Fat Mass and ObesityAssociated) and mRNA Methylation in Hippocampal Memory Formation. *Neuropsychopharmacology*, *42*(7), 1502–1510. https://doi.org/10.1038/npp.2017.31

Wang, H., Xu, B., & Shi, J. (2020). N6-methyladenosine METTL3 promotes the breast cancer progression via targeting Bcl-2. *Gene*, *722*, 144076. https://doi.org/10.1016/j.gene.2019.144076

Wang, Xiang, Feng, J., Xue, Y., Guan, Z., Zhang, D., Liu, Z., Gong, Z., Wang, Q., Huang, J., Tang, C., Zou, T., & Yin, P. (2017). Erratum: Corrigendum: Structural basis of N6adenosine methylation by the METTL3–METTL14 complex. *Nature*, *542*(7640), 260–260. https://doi.org/10.1038/nature21073

Wang, Xiao, Lu, Z., Gomez, A., Hon, G. C., Yue, Y., Han, D., Fu, Y., Parisien, M., Dai, Q., Jia, G., Ren, B., Pan, T., & He, C. (2014). N6-methyladenosine-dependent regulation of messenger RNA stability. *Nature*, *505*(7481), 117–120. https://doi.org/10.1038/nature12730

Wang, Xiao, Zhao, B. S., Roundtree, I. A., Lu, Z., Han, D., Ma, H., Weng, X., Chen, K., Shi, H., & He, C. (2015). N6-methyladenosine Modulates Messenger RNA Translation Efficiency. *Cell*, *161*(6), 1388–1399. https://doi.org/10.1016/j.cell.2015.05.014

Wang, Y., Li, Y., Toth, J. I., Petroski, M. D., Zhang, Z., & Zhao, J. C. (2014). N6methyladenosine modification destabilizes developmental regulators in embryonic stem cells. *Nature Cell Biology*, *16*(2), 191–198. https://doi.org/10.1038/ncb2902

Weng, H., Huang, H., Wu, H., Qin, X., Zhao, B. S., Dong, L., Shi, H., Skibbe, J., Shen, C., Hu, C., Sheng, Y., Wang, Y., Wunderlich, M., Zhang, B., Dore, L. C., Su, R., Deng, X., Ferchen, K., Li, C., … Chen, J. (2018). METTL14 Inhibits Hematopoietic Stem/Progenitor Differentiation and Promotes Leukemogenesis via mRNA m6A Modification. *Cell Stem Cell*, *22*(2), 191-205.e9. https://doi.org/10.1016/j.stem.2017.11.016

Widagdo, J., Zhao, Q.-Y., Kempen, M.-J., Tan, M. C., Ratnu, V. S., Wei, W., Leighton, L., Spadaro, P. A., Edson, J., Anggono, V., & Bredy, T. W. (2016). Experience-Dependent Accumulation of *N* ^{6} -Methyladenosine in the Prefrontal Cortex Is Associated with Memory Processes in Mice. *The Journal of Neuroscience*, *36*(25), 6771–6777. https://doi.org/10.1523/JNEUROSCI.4053-15.2016

Wiedmer, L., Eberle, S. A., Bedi, R. K., Śledź, P., & Caflisch, A. (2019). A Reader-Based Assay for m ^{6} A Writers and Erasers. *Analytical Chemistry*, *91*(4), 3078–3084. https://doi.org/10.1021/acs.analchem.8b05500

Wojtas, M. N., Pandey, R. R., Mendel, M., Homolka, D., Sachidanandam, R., & Pillai, R. S. (2017). Regulation of m6A Transcripts by the 3'→5' RNA Helicase YTHDC2 Is Essential for a Successful Meiotic Program in the Mammalian Germline. *Molecular Cell*, *68*(2), 374387.e12. https://doi.org/10.1016/j.molcel.2017.09.021

Xiao, W., Adhikari, S., Dahal, U., Chen, Y.-S., Hao, Y.-J., Sun, B.-F., Sun, H.-Y., Li, A., Ping, X.-L., Lai, W.-Y., Wang, X., Ma, H.-L., Huang, C.-M., Yang, Y., Huang, N., Jiang, G.-B., Wang, H.-L., Zhou, Q., Wang, X.-J., … Yang, Y.-G. (2016). Nuclear m 6 A Reader YTHDC1 Regulates mRNA Splicing. *Molecular Cell*, *61*(4), 507–519. https://doi.org/10.1016/j.molcel.2016.01.012

Xie, T., Pan, S., Zheng, H., Luo, Z., Tembo, K. M., Jamal, M., Yu, Z., Yu, Y., Xia, J., Yin, Q., Wang, M., Yuan, W., Zhang, Q., & Xiong, J. (2018). PEG10 as an oncogene: expression regulatory mechanisms and role in tumor progression. *Cancer Cell International*, *18*(1), 112. https://doi.org/10.1186/s12935-018-0610-3

Xiu, M.-X., & Liu, Y.-M. (2019). The role of oncogenic Notch2 signaling in cancer: a novel therapeutic target. *American Journal of Cancer Research*, *9*(5), 837–854. https://pubmed.ncbi.nlm.nih.gov/31218097

Xu, C., Liu, K., Ahmed, H., Loppnau, P., Schapira, M., & Min, J. (2015). Structural Basis for the Discriminative Recognition of N^6-Methyladenosine RNA by the Human YT521-B Homology Domain Family of Proteins. *Journal of Biological Chemistry*, *290*(41), 24902–24913. https://doi.org/10.1074/jbc.M115.680389

Xu, C., Wang, X., Liu, K., Roundtree, I. A., Tempel, W., Li, Y., Lu, Z., He, C., & Min, J. (2014). Structural basis for selective binding of m6A RNA by the YTHDC1 YTH domain. *Nature Chemical Biology*, *10*(11), 927–929. https://doi.org/10.1038/nchembio.1654

Yamaguchi, T., Sano, K., Takakura, K., Saito, I., Shinohara, Y., Asano, T., & Yasuhara, H. (1998). Ebselen in Acute Ischemic Stroke. *Stroke*, *29*(1), 12–17. https://doi.org/10.1161/01.STR.29.1.12

Yang, Z., Li, J., Feng, G., Gao, S., Wang, Y., Zhang, S., Liu, Y., Ye, L., Li, Y., & Zhang, X. (2017). MicroRNA-145 Modulates N^6-Methyladenosine Levels by Targeting the 3′Untranslated mRNA Region of the N^6-Methyladenosine Binding YTH Domain Family 2 Protein. *Journal of Biological Chemistry*, *292*(9), 3614–3623. https://doi.org/10.1074/jbc.M116.749689

Yoon, K.-J., Ringeling, F. R., Vissers, C., Jacob, F., Pokrass, M., Jimenez-Cyrus, D., Su, Y., Kim, N.-S., Zhu, Y., Zheng, L., Kim, S., Wang, X., Doré, L. C., Jin, P., Regot, S., Zhuang, X., Canzar, S., He, C., Ming, G., & Song, H. (2017). Temporal Control of Mammalian Cortical Neurogenesis by m6A Methylation. *Cell*, *171*(4), 877-889.e17. https://doi.org/10.1016/j.cell.2017.09.003

Yue, Y., Liu, J., Cui, X., Cao, J., Luo, G., Zhang, Z., Cheng, T., Gao, M., Shu, X., Ma, H., Wang, F., Wang, X., Shen, B., Wang, Y., Feng, X., He, C., & Liu, J. (2018). VIRMA mediates preferential m6A mRNA methylation in 3′UTR and near stop codon and associates with alternative polyadenylation. *Cell Discovery*, *4*(1), 10. https://doi.org/10.1038/s41421-018-0019-0

Zaccara S, Jaffrey SR. A Unified Model for the Function of YTHDF Proteins in Regulating m^{6}A-Modified mRNA. *Cell*. 2020;181(7):1582-1595.e18. doi:10.1016/j.cell.2020.05.012

Zhang, C., Samanta, D., Lu, H., Bullen, J. W., Zhang, H., Chen, I., He, X., & Semenza, G. L. (2016). Hypoxia induces the breast cancer stem cell phenotype by HIF-dependent and ALKBH5-mediated m ^{6} A-demethylation of NANOG mRNA. *Proceedings of the National Academy of Sciences*, *113*(14), E2047–E2056. https://doi.org/10.1073/pnas.1602883113

Zhang, C., Zhi, W. I., Lu, H., Samanta, D., Chen, I., Gabrielson, E., & Semenza, G. L. (2016). Hypoxia-inducible factors regulate pluripotency factor expression by ZNF217- and ALKBH5-mediated modulation of RNA methylation in breast cancer cells. *Oncotarget*, *7*(40). https://doi.org/10.18632/oncotarget.11743

Zhang, J.-H. (1999). A Simple Statistical Parameter for Use in Evaluation and Validation of High Throughput Screening Assays. *Journal of Biomolecular Screening*, *4*(2), 67–73. https://doi.org/10.1177/108705719900400206

Zhang, S., Zhao, B. S., Zhou, A., Lin, K., Zheng, S., Lu, Z., Chen, Y., Sulman, E. P., Xie, K., Bögler, O., Majumder, S., He, C., & Huang, S. (2017). m 6 A Demethylase ALKBH5 Maintains Tumorigenicity of Glioblastoma Stem-like Cells by Sustaining FOXM1 Expression and Cell Proliferation Program. *Cancer Cell*, *31*(4), 591-606.e6. https://doi.org/10.1016/j.ccell.2017.02.013

Zhang, Z., Theler, D., Kaminska, K. H., Hiller, M., de la Grange, P., Pudimat, R., Rafalska, I., Heinrich, B., Bujnicki, J. M., Allain, F. H.-T., & Stamm, S. (2010). The YTH Domain Is a Novel RNA Binding Domain. *Journal of Biological Chemistry*, *285*(19), 14701–14710. https://doi.org/10.1074/jbc.M110.104711

Zhao, X., Yang, Y., Sun, B.-F., Shi, Y., Yang, X., Xiao, W., Hao, Y.-J., Ping, X.-L., Chen, Y.-S.,

Wang, W.-J., Jin, K.-X., Wang, X., Huang, C.-M., Fu, Y., Ge, X.-M., Song, S.-H., Jeong, H. S., Yanagisawa, H., Niu, Y., … Yang, Y.-G. (2014). FTO-dependent demethylation of N6methyladenosine regulates mRNA splicing and is required for adipogenesis. *Cell Research*, *24*(12), 1403–1419. https://doi.org/10.1038/cr.2014.151

Zheng, G., Dahl, J. A., Niu, Y., Fedorcsak, P., Huang, C.-M., Li, C. J., Vågbø, C. B., Shi, Y., Wang, W.-L., Song, S.-H., Lu, Z., Bosmans, R. P. G., Dai, Q., Hao, Y.-J., Yang, X., Zhao, W.-M., Tong, W.-M., Wang, X.-J., Bogdan, F., … He, C. (2013). ALKBH5 Is a Mammalian RNA Demethylase that Impacts RNA Metabolism and Mouse Fertility. *Molecular Cell*, *49*(1), 18–29. https://doi.org/10.1016/j.molcel.2012.10.015

Zhong, L., Liao, D., Zhang, M., Zeng, C., Li, X., Zhang, R., Ma, H., & Kang, T. (2019). YTHDF2 suppresses cell proliferation and growth via destabilizing the EGFR mRNA in hepatocellular carcinoma. *Cancer Letters*, *442*, 252–261. https://doi.org/10.1016/j.canlet.2018.11.006

Zhou, J., Wan, J., Gao, X., Zhang, X., Jaffrey, S. R., & Qian, S.-B. (2015). Dynamic m6A mRNA methylation directs translational control of heat shock response. *Nature*, *526*(7574), 591–594. https://doi.org/10.1038/nature15377

Zhou, K. I., & Pan, T. (2018). An additional class of m6A readers. *Nature Cell Biology*, *20*(3), 230–232. https://doi.org/10.1038/s41556-018-0046-y

Zhuang, M., Li, X., Zhu, J., Zhang, J., Niu, F., Liang, F., Chen, M., Li, D., Han, P., & Ji, S.-J. (2019). The m6A reader YTHDF1 regulates axon guidance through translational control of Robo3.1 expression. *Nucleic Acids Research*, *47*(9), 4765–4777. https://doi.org/10.1093/nar/gkz157